October 2019

# Middle to Late Pleistocene Paleoenvironmental Reconstructions from Lake El'gygytgyn, Arctic Russia

Mary Helen Habicht
*University of Massachusetts - Amherst*

# MIDDLE TO LATE PLEISTOCENE PALEOENVIRONMENTAL RECONSTRUCTIONS FROM LAKE EL'GYGYTGYN, ARCTIC RUSSIA

A Dissertation Presented

by

M. HELEN HABICHT

Submitted to the Graduate School of the
University of Massachusetts Amherst in partial fulfillment
of the requirements for the degree of

DOCTOR OF PHILOSOPHY

September 2019

Department of Geosciences

**MIDDLE TO LATE PLEISTOCENE PALEOENVIRONMENTAL RECONSTRUCTIONS FROM LAKE EL'GYGYTGYN, ARCTIC RUSSIA**

A Dissertation Presented

by

M. HELEN HABICHT

Approved as to style and content by:

_____
Isla S. Castañeda, Chair

_____
Julie Brigham-Grette, Member

_____
Stephen Burns, Member

_____
Robert DeConto, Member

_____
James Holden, Member

_____
Julie Brigham-Grette, Department Head
Department of Geosciences

## ACKNOWLEDGMENTS

I would like to thank my co-advisors Isla Castañeda and Julie Brigham-Grette who have supported me and guided me throughout my time at the University of Massachusetts Amherst. Isla taught me so much about paleolimnology, biomarkers, and the field of organic geochemistry and inspired me to become a better scientist and writer. Working with Julie expanded my interest in the Arctic and climate change. Her knowledge of high latitude paleoclimate is vast and has been a valuable resource. I would also like to acknowledge my dissertation committee members Rob DeConto, Stephen Burns, and Jim Holden. Thank you for your advice, encouragement, and investment in my research.

The past few years would not have been the same without the friendly and intellectually stimulating faculty and students in the UMass Geosciences Department. I have truly appreciated being a part of this group. An additional thanks to the front office staff for their work to keep our department running smoothly. I also recognize the maintenance staff for their efforts to make this campus a safe, clean, and beautiful place to work and learn.

I would like to thank all of my Climate Center comrades through the years. I have enjoyed working in this space with you and am so grateful for your support and all the laughs. Thank you to the Biogeochem Lab members who have made long hours in the lab a wonderful experience. An extra special recognition goes to Benjamin Keisling and Dan Miller. Sharing this journey through graduate school with you both has been so rewarding and so much fun. I am proud of the things we have accomplished individually and as a group.

Finally, I thank my parents David and Mary Habicht for their love and support. Because of you, I will always do my best and have fun. Love.

## ABSTRACT

## MIDDLE TO LATE PLEISTOCENE PALEOENVIRONMENTAL RECONSTRUCTIONS FROM LAKE EL'GYGYTGYN, ARCTIC RUSSIA

SEPTEMBER 2019

M. HELEN HABICHT, B.A., ALBION COLLEGE

M.S., UNIVERSITY OF MASSACHUSETTS AMHERST

Ph.D., UNIVERSITY OF MASSACHUSETTS AMHERST

Directed by: Professor Isla S. Castañeda

Climate change is a major issue challenging the world today. Our global society faces rising temperatures, variable weather patterns, and rising sea level among other associated issues. Our action (or inaction) to address current changes will have serious ramifications for life on our planet in the coming centuries and millennia. In order to provide context for these present and future changes, we can utilize the paleo record to understand the natural variability of Earth's climate system.

One region of the world is changing more rapidly than the global average. Over recent decades, the Arctic has experienced warmer temperatures, reduced sea ice, melting permafrost, and shifts in the amount and seasonality of precipitation. Unfortunately, paleoclimate and environmental records from the terrestrial Arctic, particularly beyond the last 120 ka, are few. This is due to the repeated extensive glaciation of the northern hemisphere high latitudes during the ice ages of the Quaternary.

One area of the Arctic, in the Anadyr mountains of Chukotka, has remained unglaciated through the Pleistocene. Lake El'gygytgyn, a meteorite impact crater lake formed 3.6 million years ago lies in this area and so provides a continuous sedimentary

sequence from the Mid-Pliocene to present. This dissertation includes four studies of Lake El'gygytgyn sediments over the last 800 thousand years. A variety of biogeochemical and stable isotope proxies are used to reconstruct climate and environmental variability throughout the study interval. These studies provide novel information about the natural variations of terrestrial Arctic climate on glacial-interglacial timescales.

Chapter 2 of this dissertation involves the analysis of bacterial membrane lipids called branched glycerol dialkyl glycerol tetraethers (brGDGTs) and plant leaf wax *n*-alkanes to provide records of relative temperature change and terrestrial vegetation turnover in response to aridity during the glacial-intergacial cycles of the Mid-Pleistocene. Our data suggests that regional temperature is strongly influenced by local summer insolation while aridity changes derive from sea level driven changes in continentality. Comparison of our data with previously published paleoclimate records from Lake El'gygytgyn highlights the difference in proxy response to climatic variables and the utility of a multi-proxy approach. Additionally, we use our extensive records to identify the presence of a global climatic transition, the Mid-Brunhes Event (MBE), for the first time in the terrestrial Arctic.

In Chapter 3, we analyze algal lipid biomarkers from the same samples used in Chapter 2. We also incorporate stable carbon and nitrogen isotopes to determine changes in primary production and organic matter preservation in Lake El'gygytgyn across multiple glacial-interglacial cycles.

Chapter 4 spans the Holocene and Late Pleistocene (280 ka to present). We use the hydrogen isotopic composition of long chain plant leaf wax *n*-alkanes to reconstruct

temperature and hydroclimate changes. We find that MIS 7 was a stronger interglacial period than MIS 5e in the terrestrial Arctic and attribute the variability in hydrogen isotopes predominantly to temperature and moisture source changes.

In Chapter 5, we compare the hydrogen isotope composition of *n*-alkanes measured in Chapter 4 to the isotopic composition of *n*-alkanoic acids in the same samples previously analyzed by Wilkie (2012). This is a novel approach for paleoclimate records. Our results indicate that the type of compound selected for analysis can have a significant impact on the paleoclimatic interpretations of a study.

Finally in Chapter 6, a summary and avenues for future research are provided. Overall, this dissertation is a testament to the utility of biomarkers and stable isotopes in Arctic lake sediments. Each study provides unique information about the terrestrial Arctic climate during the Quaternary and contributes to our understanding of climatic variability and the dynamics of this sensitive region.

## TABLE OF CONTENTS

Page

## LIST OF TABLES

Table Page

## LIST OF FIGURES

# CHAPTER 1

# ARCTIC CLIMATE CHANGE

## 1.1 Overview of Arctic climate change and paleoclimatology

Anthropogenic climate change is perhaps the most critical issue facing the world today (IPCC, 2018). Humans have perturbed the climate system and induced changes with irreversible effects. Our ability to understand the extent of anthropogenic climate change and make accurate predictions about the future is dependent on our knowledge of climate changes throughout Earth's history. Studies of past warm periods are particularly pertinent, as they provide information regarding the natural variability of the climate system as well as an analog to present and future change (Loutre and Berger, 2003; Thompson and Fleming, 1996).

The Arctic is currently undergoing rapid and unprecedented climate change including rising temperatures and changes in precipitation and atmospheric circulation patterns (SWIPA, 2017). Unfortunately, the diverse terrain and variable conditions of the region have led to a sparse and incomplete system of monitoring networks thus limiting our understanding of the role and importance of the Arctic in the climate system (Fitzpatrick et al., 2010; Miller et al., 2010). The Arctic is particularly sensitive to climate change because of the impacts of polar amplification with feedback mechanisms involving oceanic, atmospheric, and terrestrial processes (IPCC, 2013). These processes do not only impact the arctic marine and terrestrial realms but also affect the cryosphere

and global climate dynamics and have major implications for climate variability in the lower latitudes (Miller et al., 2010; Walsh, 2014).

Knowledge of the paleoclimate history of this region is essential for understanding the role of these processes in modern climate change (Fitzpatrick et al., 2010). Terrestrial paleoclimate archives are rare in the Arctic due to glacial erosion (Miller et al., 2010) and little is known about the role and response of the region beyond the extent of the Greenland ice core records (~120 ka) (Andersen et al., 2004), while much longer records exist for the lower latitudes, the marine realm, and Antarctica. Thus, the generation of long, high resolution paleoclimate records from the Arctic is crucial for understanding the role and response of the region to dynamics of the climate system on longer timescales and for comparison to other globally distributed paleoclimate records.

Lakes sediments are a crucial type of terrestrial climate archive as they are widely distributed, provide high temporal resolution with continuous sedimentation, and preserve numerous geochemical proxies (Castañeda and Schouten, 2011). Lake sediments often contain abundant organic matter, providing unique records of paleoclimate and environmental changes through the preservation of source specific organic compounds or biomarkers. This dissertation focuses on applying the abundance, distribution, and isotopic signature of various organic biomarkers to address outstanding and enigmatic questions in Arctic paleoclimatology. The reconstructions from Lake El'gygytgyn, Arctic Russia presented here help fill the critical gap in knowledge surrounding this crucial region.

## 1.2 Dissertation layout

This dissertation is presented/organized in six chapters, including this introductory chapter. Four of the chapters (2-5) were prepared as manuscripts for publication in scientific journals. These chapters are written in first person plural and were composed primarily by myself with the input and advice of co-authors listed below.

Chapter 2, entitled "Middle Pleistocene temperature and vegetation change at Lake El'gygytgyn, Arctic Russia", presents a multi-proxy approach to assessing temperature and landscape scale vegetation change in the terrestrial Arctic over the interval of 200-800 ka. Two classes of organic biomarkers, branched glycerol dialkyl glycerol tetraethers and plant leaf wax *n*-alkanes, are used in combination with a suite of previously published paleoclimate data from Lake El'gygytgyn to assess the behavior of several glacial-interglacial cycles and determine the presence of a global climatic transition called the Mid-Brunhes Event. Co-authors for this publication were Isla Castañeda, Molly Patterson, and Julie Brigham-Grette. This chapter was submitted as a manuscript for publication in *Quaternary Science Reviews* and is in preparation for resubmission at the time of writing.

Chapter 3 is entitled "Lacustrine primary production and organic matter preservation during the Middle Pleistocene: an Arctic perspective from Lake El'gygytgyn, Russia." Algal biomarkers and stable isotopes are used to examine aquatic production and organic matter preservation over glacial-interglacial cycles from 200-800 ka. This chapter was prepared as manuscript for submission to *Journal of Paleolimnology* with co-authors Isla Castañeda, Stephen Burns, and Julie Brigham-Grette.

Chapter 4, entitled “Late Pleistocene Arctic climate inferred from leaf wax hydrogen isotopes in Lake El’gygytgyn, Russia”, investigates temperature and hydrologic change in the Arctic from 0-280 ka using the hydrogen isotopic composition of terrestrial plant leaf wax *n*-alkanes. Co-authors on this manuscript are Isla Castañeda, Elizabeth Thomas, Stephen Burns, Molly Patterson, and Julie Brigham-Grette. The chapter will be submitted to *Nature Geoscience*.

Chapter 5, is entitled “ A comparison of the hydrogen isotopic composition of plant leaf wax *n*-alkanes and *n*-alkanoic acids from Lake El’gygytgyn (Russia) during the past 120,000 years.” This chapters provides a novel comparison of the isotopic composition of two classes of *n*-alkyl lipids in a sedimentary sequence. The results have important implications for the use and interpretation of this proxy in paleoclimate studies. This chapter was prepared as manuscript for submission as a Note to *Organic Geochemistry* in collaboration with co-authors Elizabeth Thomas, Isla Castañeda, Stephen Burns, Jeffrey Salacup, and Julie Brigham-Grette.

The final chapter (Chapter 6) summarizes the work performed in this dissertation, its impacts, and potential directions for future work that could build on the science discussed in this thesis.

# CHAPTER 2

# MIDDLE PLEISTOCENE TEMPERATURE AND VEGETATION CHANGE AT LAKE EL'GYGYTGYN, ARCTIC RUSSIA

## 2.1 Abstract

Mid-Pleistocene climate and vegetation change in the terrestrial Arctic was investigated using branched glycerol dialkyl glycerol tetraethers and plant leaf waxes preserved in Lake El'gygytgyn (Northeast Russia) sediments. Our organic geochemical temperature and vegetation reconstructions display glacial-interglacial variability and exhibit precessional and obliquity frequencies, respectively. We compare these new records to other previously generated proxy data from Lake El'gygytgyn to assess the dynamics of glacial and interglacial periods between 200 and 800 ka. Our detailed examination of each climatic cycle illustrates that the expression of glacials and interglacials varies by proxy type. We find that marine isotope stages 7c, 9, and 17 are the three warmest interglacials, and stages 10 and 12 are the coldest glacial periods. However the intensity of these periods is not necessarily reflected in other proxies included in our analysis. The differences in proxy response can provide valuable information about the overall climate, environmental patterns and dynamics while highlighting the importance of a multi-proxy approach. The Lake El'gygytgyn proxy data also records a signal of the Mid- Brunhes Event (MBE) ~430 ka. Pre- and post-MBE differences in the proxy records are likely attributed to shifts in atmospheric circulation due to the stratification and warming in the North Pacific associated with reduced

Antarctic bottom water (AABW) production, thus providing further support for teleconnections between the high northern and southern latitudes.

## 2.2 Introduction

The Pleistocene (2.58 Ma to 11.7 ka) is characterized by periodic fluctuations between cold glacial and warm interglacial periods. Individual glacials and interglacials varied in length and intensity due to differences in boundary conditions including insolation, greenhouse gas concentrations (i.e., carbon dioxide ($CO_2$) and methane ($CH_4$)), and internal ice-driven feedbacks of continental ice sheets (Past Interglacials Working Group of PAGES, 2016). In addition to glacial-interglacial variability, a climatic shift, the Mid-Brunhes Event (MBE), occurred during the mid-Pleistocene. The MBE is a climatic transition recognized best in Antarctic ice cores at 430 ka between Marine Isotope Stages (MIS) 12 and 11 when the amplitude of glacial-interglacial cycles increased (Augustin et al., 2004; Jansen et al., 1986; Jouzel et al., 2007). In general, after MIS 12 interglacial climates are considered to have been warmer with higher atmospheric $CO_2$ (Jouzel et al., 2007; Lüthi et al., 2008). Yin (2013) suggests that pre-MBE interglacials (those prior to MIS 12) may have been cooler due to orbitally induced feedbacks resulting in increased Southern Ocean ventilation. Yet not all regions of the globe record a change in interglacial strength across the MBE inferring that it might have been a more regional event (Candy et al., 2010; Candy and McClymont, 2013). Key to understanding a cause for the MBE is determining where the event is clearly recorded.

As Earth undergoes climatic transitions associated with anthropogenic climate change, studies of paleoclimate events like the MBE become increasingly important to assess the forcing and feedbacks driving earth system processes. Due to the effect of

polar amplification, the northern high latitudes are currently the fastest warming region in the world (SWIPA, 2017). Unfortunately, high-resolution, continuous terrestrial records from the northern high latitudes beyond the last 100 ka recovered by the Greenland ice cores are rare (Miller et al., 2010). The repeated glaciation of the continents have prevented the identification and recovery of continuous sedimentary sequences throughout much of the Arctic and high northern latitudes (Miller et al., 2010). However, one part of the Arctic borderlands not impacted by large scale continental ice sheets (Glushkova, 2001; Glushkova and Smirnov, 2006), and where the MBE has yet to be detected, is Beringia – a vast land bridge reaching from the Kolyma to the MacKenzie rivers including the shallow Bering and Chukchi seas.

The Lake El'gygytgyn sediment core provides a unique and unprecedented record of climate change in the terrestrial Arctic from the Pliocene through the Pleistocene (Brigham-Grette et al., 2013; Melles et al., 2012, 2011). Here we apply two organic geochemical proxies to Lake El'gygytgyn sediments from 200-800 ka to examine temperature and vegetation change during the Mid-Pleistocene. First, we use the methylation/cyclization (MBT/CBT) ratio of branched glycerol dialkyl glycerol tetraethers (brGDGTs) (Weijers et al., 2007) as a proxy for relative temperature change. Second, we measure the average chain length (ACL) of higher plant leaf waxes ($C_{27}$ –$C_{33}$ *n*-alkanes)(Eglinton and Hamilton, 1967), to observe fluctuations in vegetation in response to climatic change. These two records, in combination with other previously published proxy data from Lake El'gygytgyn, allow us to explore the diverse expression of glacial-interglacial cycles in the Arctic during the Mid- to Late- Pleistocene. We also

examine teleconnections between high northern and southern hemisphere latitudes and investigate the presence of an MBE signal at Lake El'gygytgyn.

### 2.3 Study Area and Regional Setting

Lake El'gygytgyn, located on the Chukotka Peninsula in the Far East Russian Arctic (67°30' N, 172°5'E), was created by a meteorite impact 3.58 ± 0.04 Ma (Layer, 2000) (Figure 2.1). The catchment is 293 $km^2$ with a diameter of 18 km (Nolan and Brigham-Grette, 2007). A network of 50 small streams run into the lake and the Enmyvaam River provides an outlet to the Bering Sea (Nolan and Brigham-Grette, 2007). Today, Lake El'gygytgyn is 170 m deep, 12 km wide, and has a volume of 14.1 $km^3$ (Nolan and Brigham-Grette, 2007). The lake is monomictic and oligotrophic with summer temperatures not exceeding 4°C, except over the shallow nearshore shelves where temperatures can reach 5 °C (Nolan and Brigham-Grette, 2007). Annual overturning occurs in late summer, and lake ice formation begins by October and persists through June (Nolan and Brigham-Grette, 2007).

Modern air temperatures at Lake El'gygytgyn range from -46 °C in winter to +26 °C in summer, with a mean annual air temperature of -10.3° C (Nolan and Brigham-Grette, 2007). Cumulative annual precipitation measured from 2002 to 2007 ranged between 70 -200 mm $year^{-1}$ (Nolan, 2012). The region is affected predominantly by north-south winds (Nolan and Brigham-Grette, 2007) under the influence of two main atmospheric circulation patterns: the Siberian High and Aleutian Low (Mock et al., 1998; Nolan, 2013) (Figure 2.1). Modern vegetation at the lake is characterized as tundra, dominated by lichen and herbaceous taxa (Lozhkin et al., 2007a). Currently, the nearest conifer forests lie ~150 km southwest of the lake (Lozhkin et al., 2007a).

Lake El'gygytgyn was drilled from an ice platform during International Continental Scientific Drilling Project (ICDP) expedition 5011 in winter 2008/2009 (Melles et al., 2011). Three sediment cores were combined to create a 318 m long composite core spanning the past 3.6 Ma (Melles et al. 2011). The age model (Nowaczyk et al., 2013) is based primarily on magnetostratigraphy (Haltia and Nowaczyk, 2013) and tuning of paleo-productivity proxies to the global benthic oxygen isotope stack of Lisiecki and Raymo (2005) and regional insolation at 67 $^{o}$N (Melles et al., 2012; Nowaczyk et al., 2013).

## 2.4 Sampling and Methods

### 2.4.1 Sample Preparation

For this study, 386- 1 cm sediment samples (~1-6 grams dry weight), spanning the continuously drilled interval of 200- 800 ka were analyzed. This interval was selected because the top of the drill core is not 0 ka, as a separate gravity core collected in 2003, LZ-1024 spans the upper 200 ka. The lower limit of 800 ka was chosen to provide a direct northern hemisphere comparison with the EPICA Antarctic ice cores (Jouzel et al., 2007; Lüthi et al., 2008). Mean sedimentation rates in Lake El'gygytgyn during the last 1.0 Ma were ~ 4.02 cm ka$^{-1}$ (Nowaczyk et al., 2013), thus each 1 cm sample in this study interval integrates approximately 250 years.

Sediment samples were freeze-dried and homogenized prior to extraction. A total lipid extract (TLE) was obtained using a Dionex Accelerated Solvent Extractor (ASE 200) with a mixture of dichloromethane (DCM)/ methanol (MeOH) (9:1, v/v). The TLE from each sample was separated into apolar (9:1 DCM/hexane v/v) and polar (1:1

DCM/MeOH v/v) fractions using alumina oxide column chromatography. One half of each polar fraction was filtered through 0.45μm PTFE syringe filters using 99:1 hexane/isopropanol (v/v) and a $C_{46}$ GDGT internal standard was added to each polar fraction prior to analysis.

### 2.4.2 BrGDGT Analysis

Polar fractions were analyzed on an Agilent 1260 high performance liquid chromatograph (HPLC) coupled to an Agilent 6120 Quadrupole mass selective detector (MSD). Compound separation was achieved using two different methods, the original HPLC method developed by Hopmans et al. (2000) and Schouten et al. (2007), and subsequently a newer UHPLC method by Hopmans et al. (2016). Following the original method, GDGTs were separated on a 150 mm long, 2.1 mm diameter Prevail Cyano 3μm column. Compounds were eluted by 99:1 hexane: isopropanol for 7 minutes, then by a linear solvent gradient, ending with 1.8% isopropanol after an additional 32 minutes. Mass scanning was performed in selected ion monitoring (SIM) mode.

The newer method of Hopmans et al. (2016), which was published after most of the samples investigated here were analyzed, improves chromatography, allowing for separation of 5- and 6-methyl brGDGTs (De Jonge et al., 2013). The technique uses two Waters UHPLC columns in a series (150 mm × 2.1 mm × 1.7 μm) and isocratically elutes GDGTs using a mixture of hexane (solvent A) and hexane: isopropanol (9:1, v:v, solvent B) in the following sequence: 18% B (25 minutes), linear ramp to 35% B (25 minutes), linear increase to 100% B (30 minutes) (Hopmans et al., 2016). In this study, 113 samples were analyzed using the newer UHPLC method, while 273 samples were originally analyzed using the old method. Of these 273 samples, 62 were subsequently

run on the newer UHPLC method for comparison. Overall, no major differences were detected between the two methods as Pleistocene Lake El'gygytgyn samples contain relatively small amounts of the 6-Me brGDGTs. In total 107 samples were run in duplicate, and 21 samples in triplicate. Of these replicate samples, 64 were run in duplicate on the same method. For these samples MBT differences had a median value of 0.0 and a maximum difference of 0.05. GDGTs were quantified with respect to the $C_{46}$ standard, assuming equal ionization efficiency for all compounds.

### 2.4.3 *n*-Alkane Analysis

To analyze plant leaf waxes (*n*-alkanes), apolar fractions were injected on an Agilent 7890A dual gas chromatograph – flame ionization detector (FID) equipped with an Agilent 7693 autosampler and two 5% phenyl methyl siloxane Agilent HP-5 columns (60 m x 320 μm ID and 0.25 μm film). Helium was used as the carrier gas. The oven began at a temperature of 70 $^{o}$C, increased at 10 $^{o}$C min $^{-1}$ to 130 $^{o}$C, and again at 4 $^{o}$C min $^{-1}$ to 320 $^{o}$C, and then held for 10 minutes. *n*-Alkanes were quantified using an external calibration curve where squalane was injected at multiple concentrations ranging from 2 to 100 ng/μl, $r^2$ values for linearity tests were >0.99. The average chain length (ACL) is the weighted average of various chain lengths, usually defined as

$$ACL = \sum(C_n * n) / \sum(C_n),$$

where $C_n$ is the concentration of each *n*-alkane with *n* carbon atoms (Poynter and Eglinton, 1990). Here we incorporate carbon chain lengths of $C_{27\text{-}33}$ in the ACL calculation.

### 2.4.4 Time Series Analysis

To determine the spectral characteristics of our brGDGT and leaf wax ACL records, we used Mann and Lees (1996) robust red noise multi-taper-method (MTM) analysis in the Astrochron R program (Meyers, 2012), which has significant statistical power for identifying frequencies in the obliquity, precession, and eccentricity bands (Meyers, 2012, 2014). Time series analysis was carried out in both the depth and age domain in order to avoid circularity with assumptions made in age model development. However, the results demonstrate that power is not distorted away from significant frequencies when the age model is applied. Frequencies identified in time series in depth domain assume a time average sedimentation rate of 4.02 cm/ka derived by Nowaczyk et al., (2013) from tuning physical, sedimentological, geochemical, and pollen records to the benthic oxygen isotope stack (Lisiecki and Raymo, 2005).

## 2.5 Results and Discussion

In the following discussion, we compare our data with previously published records from Lake El'gygytgyn and global climate reconstructions. All data are plotted using the age model of Nowaczyk et al. (2013). MIS definitions are from Lisiecki and Raymo (2005) and sub-stage definitions are made following Railsback et al. (2015). We begin with a discussion of proxy interpretations and then examine the characteristics of each glacial and interglacial period. Finally, we explore global changes observed in our record and the MBE climatic transition.

### 2.5.1 BrGDGTs

Paleotemperature reconstructions are based on brGDGTs, which are membrane lipids presumably produced by the ubiquitous soil bacteria, Acidobacteria (Sinninghe Damsté et al., 2014; 2011; Weijers et al., 2006). brGDGTs are composed of glycerol bound, ether bonded alkyl chains that vary by the number of methyl branches (4-6) and cyclopentyl moieties (0-2) (Weijers et al., 2007). Weijers et al. (2007) developed a proxy for mean annual air temperature (MAAT) based on the distribution of brGDGTs, expressed by their degree of methylation (**M**ethylation Index of **B**ranched **T**etraethers; MBT) and cyclization (**C**yclization Index of **B**ranched **T**etraethers; CBT). In the initial calibration, CBT was negatively correlated to pH, while MBT was positively correlated with MAAT and to a lesser extent, negatively correlated to pH (Weijers et al., 2007). However, subsequent analysis of brGDGTs and improved chromatography has since shown that the apparent dependence of MBT on pH was an artifact of incomplete separation of 5- and 6-methyl brGDGT isomers (De Jonge et al., 2013).

Application of the improved chromatography method of Hopmans et al. (2016) has indicated 6-methyl brGDGT isomers may be abundant in environmental samples (De Jonge et al., 2014b). Failure to account for the presence of these isomers can have significant implications for the use of the MBT/CBT proxy (De Jonge et al., 2014a, 2014b, 2013). Here, we report brGDGT indices calculated from samples run on the original HPLC methods (Hopmans et al. 2000; Schouten et al. 2007) and the newer UHPLC method of Hopmans et al. (2016). The fractional abundances of the 6-methyl brGDGTs are relatively low throughout the study interval, with total 6-methyl compounds ranging from 2- 22% with an average of 9%, indicating results from the old

method are still robust. For samples run on both methods, the mean difference in MBT ratios was 0.02 and the maximum difference was 0.06. The relative amounts of the 6-methyl isomers expressed as the isomer ratios (e.g. De Jonge et al., 2014b) had relatively low averages of 0.11, 0.29, 0.04, 0.14, and 0.11 for compounds 1050', 1048', 1046', 1036', and 1034'. Interestingly, 1032' was not present in any samples.

Since initial MBT/CBT proxy development in 2007, brGDGTs have been utilized to reconstruct temperature and pH in a variety of environments and locations including Lake El'gygytgyn (D'Anjou et al., 2013; Holland et al., 2013; de Wet et al., 2016; Keisling et al., 2016). BrGDGTs were initially presumed to be produced in soils, and their presence in aquatic sediments to be a result of erosion (Hopmans et al., 2004). More recently, evidence for *in situ* production in lakes, rivers, and their sediments has been noted (e.g. Bechtel et al., 2010; Buckles et al., 2014; De Jonge et al., 2015; Loomis et al., 2014, 2012; Schoon et al., 2013; Tierney et al., 2010; Tierney and Russell, 2009; Weber et al., 2015; Zell et al., 2013; Zhu et al., 2011). There are several possible sources of brGDGTs at Lake El'gygytgyn, including watershed soils/permafrost, inflowing streams, aeolian inputs, and *in situ* production within the water column. Although modern samples were not available to directly determine the main source of brGDGTs, we can make some likely inferences, based on the physical characteristics of the lake. Lake El'gygytgyn drains a relatively small catchment and is surrounded by permafrost with a shallow (<0.5 m) active layer that contains brGDGTs (Bischoff et al., 2014). However, watershed soils and permafrost are unlikely to be the main source of brGDGTs in Lake El'gygytgyn sediments as a yearly snowmelt freshet is the main hydrological event and occurs when the ground is still frozen, thus limiting erosion (Nolan and Brigham-Grette, 2007). Spring

snowmelt fills fifty small streams that drain into Lake El'gygytgyn (Nolan and Brigham-Grette, 2007). Although brGDGTs have been found in many rivers (Herfort et al., 2006; Kim et al., 2007; van Dongen et al., 2008) and *in situ* production within rivers can occur (De Jonge et al., 2015) , it is unlikely these streams are a major source of the compounds at Lake El'gygytgyn as they are highly seasonal and many are only active during the brief snowmelt period (Nolan and Brigham-Grette, 2007). Additionally, aeolian inputs are unlikely to be a major source of brGDGTs as they comprise less than 2% of the Lake El'gygytgyn sediment flux (Fedorov et al., 2013). Soils, streams, and dust may all introduce small amounts of brGDGTs to Lake El'gygytgyn but we posit most accumulation in the lake sediments is due to autochthonous surface water production, as has been reported for other lakes (e.g. Blaga et al., 2008; Bechtel et al., 2010; Tierney et al., 2010; Loomis et al., 2014). Although production within the lake sediments themselves cannot be ruled out, much of the recent literature suggests that brGDGTs are produced within the upper water column (Buckles et al., 2014; Loomis et al., 2014). Furthermore, the bottom water temperature of Lake El'gygytgyn remains at ~4 °C throughout the year (Nolan and Brigham-Grette, 2007), and given the size and depth of the lake, this is unlikely change significantly, even across glacial- interglacial cycles yet our temperature reconstructions indicate significant variability. Thus, we surmise that brGDGTs are likely produced in the surface waters of Lake El'gygytgyn.

Many biological based temperature proxies exhibit a seasonal growth bias. We also assume that brGDGTs likely represent a summer temperature at Lake El'gygytgyn. Currently, Lake El'gygytgyn is only ice free for ~ 2 months (July and August), thus restricting most primary productivity to these times (Nolan and Brigham-Grette, 2007). A

seasonal bias has been noted in brGDGT distributions in modern lakes from mid- to high-latitudes (Pearson et al., 2011; Shanahan et al., 2013b; Sun et al., 2011). Shanahan et al. (2013) suggest that a summer temperature bias in Arctic lakes is due to increased productivity and conductivity due to favorable conditions including higher temperatures, increased light availability, and reduced ice cover. Indeed, the great majority of primary productivity at Lake El'gygytgyn occurs during the short summer ice-free period (Nolan and Brigham-Grette, 2007).

A number of lacustrine brGDGT calibrations to temperature and pH were developed following strong evidence for *in situ* production (e.g. Tierney and Russell, 2009; Tierney et al., 2010; Pearson et al., 2011; Sun et al., 2011; Loomis et al., 2012; Buckles et al., 2014; Loomis et al., 2014). However, many of these calibrations are geographically restricted (e.g. Tierney et al., 2010; Foster et al., 2016) or based on small sample sets (e.g. Zink et al., 2010; Foster et al., 2016). For this study, we apply the lake calibration of Sun et al. (2011). This calibration is the only one incorporating Eurasian lakes, making it the closest geographically available for Lake El'gygytgyn. It also yields values in general agreement with pollen based summer temperature reconstructions for Lake El'gygytgyn from Melles et al. (2012) and yields absolute temperatures in the middle of the range when applying all available lacustrine calibrations. Relationships between MBT/CBT, temperature, and pH vary widely between calibrations and produce a large range of reconstructed temperatures. Regardless, similar patterns of temperature variability (i.e., warming and cooling trends) are recorded. It should also be noted that although the reproducibility of the data is excellent, with an analytical error of <<1 $^{o}$C, the Sun et al. (2011) calibration has an uncertainty of +/- 5.24 $^{o}$C. Therefore, caution

should be taken before interpreting MBT/CBT reconstructions as absolute temperatures although trends are meaningful. We stress that without a site- specific calibration, or direct investigations of local brGDGT sources, reconstructing absolute temperature is not possible. However, our data reveals strong glacial-interglacial temperature variability in agreement with global climate records (Figure 2.2), supporting use of MBT/CBT as a proxy to examine relative temperature variability, and revealing new insights into Arctic paleoclimate.

### 2.5.2 Plant Leaf Waxes

Plant leaf waxes (*n*-alkanes) are useful indicators of environmental change. They are widespread in lacustrine sediments and can be derived from autochthonous and allochthonous sources (Didyk et al., 1978; Eglinton and Hamilton, 1967). Principally, the sources of *n*-alkanes in lake sediments are algae, aquatic macrophytes, and vascular plants that reside around the lake. Short chain *n*-alkanes ($C_{15}$-$C_{21}$) are attributed to algae and photosynthetic bacteria (Cranwell et al., 1987; Meyers, 2003), whereas submerged and emergent aquatic plants are the main producers of mid-chain ($C_{21}$, $C_{23}$, and $C_{25}$) *n*-alkanes (Ficken et al., 2000). Moreover, long-chain compounds ($C_{27}$- $C_{33}$) are characteristic of higher terrestrial plants (Cranwell et al., 1987; Eglinton and Hamilton, 1967). Although shorter chain lengths are present in our samples, the dominant chain length in this record ranges from 27-29 carbon atoms with a mean long chain ($C_{27}$-$C_{33}$) ACL value of 29.4. Leaf waxes in Lake El'gygytgyn sediments are likely predominantly sourced from higher terrestrial plants in the catchment (Holland et al., 2013; Wilkie et al., 2013). Here, we use the distribution of $C_{27}$ to $C_{33}$ *n*-alkanes to assess climatically driven vegetation changes.

The *n*-alkane average chain length (ACL) can be used to assess aridity and temperature changes (Bush and McInerney, 2015). Plants stressed by high temperature or arid conditions synthesize longer chain lengths to enhance their epicuticular waxes and minimize water loss (Shepherd and Wynne Griffiths, 2006). However, evidence for a correlation between temperature, aridity, and ACL is mixed, and the predominant driver of ACL seems to vary regionally (Bush and McInerney, 2015). In some locations, high ACL values are associated with higher temperatures (e.g., Castañeda et al., 2009; Bush and McInerney, 2015) while in others, including the Arctic, arid conditions are associated with higher ACL values (e.g. Andersson et al., 2011). At Lake El'gygytgyn, changes in ACL have been found to correlate most strongly with aridity during the Plio-Pleistocene transition but also to some extent with temperature and vegetation shifts (Keisling et al., 2016). Changes in the *n*-alkane distribution throughout this record therefore likely suggests a response to temperature or moisture variability either by individual plants (e.g. Bush and McInerney, 2015) or a systematic change in the distribution of vegetation in the catchment. Analysis of pollen assemblages indicates major shifts in the vegetation of Lake El'gygytgyn's catchment across glacial-interglacial cycles (Lozhkin et al., 2007a; Lozhkin and Anderson, 2013; Melles et al., 2012). These studies show that trees and shrubs dominate the catchment during interglacials while shrubs and herbaceous taxa dominate under glacial conditions. Climatically driven changes in dominant taxa likely shifted distributions of leaf waxes, influencing ACL values. We posit that the Lake El'gygytgyn ACL record represents landscape scale vegetation changes driven by climate, and likely mainly associated with precipitation variability.

ACL values clearly display glacial-interglacial cyclicity and resemble the global benthic oxygen isotope stack (Lisiecki and Raymo 2005) (Figure 2.2). Higher ACL values (29-30) occur during glacial periods, while lower values (28-28.5) are associated with interglacials (Figure 2.2). MBT/CBT temperatures and ACL values record different patterns throughout the study interval and are not statistically correlated ($R^2$=0.0038; p=0.265), further suggesting ACL may be responding to a different climatic parameter. Temperature cannot be entirely ruled out based on the insignificance of the correlation but if it were the main control on ACL at Lake El'gygytgyn, then higher ACL values would be expected when it was warmer contrary to what is noted here (Figure 2.2). Annual precipitation estimates based on pollen indicate elevated precipitation during interglacials (Melles et al., 2012). Furthermore, a study of clay mineralogy, sediment hue and sediment geochemistry also indicates wetter conditions at Lake El'gygytgyn during stages 11 and 9 (Wei et al., 2014). Therefore, we suggest that ACL variability at Lake El'gygytgyn during the Pleistocene is mainly driven by variations in precipitation but recognize that interpreting this record as solely an aridity record is likely an oversimplification.

### 2.5.3 Main Features of the Entire Record

In the following sections, we closely examine individual glacial and interglacial periods. To ease comparison, we report MBT/CBT temperatures as deviations from the mean value of the entire record (10.8 $^{o}$C), when applying the Sun et al. (2011) calibration. We emphasize that the temperatures and amplitudes of change reported here are calibration dependent, and absolute temperatures should be interpreted with caution. Additionally, we caution against direct interpretation of ACL as a precipitation proxy due

to the potential for numerous factors controlling vegetation type, as discussed above, although we believe this record is largely responding to changes in aridity. For each of the subdivided glacial-interglacial intervals we compare our biomarker reconstructions to other previously published proxy data from Lake El'gygytgyn. These include the percent biogenic silica as a proxy for diatom productivity (Meyer-Jacob et al., 2014) ranging from ~10 during glacials to a maximum of 56% during interglacials, and the percent tree and shrub pollen as a proxy for catchment vegetation cover, which ranges from values of 1-18% during glacials and ~30-90% during interglacials (Lozhkin et al., 2017, 2007a, 2007b; Lozhkin and Anderson, 2013).

The brGDGT temperature and plant leaf wax *n*-alkane records from Lake El'gygytgyn show significant glacial-interglacial variability throughout the study interval (Figure 2.2, 2.3, and 2.4). The warmest interglacial periods are MIS 7c, 9, and 17 while the coldest glacials are MIS 10 and 12 (Fig 2.2, 2.3, and 2.4). The wettest (low ACL) interglacials are 9, 17, and 11 and likely driest (high ACL) glacials are 12 and 18 (Figure 2, 3, and 4). Although the proxies were measured on the same samples, they do not vary synchronously, suggesting they respond to different climatic parameters. When we compare our new proxy records to other global and Lake El'gygytgyn proxy data, we observe that the relative intensity of glacial and interglacial periods is proxy dependent (Figure 2.3 and 2.4). Although there are overall trends in intensity (e.g. MIS 11 is relatively strong, while MIS 15e is relatively weak) there is significant variability in proxy response (Figure 2.3 and 2.4). Indeed, even three proxies for primary productivity (biogenic silica, Si/Ti ratio, and diatom abundance) record different relative intensities of interglacials and glacials (Figure 2.3 and 2.4). The timing of glacial-interglacial changes

also varies by proxy, providing insight into climate dynamics and the associated environmental responses.

#### 2.5.3.1 MIS 19-17 (800 to 676 ka)

Climate variability during MIS 19-17 is moderate in many globally distributed records with relatively mild interglacial and glacial conditions (Lang and Wolff, 2011; Past Interglacials Working Group of PAGES, 2016). At Lake El'gygytgyn, MIS 19-17 is marked by highly variable temperature fluctuations, with MBT/CBT temperatures ranging from 8$^{o}$C above to 6$^{o}$C below the mean (Figure 2.5). Interestingly, MIS 19 is relatively cool for an interglacial at this site, at 4-6 $^{o}$C above the mean, whereas relatively high temperatures occur during MIS 18. During MIS 17c temperatures are ~8 $^{o}$C higher than the record mean, making it the third warmest interglacial in our record (Figure 2.3). Temperature variations do not clearly track glacial-interglacial fluctuations throughout this interval but instead seem strongly driven by local precession forcing (Figure 2.5). In contrast to the brGDGT record, the ACL record indicates strong glacial- interglacial fluctuations throughout this interval (Figure 2.5). During MIS 19 values are low suggesting a vegetation response to interglacial conditions and subsequent fluctuations in ACL correspond to glacial substages 18a-e. Afterwards, ACL values fall during MIS 17 indicating the return of interglacial conditions.

We note both similarities and differences between our biomarker records and other Lake El'gygytgyn proxy data. MIS 19 is extremely weak in the pollen data with <40% tree and shrub pollen present in the sediments (Lozhkin et al., 2016) (Figure 2.3 and 2.5). Comparable pollen percentages occur during MIS 18b-d (Figure 2.4 and 2.5), suggesting relatively warm and wet conditions during this glacial period. The MIS 17

pollen record indicates trees and shrubs were abundant with percentages <70%, although values are not as high as other more recent interglacials occurring (Lozhkin et al. 2016) (Figure 2.3 and 2.5). Biogenic silica percentages indicate similar patterns, with higher values occurring during MIS 17a and little change associated with MIS 19 (Figure 2.3 and 2.5). Overall, the Lake El'gygytgyn proxy records generally agree that here MIS 19 is a relatively weak interglacial, MIS 18 is a warm and wet glacial, and MIS 17 is a warm interglacial (Figure 2.3, 2.4, and 2.5). However, differences in timing and intensity of glacial-interglacial changes is apparent when comparing the records (Fig 2.5).

#### 2.5.3.2 MIS 16-13 (621 to 478 ka)

MIS 16 stands out as a particularly strong glacial period in marine isotopic records (Lisiecki and Raymo, 2005) with low atmospheric $CO_2$ concentrations (Lüthi et al., 2008) while MIS 15 is generally regarded as a relatively weak interglacial (Lang and Wolff, 2011; Past Interglacials Working Group of PAGES, 2016). Both MIS 15 and the subsequent weak interglacial MIS 13, show a complex structure in many records with two peaks of comparable magnitude separated by a cooler interval (Lang and Wolff, 2011; Past Interglacials Working Group of PAGES, 2016). Moreover, the entire interval of MIS 15-13 has low amplitude variability in a range of records, with MIS 14 occurring as a very weak glacial (Lang and Wolff, 2011). Indeed, it is sufficiently weak that its designation as a glacial has been brought into question (Lang and Wolff, 2011) and recently the entire interval of MIS 15-13 has been proposed to be an extended interglacial period with warm, humid conditions noted on the Chinese Loess Plateau (Hao et al., 2015). Indeed, at Lake El'gygytgyn, it appears that warm conditions with muted vegetation variability prevailed from MIS 16 -13 (Figure 2.3, 2.4, and 2.6).

Warm conditions are recorded in MBT/CBT temperatures during MIS 15 (Figure 2.6). This warmth is outstanding and contrasts with most records compiled in interglacial comparison studies (e.g. Lang and Wolff, 2011; Past Interglacials Working Group of PAGES, 2016). In the MBT/CBT temperature record, substage 15a is notable with temperatures reaching ~6 ºC above the mean, while stage 15e does not stand out (Figure 2.6). ACL values during MIS 15 are the highest observed in any interglacial in our study, suggesting relatively arid conditions, and show a decreasing trend throughout the interval (Figure 2.3 and 2.6).

Anomalously warm conditions are also reconstructed during MIS 13 (Figure 2.6). Although there are significant fluctuations, maximum temperatures associated with substage 13a are up to 8 ºC higher than the mean, and much of the interglacial is 4 ºC above the mean (Figure 2.6). Substage 13c does not stand out as strongly as 13a, with reconstructed temperatures of 2 ºC above the mean (Figure 2.6). The outstanding warmth of substage 13a at Lake El'gygytgyn is unusual, as many records indicate MIS 13 was a relatively weak interglacial (Lang and Wolff, 2011; Past Interglacials Working Group of PAGES, 2016). A significant cooling excursion between 491 and 484 ka is present (Figure 2.6), interrupting the warm conditions. This fluctuation suggests a strong and brief stadial occurred with much lower temperatures. In the ACL record, substages 13a and c are present although values decrease throughout the interglacial, perhaps suggesting a continual change in plant communities associated with progressively wetter conditions (Figure 2.6).

Glacial periods MIS 14 and 16 also display similar characteristics. During MIS 16, temperatures fluctuate +/- 4 ºC around the mean without a discernable pattern (Figure

2.6). During MIS 14, reconstructed temperatures are moderate, with an average close to the record mean. Changes in ACL are minimal during MIS 16, although some lower amplitude cyclicity is present during this interval, perhaps related to local insolation changes associated with precession. The shift to higher ACL values associated with glacial periods is also reduced during MIS 14 (Figure 2.6).

Other proxy data from Lake El'gygytgyn show shifts in vegetation and primary productivity associated with the warmth and muted precipitation as suggested by the biomarker records. Pollen assemblage analysis indicates alternation between tree and shrub and herbaceous dominated taxa associated with interglacials and glacials respectively (Lozhkin et al., 2016). As in the temperature reconstructions, substage 15a stands out strongly with >80% trees and shrubs, while stages c-e are less pronounced (Lozhkin et al., 2016). Pollen percentages increase throughout MIS 13 reaching up to 77% tree and shrub pollen during MIS13a (Figure 3), while 13c has much lower amounts (Figure 2.6) thus corroborating vegetation change recorded by the continually decreasing ACL values. The pollen data indicate MIS 16 is slightly colder than MIS 14, with decreased trees and shrubs and increased herbaceous taxa (Lozhkin et al. 2016) but neither period is as severe as other glacials in the last 800 ka (Lozhkin et al., 2007b, 2007a) (Figure 2.4). Thus, the relatively high summer temperatures and higher precipitation during these glacials likely allowed more trees and shrubs to remain on the landscape. Percentages of biogenic silica in Lake El'gygytgyn sediments are relatively low throughout this interval, ranging from 8-20% (Meyer-Jacob et al., 2014) (Figure 2.3, 2.4, and 2.6). Peaks associated with MIS 15a and 15e are present, but weak, while MIS 13 does not stand out at all. Total diatom counts are also low throughout this interval,

suggesting diatom productivity was minimal (Snyder et al., 2013) (Figure 2.3, 2.4, and 2.6).

#### 2.5.3.3 MIS 12 and 11 (478 to 375 ka)

MIS 12 is recognized as a strong glacial period in marine and terrestrial records (Lang and Wolff, 2011), followed by MIS 11, which is recognized at numerous locations as a strong and exceptionally long (~30 ka) interglacial (Lang and Wolff, 2011; Loutre and Berger, 2003; Lüthi et al., 2008). MIS 11 is paradoxical given its weak astronomical forcing and relatively moderate atmospheric $CO_2$ concentrations (Yin and Berger, 2010). The length and warmth of "super interglacial" MIS 11 and the severity of MIS 12 have been noted in regional and globally distributed records including marine sediment cores from the North Atlantic (Lawrence et al., 2009; Voelker et al., 2010), the Bering Sea (Caissie et al. 2016), the Arctic Ocean (Cronin et al., 2014; Marzen et al., 2016), from the terrestrial Arctic including Lakes Baikal (Prokopenko et al., 2010) and El'gygytgyn (Melles et al., 2012), and Antarctic ice core records (Lüthi et al., 2008). At Lake El'gygytgyn, MIS 11 was labeled a "super interglacial" because of strong responses in certain proxies including outstandingly high silica/titanium and biogenic silica values and warm summer temperatures (15 $^{o}$C) and elevated annual precipitation (800 mm/yr) estimates from pollen (Melles et al., 2012) although it does not appear as strong in the organic proxies examined here (Figs 2.2, 2.3, and 2.7).

Many records including marine, ice core, and terrestrial archives indicate Stage 12 was the strongest glacial of the past 800 ka (Lang and Wolff, 2011). Interestingly, the Lake El'gygytgyn temperature record does not indicate a similar severity. Although MIS 12 is the second coldest glacial in our study interval (Figure 2.4),

it does not appear to have the intensity observed in other global records (Figure 2.2 and 2.7). BrGDGT based temperature reconstructions are highly variable, with a range of 15 $^{o}$C, but overall they suggest relatively mild conditions similar to the record mean (Figure 2.7). Throughout the whole record, brGDGT temperatures and local summer insolation seem to covary. Relatively moderate insolation forcing at 67 $^{o}$N (460-500) during Stage 12 (Figure 2.2), may have led to the mild temperatures reconstructed here. Mild conditions have also been noted at Lake Baikal during MIS 12 (Prokopenko et al., 2006, 2001) suggesting a warm continental pattern for Eurasia during this glacial.

Despite relatively high temperatures, the terrestrial Arctic may have been arid for much of MIS 12. ACL values are the highest of any glacial (Figure 2.4), with values close to 30 observed throughout most of the period. There is a short deviation from 437-432 ka when values drop to 28.8, before returning to 29.9 prior to the termination (Figure 2.7). Pollen assemblages indicate terrestrial vegetation was dominated by tundra shrubs and herbs throughout MIS 12 (Lozhkin and Anderson, 2013) and does not record a shift at 437-432ka. Perhaps this excursion was too short to produce a major change in dominant plant taxa at Lake El'gygytgyn but the drop in ACL values may be associated with a response of individual plants to a brief interval of wetter conditions. Analysis of sediment hue and mineralogy has suggested MIS 12 was generally dry at Lake El'gygytgyn, but some wet periods also occurred (Wei et al., 2014). A shift in sediment facies is observed at 434 ka (Melles et al., 2012), which may reflect increased precipitation prior to the glacial termination. At the termination, ACL values decrease and vegetation shifts abruptly to tree and shrub dominated taxa at the beginning of MIS 11 (Lozhkin and Anderson, 2013).

MIS 11 was particularly warm in the Northern Hemisphere high latitudes. Planktic foraminifera assemblages suggest summer sea surface temperatures (SSTs) in the Arctic Ocean may have been 8-10 ºC warmer than present (Cronin et al., 2014). The Bering Strait was flooded, and the Bering Sea was highly productive, although SSTs were seemingly not as warm as the Arctic Ocean (Caissie et al., 2016). Continental temperatures were also warm with pollen estimates suggesting summer air temperatures at Lake Baikal were 2 ºC higher (Prokopenko et al., 2010) and 4 ºC higher than present at Lake El'gygytgyn (Lozhkin and Anderson, 2013). MBT/CBT temperature reconstructions from this study indicate higher than average conditions during MIS 11, suggesting this stage was significantly warmer than present summer temperatures (Figure 2.7).

The extended interglacial warmth significantly altered terrestrial vegetation and ecosystem productivity in the high latitudes. High concentrations of aquatic biomarkers (D'Anjou et al., 2013), high silica/titanium ratios (Melles et al., 2012), and high biogenic silica percentages (Meyer-Jacob et al., 2014) in Lake El'gygytgyn sediments indicate enhanced primary production throughout the interglacial (Figure 2.3 and 2.7). Exceptionally abundant and diverse diatoms are observed in Lake El'gygytgyn sediments at this time (Snyder et al., 2013) (Figure 2.3 and 2.7). Biogenic silica and diatom counts from Lake Baikal sediments also suggest significantly higher productivity (Prokopenko et al., 2010) (Figure 2.2). Substantial spruce pollen is evident in MIS 11 sediments (Melles et al., 2012) suggesting forests around or near the lake, and this proxy is supported by increased concentrations of arborinol (D'Anjou et al., 2013a), a biomarker for trees (Jacob et al., 2005). Pollen reconstructions from the North Atlantic suggest a boreal forest

may have extended across much of southern Greenland (Vernal and Hillaire-Marcel, 2008).

In many MIS 11 paleoclimate records display a pattern of gradually increasing values that reach a maximum late in the interglacial (~400 ka) (Past Interglacials Working Group of PAGES, 2016) (Figure 2.2). Previous work at Lake El'gygytygn suggests a similar pattern. Pollen data indicate mean summer temperature peaked at 415 ka (~ 15 ºC) with relatively warm conditions maintained between 420 ka- 395 ka (Melles et al., 2012) mean summer temperature ranging from 10-15 ºC (Vogel et al., 2013) (Figure 2.7). Conversely, MBT/CBT reconstructed temperatures reach maximum values early in the interglacial during MIS 11e at ~424 ka, with temperatures transitioning quickly from 1 °C below average at the end of MIS 12 to temperatures of 7 ºC above average at ~425 ka (Figure 7). This warmth is not sustained throughout the interglacial but instead immediately begins to decrease, reaching below average values at 413 ka before subsequently increasing again to 4 ºC above average at 398 ka before finally cooling to 7 ºC below average at the end of the interglacial (Figure 2.7). Vogel et al. (2013) suggest a similar abrupt warming from 425- 424 ka and a brief cooling between 424 and 420 ka recorded in pollen data, corresponding to the abrupt drop in MBT/CBT temperatures. However, the pollen temperature estimates rebound and remain at ~15 ºC for the next 20 ka (Figure 2.7) while total tree and shrub pollen also suggest a long interglacial with sustained warmth (Vogel et al., 2013) (Figure 2.7). We note that percent deciduous pollen displays the same pattern as the brGDGT temperatures, suggesting that deciduous taxa were sensitive to the changing summer conditions. Interestingly, an early interglacial peak with subsequent abrupt decline is also noted in Bering Sea diatom

productivity (Caissie et al., 2016) (Figure 2.7) suggesting this early warming may have been a regional climatic pattern related to insolation forcing.

Significant changes in precipitation are also recorded at Lake El'gygytgyn during MIS 11. Pollen based precipitation reconstructions indicate annual precipitation averaged 700 mm/yr, approximately 4 times that of Holocene values (Melles et al., 2012) (Figure 2.7). Increased precipitation across MIS 11 is also evident in work by Wei et al. (2014) with sediment hue (iron oxide staining) indicating wetter conditions. In this record *n*-alkane ACL, interpreted as reflecting catchment vegetation changes largely due to precipitation variability, strongly resembles the pollen based precipitation record of Melles et al. (2012) (Figure 2.7). Both records display a more gradual change after the glacial termination of MIS 12 with peak values sustained throughout much of the interglacial. Low ACL values are maintained from 424 ka to 401ka corresponding to the extremely wet conditions (700 mm/year) (Melles et al., 2012) recorded by the pollen (Figure 2.7). The most humid period recorded in Lake Baikal sediments is from 420 to 405 ka when annual precipitation was around 500 mm/yr (Prokopenko et al., 2010), similar to the pattern observed in the Lake El'gygytgyn records.

#### 2.5.3.4 MIS 10-7 (374 to 200 ka)

##### 2.5.3.4.1 MIS 10

MIS 10 at Lake El'gygytgyn displays anomalous behavior for a glacial interval. Although initiating with low temperatures, around 7 $^{o}$C below average, subsequently temperatures rapidly rise to 6 $^{o}$C above average before slowly declining and oscillating around the record mean for the remainder of the period (Figure 2.8). ACL

values fluctuate throughout MIS 10 suggesting plant taxa may have been responding to significant moisture variability at Lake El'gygytgyn (Figure 2.8). The relatively warm and wet conditions of MIS 10 may also have led to anomalous environmental and ecosystem changes at Lake El'gygytgyn. D'Anjou et al. (2013) found MIS 10 had elevated terrestrial plant n-alkane inputs and higher concentrations of arborinol than either MIS 8 or 12. Significant aquatic production may have also occurred as concentrations of algal lipids, aquatic productivity biomarkers, are also elevated (D'Anjou et al., 2013a).

#### 2.5.3.4.2 MIS 9

MIS 9 is the 4$^{th}$ strongest interglacial of the past 800 ka in the global benthic oxygen isotope stack (Lisiecki and Raymo, 2005; Past Interglacials Working Group of PAGES, 2016). Sea water $\delta^{18}O$ suggests MIS 9 has the second lowest (after MIS 11) global ice volume (Elderfield et al., 2012) but this has yet to be confirmed by other studies (Past Interglacials Working Group of PAGES, 2016). MIS 9 has the highest atmospheric $CO_2$ and methane concentrations of any interglacial of the past 800 ka, with a peak value of 300 ppm $CO_2$ and 800 ppb $CH_4$ (Lüthi et al., 2008) (Figure 3). Although MIS 9 is recorded as the warmest interglacial in several marine records and in Antarctica, the warmth was brief as the period has an exceptionally short peak (Lang and Wolff, 2011; Past Interglacials Working Group of PAGES, 2016).

At Lake El'gygytgyn, the MBT/CBT temperature record is variable within MIS 9. Early in this interglacial, temperatures are cool, ranging from 6 $^{o}$C below to 4 $^{o}$C above average (Figure 2.8). But intense warming to 10 $^{o}$C above average occurs at 308 ka, substage 9e, after which temperatures start to decline (Figure 2.8). Stages 9d and c are

represented as a shoulder along the decreasing trend, with temperatures fluctuating between around 5 $^{o}$C above the record mean (Figure 2.8). Stage 9b is present as significant cooling before temperatures rebound again during 9a (Figure 2.8). ACL values are out of phase with the temperature record. Lower values are recorded earlier in the interglacial (334 to 318 ka) and higher values occur later (316 to 300 ka), suggesting MIS 9 may have transitioned from relatively cool and wet to warmer but drier conditions (Figure 2.8). Lake El'gygytgyn super interglacial sediment Facies C is present during MIS 9, indicating intervals of warmth strong enough to increase surface water productivity, and wet conditions also likely occurred (Melles et al., 2012; Wei et al., 2014).

The warmth and moisture in MIS 9 created environmental conditions favorable for primary producers. The preservation of organic biomarkers D'Anjou et al. (2013) suggest enhanced primary productivity at this time based on biomarkers in Lake El'gygytgyn sediments , which is corroborated by elevated biogenic silica percentages (Meyer-Jacob et al., 2014) (Figure 2.3 and 2.8). The terrestrial landscape was also impacted, as pollen counts indicate a significant increase in trees and shrubs (Lozhkin et al., 2007a, 2007b)(Figure 2.3 and 2.8) and arborinol concentrations are high (D'Anjou et al., 2013a) both indicating vegetation growth associated with warmer temperatures.

#### 2.5.3.4.3 MIS 8

At many globally distributed sites, MIS 8 is recorded as a weak glacial (Lang and Wolff, 2011). Our Lake El'gygytgyn records suggest MIS 8 was relatively warm and had significant moisture fluctuations (Fig 2.4 and 2.8). MBT/CBT temperatures average 1 $^{o}$C below the record mean throughout the glacial period (Figure

2.8). The n-alkane ACL exhibits a large change from low to high values (Figure 2.8) suggesting vegetation fluctuations throughout the glacial. A wet interval has also been noted in the Lake El'gygytgyn sedimentological hue record at this time (Wei et al. 2014).

#### 2.5.3.4.4 MIS 7

MIS 7 is an unusual interglacial with a complex structure. Three peaks vary in intensity across different records (Lang and Wolff, 2011). At many sites, MIS 7 is characterized by the highest values being reached early in the interglacial (Stage 7e) after which climatic parameters slowly decline (Tzedakis et al., 2012b, 2012a). However, some records indicate peak temperatures were reached later in the interglacial (Stage 7c) and may have extended to 7a while others show near glacial conditions occurring between the warmer interglacial substages (Lang and Wolff, 2011). Regardless of when peak warmth was regionally achieved, MIS 7 is generally a relatively weak interglacial, comparable in strength to interglacials prior to 450 ka (PAGES, 2016). Lower temperatures are observed in many globally distributed marine and terrestrial records (Lang and Wolff, 2011; Past Interglacials Working Group of PAGES, 2016) and $CO_2$ forcing was moderate (Augustin et al., 2004) (Figure 2.3).

Although our Lake El'gygytgyn record does not span the entirety of MIS 7, much of the complex structure observed in other records is reproduced here (Figure 2.8). After the termination of MIS 8, temperatures rise 5 $^{o}$C above average during 7e at ~244 ka. Temperature then decreases through substage 7d before rising again and maximizing at 11 $^{o}$C above average at 216 ka during stage 7c. After this abrupt peak, temperatures drop significantly. Interestingly, at Lake El'gygytgyn, we observe the warmest temperatures of this 600 ka record during MIS 7 (Figure 2 and 3). This is contradictory to the general

patterns discussed above. Strong, in phase precession and obliquity forcing during 7c is likely responsible for the extreme warmth recorded at Lake El'gygytgyn. MIS 7 in the Lake Baikal biogenic silica record is a relatively low compared to other interglacials, although several peaks (MIS 7 a-e) are associated with precession (Prokopenko et al., 2006). The higher latitude location of Lake El'gygytgyn may have led to more significant insolation forcing, creating the exceptionally warm temperatures observed in the brGDGT temperatures.

Although MIS 7 is not considered to be among the super interglacials as identified by Melles et al. (2012), the interval represents a period that may have been dominated by strong interhemispheric teleconnections. Ice sheet modeling suggests the West Antarctic Ice Sheet (WAIS) may have collapsed (Pollard and DeConto, 2009) in MIS 7, signaling significant warming in the southern hemisphere high latitudes. However, proxy records of WAIS collapse are currently lacking due to unconformities in the ANDRILL record (Naish et al., 2009), and further investigation is required.

The ACL record from Lake El'gygytgyn indicates vegetation shifts associated with substages 7c-e (Figure 2.8). The pollen data also indicate variations in trees and shrubs, although the total percentages are generally low (Figure 2.3 and 2.8). Primary productivity is also relatively limited throughout the interglacial (Figure 2.3 and 2.8). The insolation driven peak in temperature may have been too short-lived to promote major vegetation growth or increased primary production during MIS 7. The low biogenic silica percentages during warm MIS 7, but high percentages during more moderate interglacials such as MIS 11 (Fig 2.3), suggest paleoproductivity likely responds to other climatic variables in addition to temperature. Therefore, previous interpretations that biogenic

silica provides a temperature indicator (e.g. Melles et al., 2012; Meyer-Jacob et al., 2014) should be interpreted with caution.

#### 2.5.3.5 Orbital Forcing of Biomarker Records

MBT/CBT temperatures and ACL values reveal strong glacial- interglacial variability across the study interval of 800-200 ka (Figure 2.2). Generally higher temperatures are present during interglacials and lower temperatures are present during glacials but higher frequency variations predominate (Figure 2.2 and 2.3). When analyzed according to both depth and age, significant spectral peaks that satisfy 85% confidence level (Meyers, 2012) are identified in the brGDGT record (Fig 2.9 and Table 2.1). These frequencies are consistent with eccentricity E2 (121.18 k.y.), E3 (97.56 k.y.), and precession P1 (23.60 k.y.) and P3 (18.98 k.y.) identified in MTM analysis of eccentricity-tilt-obliquity (ETP) following the Laskar et al., (2011) solution. Thus, spectral analysis demonstrates the significant precession component to the brGDGT data that is consistent with dominate role of precession influencing summer insolation intensity at 67°N (Figure 2.2 and 2.3). Frequencies identified in the leaf wax ACL record are consistent with the three dominate components of obliquity (O1-O3) (Figure 2.9 and Table 2.1). Notably, when the age model is applied to the ACL record there is a slight redistribution of power toward the eccentricity (E3) band (Figure 2.9 and Table 2.1). Significant variability surrounding the obliquity frequency implies changes in ACL correspond to an amplification of the seasonal cycle and 100-k.y. changes in ice volume, which is also visually obvious (Figure 2.2). Thus, the brGDGT and *n*-alkane records reflect glacial-interglacial variability, but importantly do not change synchronously, suggesting the proxies are responding to different components of the climate system.

The obliquity driven frequency observed in the ACL record infers vegetation mainly responded to variables other than summer temperature. Notably, cooling and ice volume growth via ice-driven feedbacks in response to changes in mean annual insolation are primarily driven by obliquity (Martin et al., 1987; Ruddiman, 2014). Given the close association between ice-volume and aridity, we posit that precipitation induced changes in vegetation are mainly driving the ACL shifts. Thus, increased aridity in Beringia associated with cooling, ice accumulation, and changes in sea level, causing emergence of the vast Bering Land Bridge, could manifest the 41 k.y. frequency we observe. The strong response to obliquity recorded in the ACL record may also be associated with plant response to seasonality changes. Variations in obliquity amplify or reduce summer and winter seasonality, which would potentially significantly impact plant growth and drive terrestrial vegetation turnover.

The region of Beringia is particularly sensitive to changes in global sea level. The Bering Strait has a present depth of ~50 m. Today, relatively fresh North Pacific water flows through the strait at a rate of approximately 0.8 Sverdrups (Woodgate and Aagaard, 2005). This northward flux of water has significant regional and global impacts and affects Chukchi Sea and Arctic Ocean hydrography as well as the Atlantic Meridional Overturning Circulation (Woodgate and Aagaard, 2005). Pleistocene ice volume changes effectively opened and closed the Bering Land bridge, assuming little influence from dynamic topography or glacial isostatic influences (Clark et al., 2014; Milne and Mitrovica, 2008). This opening and closing, or reduction of flow, has significant impacts on global ocean circulation and climate (Hu et al., 2010; Knudson and Ravelo, 2015) as well as regional climatology (Bartlein et al., 2015). Trends in plant leaf wax ACL

throughout the Lake El'gygytgyn record show a marked resemblance to global sea level changes (manifested by ice volume growth) (Rohling et al., 2014) (Figure 2.2). We suggest changes in continental ice volume, likely created shifts in precipitation and humidity at Lake El'gygytgyn and local vegetation changes in response to these conditions are manifested in the ACL variations.

### 2.5.4 The MBE and Arctic Climate

Statistical analysis of bulk geochemical data (Melles et al., 2012) and organic biomarker proxy data presented here was performed to test for the presence of an MBE signal at Lake El'gygytgyn. Data spanning the interval of 0- 800 ka (and 200-800 ka for the organic biomarker data) was divided into pre- MBE (800-430 ka) and post-MBE (429- 0 ka) intervals and a two-sample Student's t-test ($p < 0.05$) was applied. Climatic parameters from Lake El'gygytgyn exhibited statistically significant differences between the pre- and post- MBE data sets at the 95% confidence level (Figure 2.10), suggesting the terrestrial western Arctic experienced a climatic shift and environmental changes associated with the MBE.

Although the pre- and post-MBE data are significantly different, the change associated with this transition is not consistent among the examined proxy records. However, most parameters exhibit a change in the mean as well as an increase in amplitude of values, similar to the patterns recorded in the global benthic oxygen isotope stack (Lisiecki and Raymo, 2005) and the EPICA Dome C $CO_2$ record (Lüthi et al., 2008) (Figure 2.10A and B). We note that despite both the highest and lowest MBT/CBT reconstructed temperatures occurring in the post- MBE interval (Figure 2.2), they are not within in the $5^{th}$ and $95^{th}$ percentile outliers shown in the boxplots (Figure 2.10C).

Overall, MBT/CBT temperatures indicate a negative shift in the mean and median value and instead of a general warming associated with post MBE interglacials, the temperature reconstructions indicate an overall cooling trend (Figure 2.10C). Although intensely warm "super interglacials" are indicated in some Lake El'gygytgyn proxy records, generally the MBT/CBT reconstructed temperatures show cooler conditions post-MBE. Yin and Berger (2012) suggest that the MBE signal is mainly a characteristic of climatic variables influenced by greenhouse gases, while those more strongly controlled by insolation do not record MBE signals. Lake El'gygytgyn MBT/CBT temperatures are strongly dominated by summer insolation, which may cause them to not show the expected trends associated with an MBE signal. We note that although the temperatures do not show the expected warming trend, a statistical difference between pre- and post-MBE intervals is present in the data, which we interpret as an MBE signal.

A statistically significant MBE signal is also recorded in the other proxy records examined here. ACL values also show a shift in mean and median values, with lower values predominating after the MBE implying landscape scale vegetation changes responded to climatic shifts associated with the MBE (Figure 2.10D). Biogenic silica percentages show increased amplitude with higher mean and median values post-MBE indicating increased diatom productivity (Figure 2.10E). Total organic carbon (Melles et al., 2012) also implies enhanced productivity, with higher mean and median values after the MBE (Figure 2.10F). Mn/Fe ratios (Melles et al., 2012) (a proxy for oxygenation and mixing) record higher values post-MBE, implying enhanced mixing and bottom water oxygenation (Figure 2.10G). This enhanced mixing may have led to the increased productivity indicated by other proxies. Percent tree and shrub data have similar mean

and median values but a greater range after the MBE (Figure 2.10H), indicating more trees were present around Lake El'gygytgyn during post- MBE interglacials than pre-MBE interglacials.

Although the mechanism for the MBE is debated, a prevailing hypothesis by Yin (2013) suggests changes in Antarctic bottom water (AABW) production, produced by variations in insolation and associated feedbacks via the location of the polar front, salinity changes, and sea ice formation, caused the climatic shift observed in many records. Prior to the MBE, AABW production was enhanced and led to cooler interglacials while warmer interglacial conditions post-MBE are associated with reduced AABW production (Yin, 2013). Changes in thermohaline circulation and atmospheric fronts have been connected to the mechanism for MBE expression in several other records (Candy and McClymont, 2013; Castañeda et al., 2016). A compilation of records from the North Atlantic and Nordic seas finds no evidence of the MBE in the mid-latitudes of the Atlantic but suggests a signal is preserved at latitudes above 56 $^{o}$N (Candy and McClymont, 2013). The authors attribute cooler pre-MBE interglacials to a southward migration of the polar front creating an enhanced temperature gradient between the mid and high latitudes of the North Atlantic (Candy and McClymont, 2013). Migrations of the polar front within the North Atlantic between 800 and 400 ka have also been noted by (Alonso-Garcia et al., 2011). As a major source of deep water formation, the high latitudes of the North Atlantic are sensitive to changes in ocean circulation. Since the likely mechanism for the MBE likely involves changes in thermohaline circulation, areas strongly influenced by/associated with deep water formation or

upwelling, such as the Southern Ocean, North Atlantic, and North Pacific, may be more likely to capture a signal of the event.

Teleconnections between the northern and southern hemisphere climates have been suggested based on the similarities between the Lake El'gygytgyn record and the ANDRILL 1B record, as noted by Melles et al. (2012) and northwest Pacific Ocean records (Woodard et al., 2014). The coupling of the two hemispheres is indicated through the correspondence between "super interglacials" in the Lake El'gygytgyn record (Melles et al., 2012) and diatomite layers in the ANDRILL 1B record (McKay et al., 2012), which reflect a diminished West Antarctic Ice Sheet (WAIS) and open water in the Ross Embayment (Pollard and DeConto, 2009). Melles et al. (2012) hypothesized that periods of correlation between the two hemispheres are the result of a decrease in Antarctic sea ice, leading to a reduction in AABW formation and Southern Ocean ventilation, both of which would affect thermohaline circulation and reduce upwelling in the North Pacific, thereby producing a stratified water column and increasing SSTs during super interglacials (Melles et al., 2012). Relative to North Atlantic Deep Water (NADW), less AABW flowed into the southwest Pacific during MIS 11 (Hall et al., 2001; Elderfield et al., 2012), while reduced upwelling in the Pacific is indicated by low biogenic silica concentrations in ODP site 882 sediments covering this interval (Haug et al., 1995; Jaccard et al., 2010). These changes may have impacted the dominant atmospheric pressure patterns causing displacement of the Aleutian Low at Lake El'gygytgyn, resulting in increased air temperatures and elevated precipitation over northeast Arctic Russia (Melles et al., 2012). We suggest that these shifts may also be responsible for the MBE signals we observe recorded in the proxy records at Lake El'gygytgyn. Notably, the

strength and position of the Aleutian Low may have played a crucial role in linkages between Atlantic Meridional Overturning Circulation (AMOC) anomalies and the production of NADW (i.e., Manabe et al., 1988; Thompson et al., 2000; Timmermann et al., 2007). Thus, the Lake El'gygytgyn record may have even broader scale relevance to studies in the North Atlantic.

## 2.6 Conclusions

Organic geochemical analysis of the unique Lake El'gygytgyn sedimentary record yields numerous insights to mechanisms of terrestrial Arctic climate variability and the strength of glacial-interglacial periods during the Mid-Pleistocene. We find precessional forcing is a major determinant of summer temperatures during the Mid-Pleistocene with MBT/CBT temperatures varying at ~23 and 19 ka. The plant leaf wax ACL record suggests a dependence of Arctic climate and vegetation on glacial- interglacial cooling/ice volume changes with a dominant periodicity of 41 ka. The marked correspondence between ACL and sea level supports the role of global changes in terrestrial Arctic climate. We note that the "super interglacial" nature of MIS 11 recorded by biogenic silica is not echoed in our MBT/CBT temperature record. Instead, greatest warmth is recorded by brGDGTs during periods of strong isolation forcing, such as MIS 7, which is not recognized as a super interglacial. Overall, our organic geochemical records suggest that MIS 7, 9, and 17 were the warmest interglacials, while MIS 10 was the coldest glacial period. One interval of interest which stands out in our records is MIS 16-13, where, in both the MBT/CBT and ACL records, we observe muted climatic variability with MIS 14 preserved as an especially weak glacial. Overall, our proxy records indicate the Arctic experienced an MBE associated shift in glacial- interglacial

behavior over the interval of 200- 800 ka. Our record is the first to demonstrate preservation of an MBE signal in the terrestrial Arctic, an area with key implications for global climate change.

An important outcome of our multi-proxy approach is that the intensity and timing of climatic cycles, as well as the orbital signals these records contain, varies by proxy type, even within the same sedimentary archive and when measured on the same samples. We suggest high resolution, multi-proxy analysis of additional paleoclimate archives is essential for improved understanding of the complexities of the earth climate system as these differences can provide valuable information about climate and environmental patterns and dynamics. We caution basing interpretations on one proxy or parameter, particularly when comparing different proxy records between multiple locations, and instead promote the use of multiple proxies to examine past climate variability at any site.

## 2.7 Acknowledgements

MHH thanks Benjamin Keisling and Greg de Wet for helpful feedback and discussions. Jeff Salacup is acknowledged for his technical laboratory assistance. Julie Chessia and Geoffrey Small are recognized for their help with sample preparation. We thank Martin Melles, Pavel Minyuk, Patricia Anderson, Anatoly Lozhkin, Volker Wennrich, Norbert Nowaczyk, and Robert DeConto for ongoing collaboration on the Lake El'gygytgyn project. Drilling operations at Lake El'gygytgyn were funded by the International Continental Scientific Drilling Program (ICDP), The US National Science Foundation (NSF), the German Federal Ministry of Education and Research (BMBF), Alfred Wegener Institute (AWI) and Geo-Forschungs Zentrum Potsdam (GFZ), the

Russian Academy of Sciences Far East Branch (RAS FEB), the Russian Foundations for Basic Research (RFBR), and the Austrian Federal Ministry of Science and Research (BMWF). Primary funding for this research was provided by NSF grant #1204087. Sample material used in this project, as well as sampling assistance, was provided by LacCore at the University of Minnesota. Data associated with this study will be made available on the NOAA National Centers for Environmental Information paleoclimatology database and on PANGAEA data publisher for earth and environmental science.

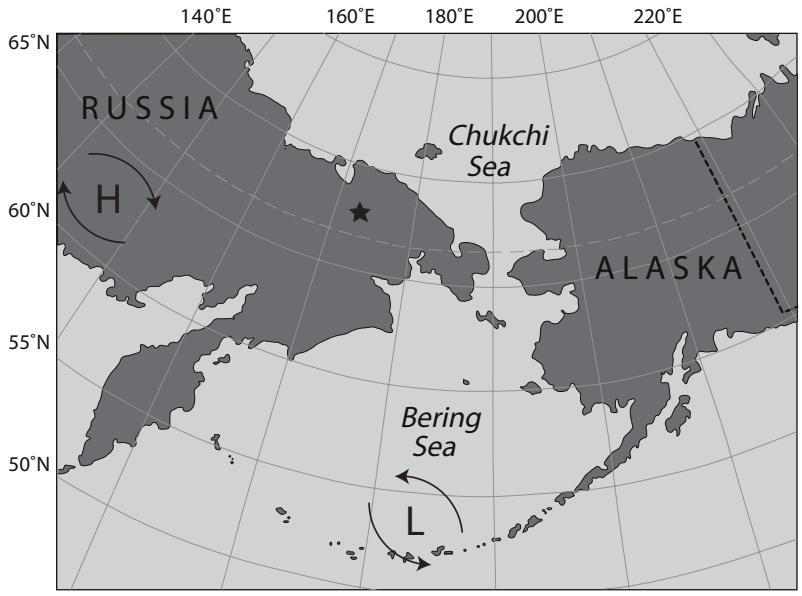


**Figure 2.1 Location of Lake El'gygytgyn in northeast Arctic Russia (star). Relative locations of the dominant atmospheric circulation patterns: the Siberian high (H) and Aleutian low (L) are indicated.**

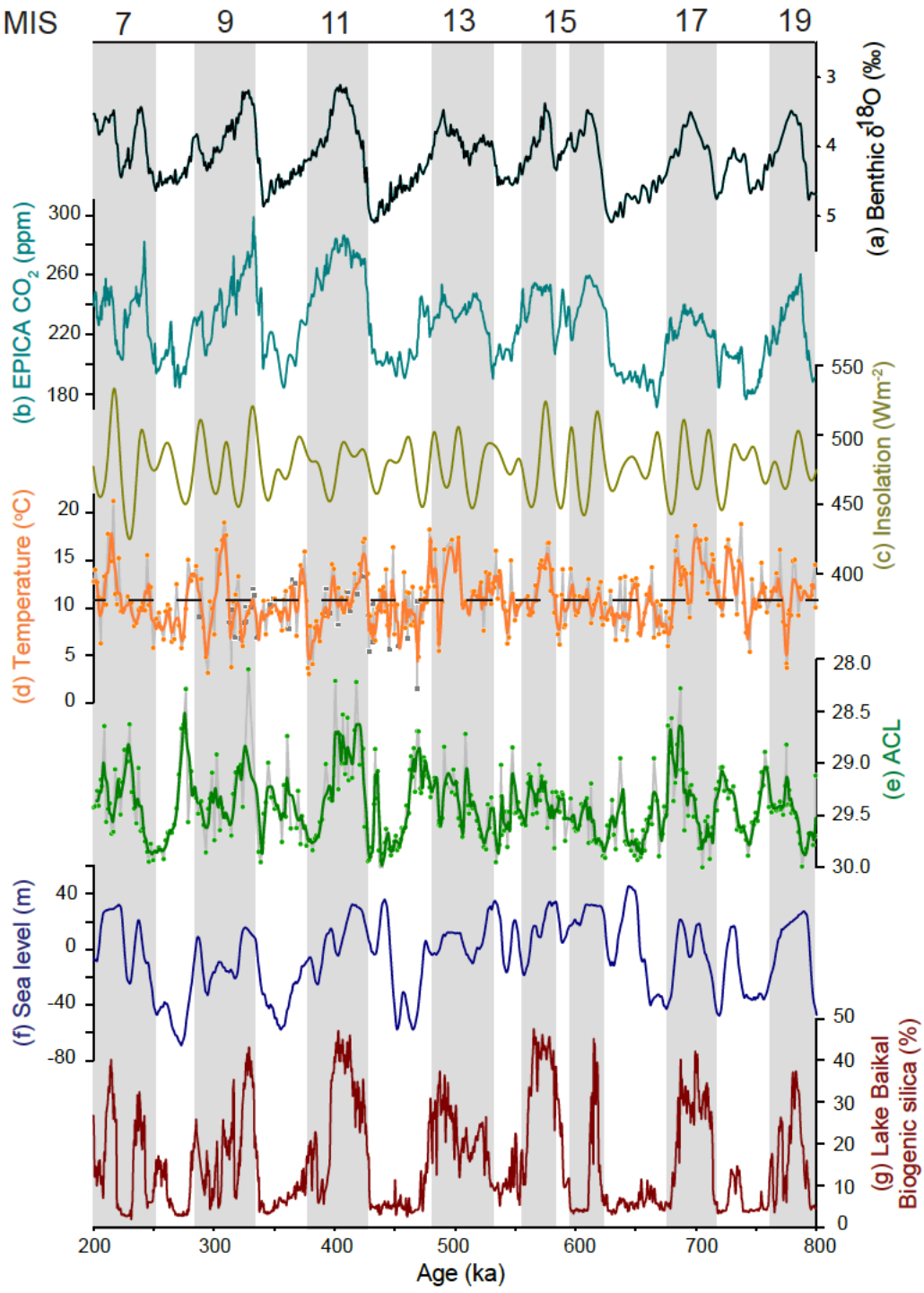
MIS
7
9
11
13
15
17
19
(a) Benthic δ18O (‰)
3
4
5
(b) EPICA CO2 (ppm)
300
260
220
180
(c) Insolation (Wm-2)
550
500
450
400
(d) Temperature (°C)
20
15
10
5
0
(e) ACL
28.0
28.5
29.0
29.5
30.0
(f) Sea level (m)
40
0
-40
-80
(g) Lake Baikal Biogenic silica (%)
50
40
30
20
10
0
200
300
400
500
600
700
800
Age (ka)

**Figure 2.2 Lake El'gygytgyn and global climate proxy records from 200- 800 ka. A) Global benthic oxygen isotope stack (Lisiecki and Raymo, 2005). B) EPICA Dome C atmospheric $CO_2$ record (Lüthi et al., 2008). C) Local summer insolation at 67 $^{o}$N (Laskar et al., 2004). D) MBT/CBT temperature reconstruction from this study raw data (orange circles) and D'Anjou et al. (2013) (gray squares) and three point running mean (solid orange line). The record mean (10.8 $^{o}$C) is denoted with the black dashed line. E) *n*-alkane ACL, raw data (circles) and three point running mean (solid green line). F) Global mean relative sea level (Rohling et al., 2014). G) Lake Baikal biogenic silica record (Prokopenko, 2006). Marine isotope stages are labeled and highlighted in grey.**

| MIS | 7c | 7e | 9 | 11 | 13 | 15a | 15e | 17 | 19 | |
|---|---|---|---|---|---|---|---|---|---|---|
| LR04 | 3.48 | 3.44 | 3.19 | 3.11 | 3.47 | 3.39 | 3.49 | 3.5 | 3.48 | 1 |
| CO2 (ppm) | 257 | 275 | 291 | 286 | 247 | 254 | 259 | 237 | 259 | 2 |
| Insolation at 67 oN | 533 | 500 | 518 | 494 | 502 | 522 | 515 | 509 | 499 | 3 |
| | | | | | | | | | | |
| Biogenic silica (%) | 11.6 | 19 | 30.3 | 56.2 | 17.9 | 19 | 15.3 | 24.2 | 15 | 4 |
| Si/Ti | 0.68 | 0.79 | 1.34 | 2.35 | 0.97 | 1.03 | 1.04 | 1.31 | 1.11 | 5 |
| Diatom abundance | 3.70E+09 | 2.70E+09 | 5.60E+09 | 1.50E+10 | 8.10E+09 | 1.90E+09 | 1.50E+09 | 3.90E+09 | 1.25E+09 | 6 |
| Mn/Fe | 9.13 | 12.47 | 11.66 | 49.73 | 15.44 | 12.16 | 11.52 | 22.04 | 13 | 5 |
| Tree and shrub pollen (%) | 36.38 | 41.85 | 77.73 | 88.13 | 77.79 | 86.75 | 54.55 | 73.25 | 31.62 | 7,8,9 |
| brGDGT temperature (oC) | 21.28 | 15.56 | 19 | 17.29 | 18.26 | 16.84 | 14.12 | 18.68 | 16.13 | this study |
| ACL | 28.64 | 28.62 | 28.09 | 28.22 | 28.69 | 29.01 | 29.19 | 28.11 | 28.82 | this study |

weakest strongest

**Figure 2.3 Maximum values for interglacial periods from global and Lake El'gygytgyn proxy records. The values are color coded according to strength with the darkest red colors corresponding to the strongest interglacials through to the light beige representing the weakest. References are as follows 1) Lisiecki and Raymo, 2005; 2) Lüthi et al., 2008; 3) Laskar et al., 2004; 5) Meyer-Jacob et al., 2014; 6) Melles et al., 2012; 7) Snyder et al., 2013; 8) Melles et al., 2012; 7-9) Lozhkin et al., 2007, 2017; Lozhkin and Anderson, 2013.**

| MIS | 8 | 10 | 12 | 14 | 16 | 18 | Reference |
|---|---|---|---|---|---|---|---|
| LR04 | 4.63 | 4.84 | 5.08 | 4.55 | 5.08 | 4.75 | 1 |
| CO2 (ppm) | 195 | 201 | 199 | 190 | 189 | 184 | 2 |
| Insolation at 67 oN | 478 | 455 | 460 | 472 | 462 | 492 | 3 |
| | | | | | | | |
| Biogenic silica (%) | 6 | 8 | 6 | 7 | 6 | 6 | 4 |
| Si/Ti | 0.38 | 0.37 | 0.36 | 0.43 | 0.45 | 0.36 | 5 |
| Diatom abundance | 1.03E+09 | 1.43E+09 | 2.76E+08 | 8.81E+07 | 3.56E+08 | 1.26E+08 | 6 |
| Mn/Fe | 7.42 | 5.78 | 6.43 | 5.82 | 6.45 | 5.81 | 5 |
| Tree and shrub pollen (%) | 3.55 | 3.53 | 1.56 | 18.14 | 4.52 | 14.88 | 7,8,9 |
| brGDGT temperature (oC) | 5.77 | 3.74 | 5.43 | 6.23 | 6.64 | 9.21 | this study |
| ACL | 29.94 | 29.95 | 30.02 | 29.95 | 29.91 | 29.99 | this study |
| | | | | | | | |
| weakest | | | | | | | strongest |

**Figure 2.4 Minimum values for each glacial from global and Lake El'gygytgyn proxy records. The values are color coded for strength with dark blue as the strongest and seafoam green as the weakest glacials. References are as follows 1) Lisiecki and Raymo, 2005; 2) Lüthi et al., 2008; 3) Laskar et al., 2004; 5) Meyer-Jacob et al., 2014; 6) Melles et al., 2012; 7) Snyder et al., 2013; 8) Melles et al., 2012; 7-9) Lozhkin et al., 2007, 2017; Lozhkin and Anderson, 2013.**

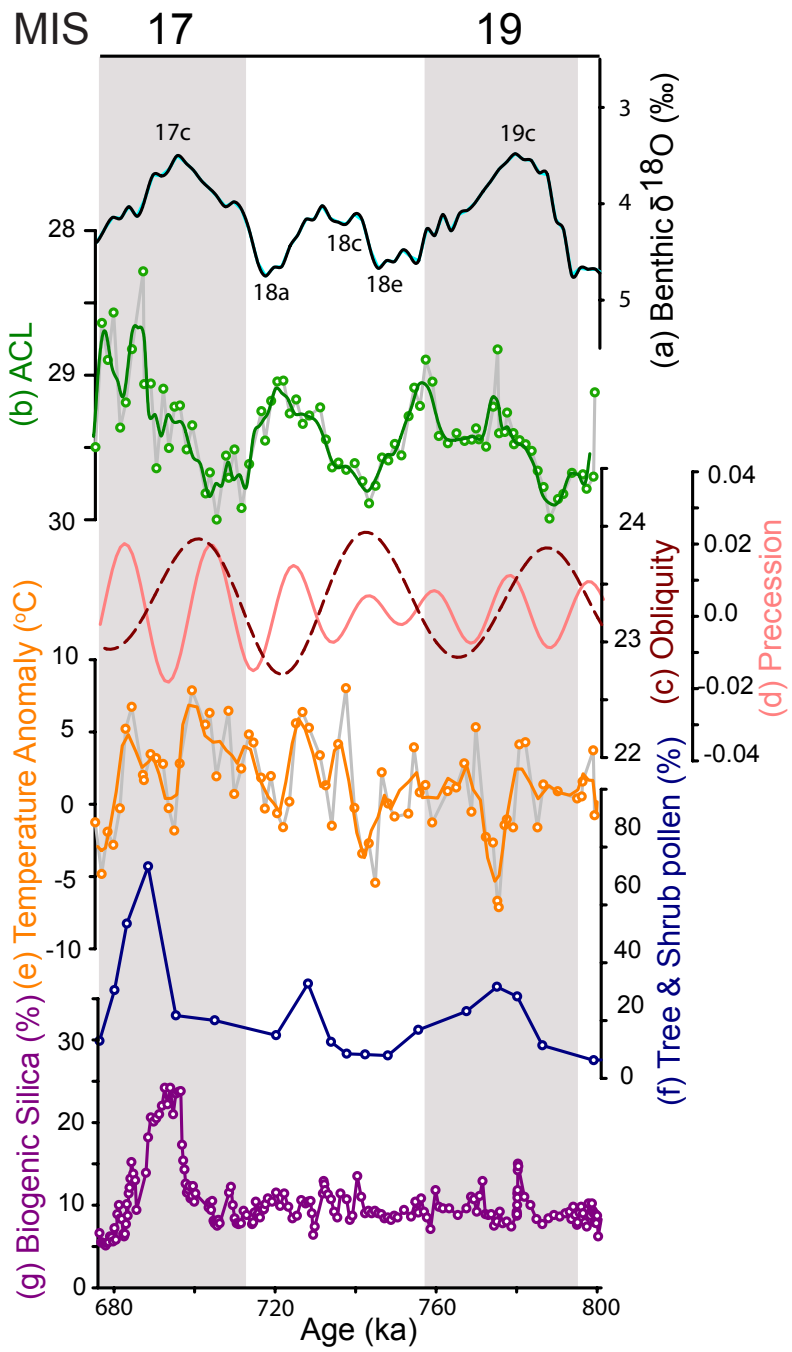


**Figure 2.5 MIS 17-19. A) Global benthic oxygen isotope stack (Lisiecki and Raymo, 2005). B) *n*-alkane average chain length raw data (circles), three point running mean (solid green line). C Local obliquity (dashed red) at 67 ºN). D Local precession (pink). E) MBT/CBT temperature reconstruction raw data (circles), three point running mean (orange line). F) Percent trees and shrubs data (Lozhkin et al., 2017). G) Percent biogenic silica (Meyer-Jacob et al., 2014). Gray bars indicate marine isotope stages.**

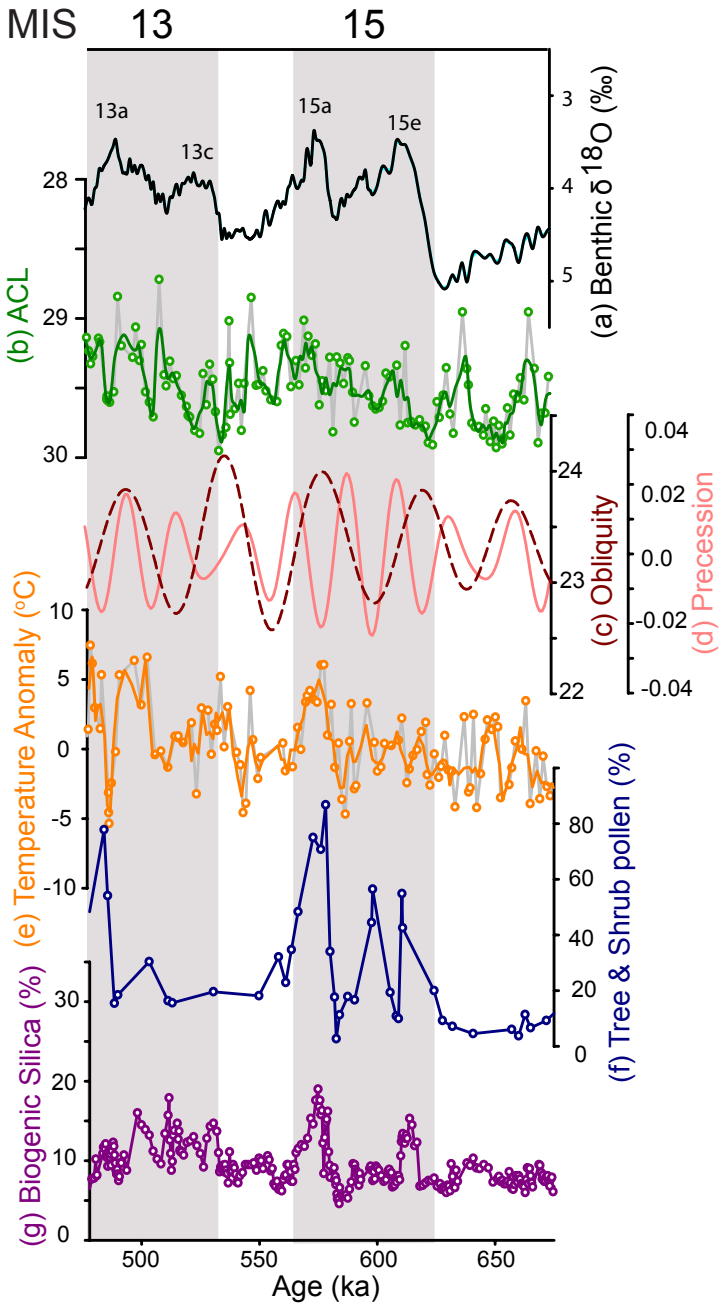


**Figure 2.6 MIS 13-15 A) Global benthic oxygen isotope stack (Lisiecki and Raymo, 2005). B) *n*-alkane average chain length raw data (circles), three point running mean (solid green line). C Local obliquity (dashed red) at 67 ºN). D Local precession (pink). E) MBT/CBT temperature reconstruction raw data (circles), three point running mean (orange line). F) Percent trees and shrubs data (Lozhkin et al., 2017). G) Percent biogenic silica (Meyer-Jacob et al., 2014). Gray bars indicate marine isotope stages.**

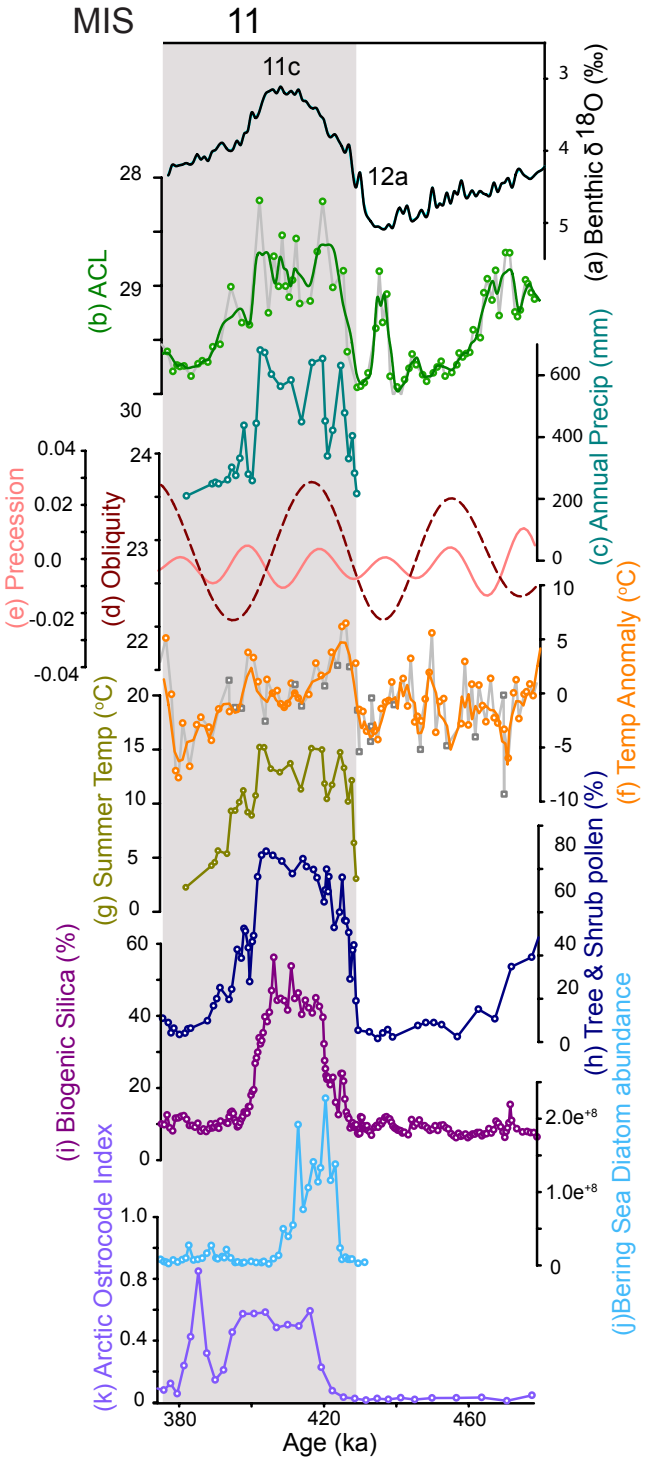
MIS 11
11c
12a
(a) Benthic δ18O (‰)
(b) ACL
(c) Annual Precip (mm)
(d) Obliquity
(e) Precession
(f) Temp Anomaly (°C)
(g) Summer Temp (°C)
(h) Tree & Shrub pollen (%)
(i) Biogenic Silica (%)
(j)Bering Sea Diatom abundance
(k) Arctic Ostrocode Index
Age (ka)

**Figure 2.7 MIS 11-12. A) Global benthic oxygen isotope stack (Lisiecki and Raymo, 2005). B) *n*-alkane average chain length raw data (circles), three point running mean (solid line). C) Pollen based mean annual precipitation estimate (Melles et al., 2012). D) Local obliquity (dashed red) at 67 ºN. E) Local precession (pink). F) MBT/CBT temperature reconstruction raw data from this study (orange circles), from D'Anjou et al. (2013) (gray squares, three point running mean (orange line). G) Pollen based mean temperature of the warmest month estimate (Melles et al., 2012). H) Percent trees and shrubs data (Lozhkin et al., 2017). I) Percent biogenic silica (Meyer-Jacob et al., 2014). J) Bering Sea diatom abundance (Caissie et al., 2016). K) Arctic Ostrocode Index (Marzen et al., 2016). Gray bar indicates marine isotope stages.**

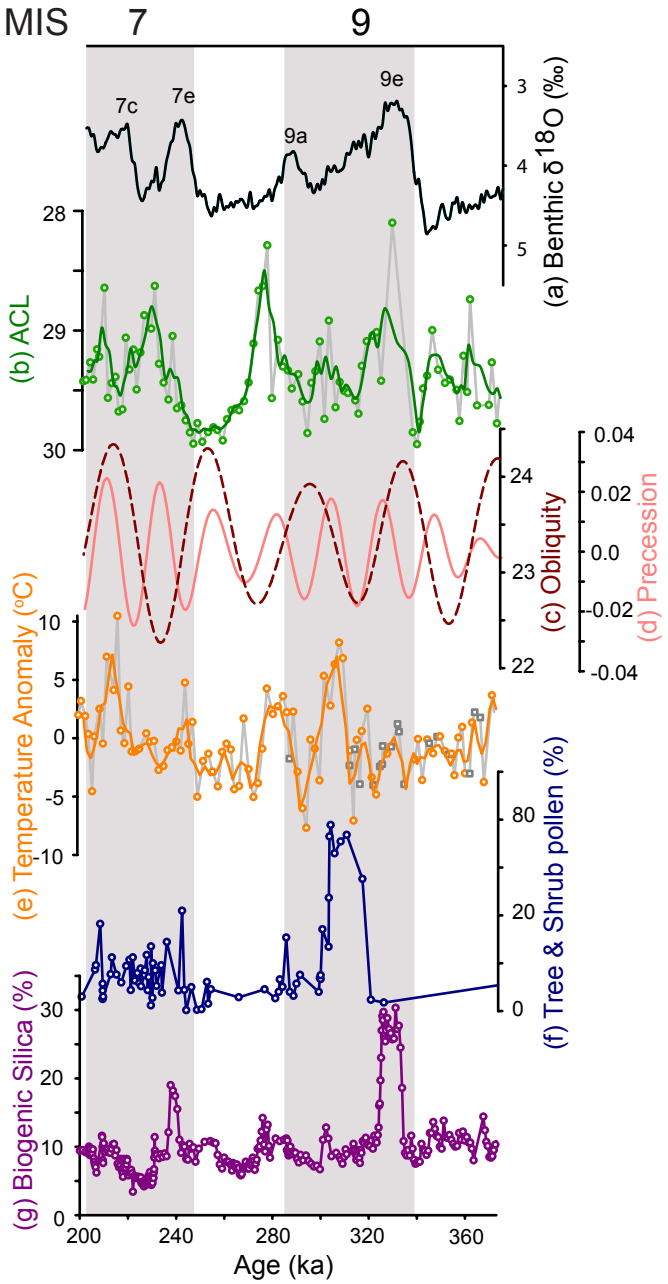


**Figure 2.8 MIS 7-10. A) Global benthic oxygen isotope stack (Lisiecki and Raymo, 2005). B) *n*-alkane average chain length (ACL) raw data (circles), three point running mean (solid green line). C Local obliquity (dashed red) at 67 °N). D Local precession (pink). E) MBT/CBT temperature reconstruction raw data (circles), three point running mean (orange line). F) Percent trees and shrubs data (Lozhkin et al., 2017). G) Percent biogenic silica (Meyer-Jacob et al., 2014). Gray bars indicate marine isotope stages.**

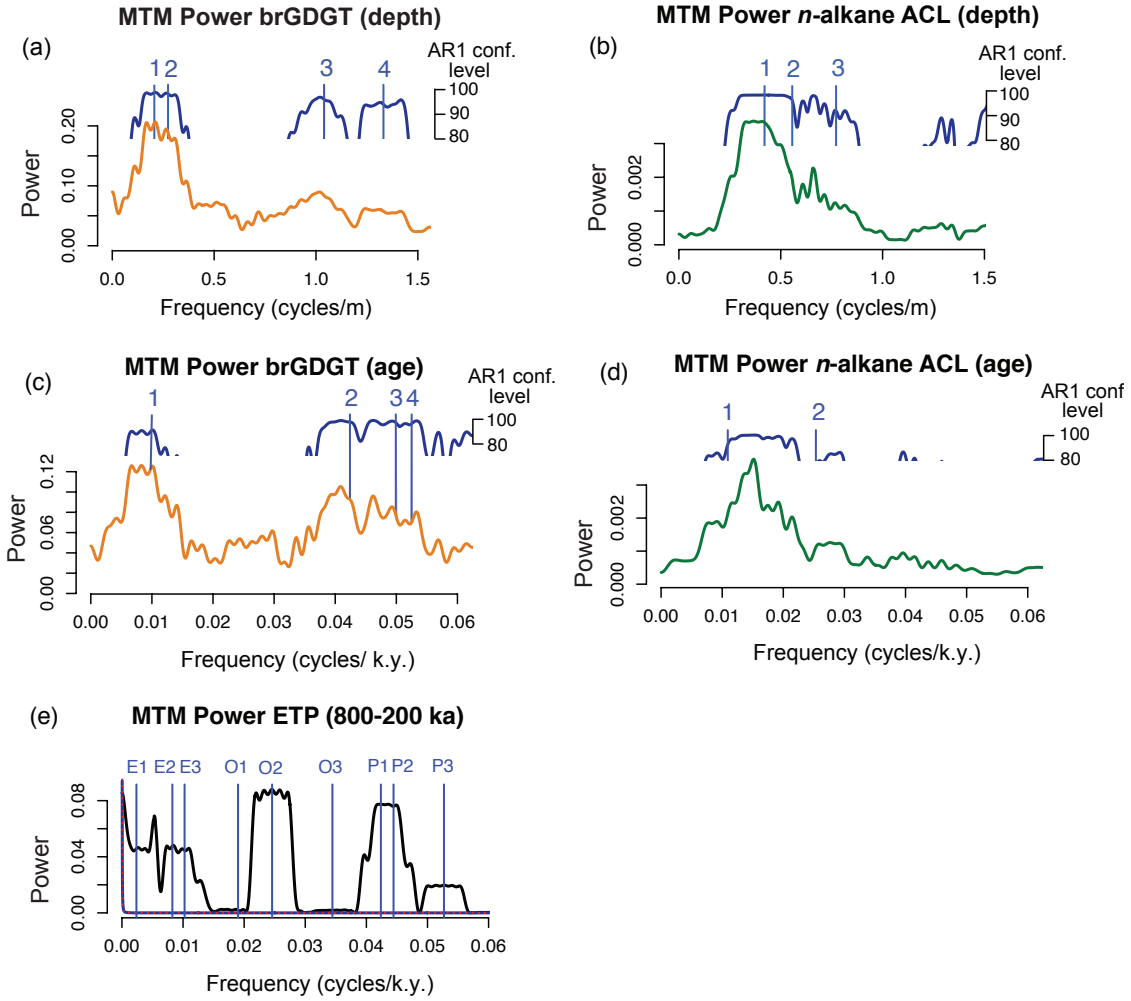


**Figure 2.9 MTM spectral characteristics of Lake El'gygytgyn proxy records (MBT/CBT temperature and *n*-alkane ACL), and eccentricity-tilt-precession (ETP) solution (Laskar et al., 2011) using the ML96 Robust AR1 method (Mann and Lees, 1996). A-B) is proxy data using the depth domain with no tuned age model assumptions. C-D) is proxy data using the tuned age model of Nowaczyk et al., (2013). E) MTM Power ETP solution. Numbered blue lines indicate significant spectral peaks that satisfy the MTM harmonic F-test 85% confidence levels.**

| ID | Data set | Observed frequency (cycles/m) or (cycles/ky) | MTM_ML96 harmonic probability (%) | Observed periodicity (k.y.) | Orbital interpretation (k.y.) |
|---|---|---|---|---|---|
| 1 | brGDGT (depth) | 0.206 | 92.00 | 120.76 | 121.18 (E2) |
| 2 | brGDGT (depth) | 0.274 | 96.86 | 90.79 | 97.56 (E3) |
| 3 | brGDGT (depth) | 1.041 | 85.75 | 23.90 | 23.60 (P1) |
| 4 | brGDGT (depth) | 1.330 | 99.73 | 18.70 | 18.98 (P3) |
| 1 | ACL (depth) | 0.420 | 99.93 | 59.23 | 52.63 (O1) |
| 2 | ACL (depth) | 0.556 | 95.68 | 44.74 | 40.70 (O2) |
| 3 | ACL (depth) | 0.770 | 87.12 | 32.31 | 29.03 (O3) |
| 1 | brGDGT (age) | 0.011 | 95.30 | 95.19 | 97.56 (E3) |
| 2 | brGDGT (age) | 0.042 | 23.58 | 23.58 | 23.60 (P1) |
| 3 | brGDGT (age) | 0.050 | 20.03 | 20.03 | 22.50 (P2) |
| 4 | brGDGT (age) | 0.053 | 19.04 | 19.04 | 18.98 (P3) |
| 1 | ACL (age) | *0.011* | *96.45* | 91.64 | 97.56 (E3) |
| 2 | ACL (age) | 0.025 | 99.48 | 39.47 | 40.70 (O2) |

**Table 2.1 Predicted and observed periods for the brGDGT temperatures and *n*-alkane ACL proxy data.**

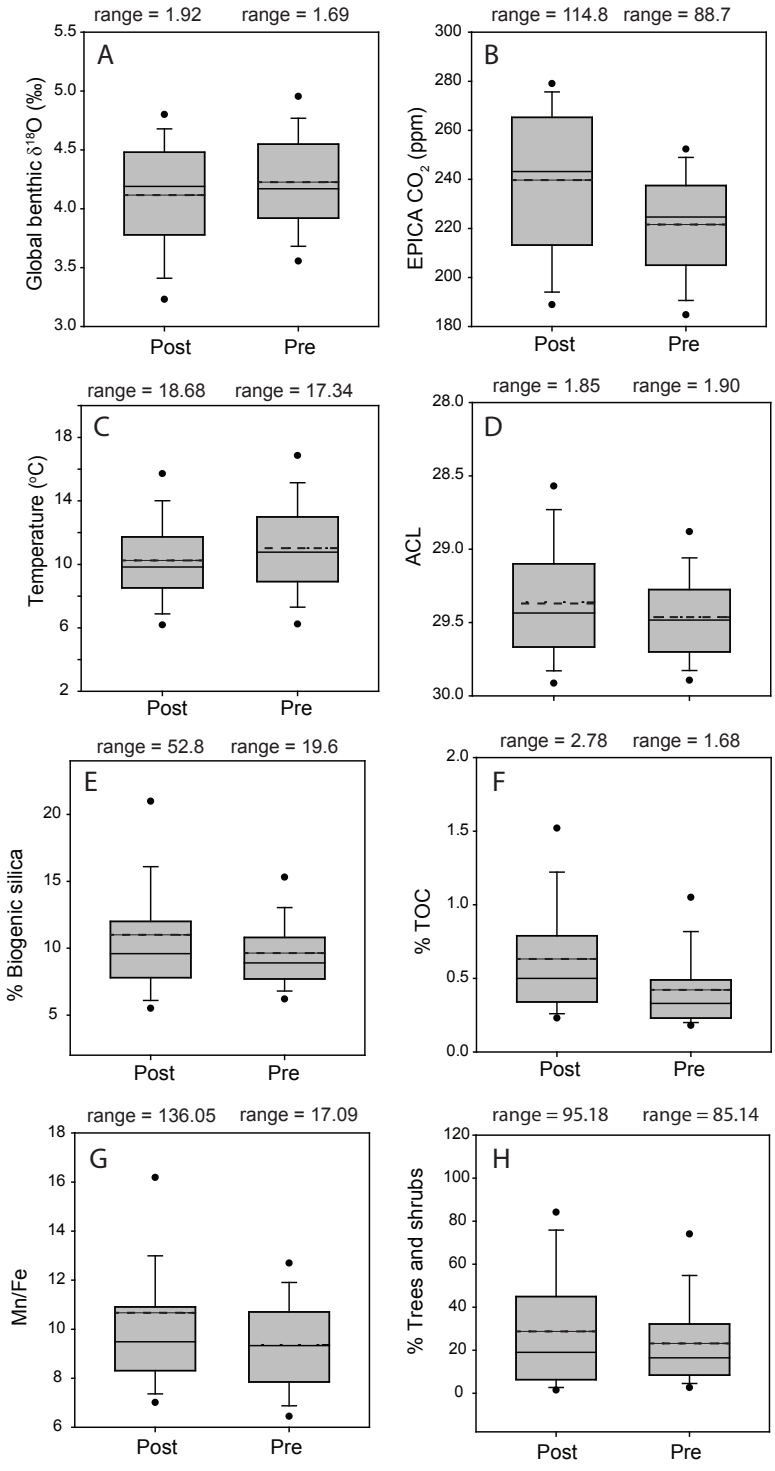
range = 1.92
range = 1.69
A
Global benthic δ18O (‰)
5.5
5.0
4.5
4.0
3.5
3.0
Post
Pre
range = 114.8
range = 88.7
B
EPICA CO2 (ppm)
300
280
260
240
220
200
180
Post
Pre
range = 18.68
range = 17.34
C
Temperature (°C)
18
14
10
6
2
Post
Pre
range = 1.85
range = 1.90
D
ACL
28.0
28.5
29.0
29.5
30.0
range = 52.8
range = 19.6
E
% Biogenic silica
20
15
10
5
Post
Pre
range = 2.78
range = 1.68
F
% TOC
2.0
1.5
1.0
0.5
0.0
Post
Pre
range = 136.05
range = 17.09
G
Mn/Fe
18
16
14
12
10
8
6
Post
Pre
range = 95.18
range = 85.14
H
% Trees and shrubs
120
100
80
60
40
20
0
Post
Pre

**Figure 2.10 Box and whisker plots showing the differences between pre-and post-MBE intervals. In all plots the bottom and top of the box indicate the first and third quartiles, the solid line inside the box indicates the median, and the dashed line indicates the mean. In a few cases the mean plots on top of the median line. The tips of the whiskers represent the smallest and largest values that are not more than 1.5 times the interquartile range above or below the median. The dots represent the $5^{th}$ and $95^{th}$ percentile outliers. For all plots, a Student's t-test significant at a 95% confidence level was first performed to test the null hypothesis that the pre-and post-MBE intervals are the same; for all parameters, the null hypothesis was rejected. The range listed above the plots is the difference between the maximum and minimum values in each interval.**

# CHAPTER 3

# PRIMARY PRODUCTION AND ORGANIC MATTER PRESERVATION DURING THE MIDDLE PLEISTOCENE: AN ARCTIC PERSPECTIVE FROM LAKE EL'GYGYTGYN, RUSSIA

## 3.1 Abstract

As the climate warms under the effects of anthropogenic climate change, the sensitive ecosystems in and around Arctic lakes are expected to be significantly impacted. These changes will likely influence primary production and carbon cycling, with potential implications for global climate. Examination of primary productivity variations during past climate fluctuations and warm periods help constrain how Arctic lacustrine ecology, organic matter production, and carbon cycling may change in the future. Here we reconstruct primary productivity and organic matter preservation changes in Lake El'gygytgyn, Arctic Russia. Organic biomarkers and stable carbon and nitrogen isotopes are used to assess changes in autochthonous and allochthonous organic matter production and preservation across glacial-interglacial cycles during the Mid-Pleistocene from Marine Isotope Stage (MIS) 19 to 7 (800 to 200 ka). We find climatically induced shifts in the algal community of Lake El'gygytgyn and note periods of enhanced productivity and preservation during both glacial and interglacial periods. We find ice cover to be a particularly important determinant of organic matter preservation in our record. We also note orbital signals in our records and highlight the influence of the length and intensity of the summer season (e.g. obliquity and precession) on aquatic ecosystem productivity and organic matter preservation at Lake El'gygytgyn.

## 3.2 Introduction

Lakes can impact climate at a regional scale through exchange of heat and water with the atmosphere and can also impact global climate through their role in the global carbon cycle (Tranvik et al., 2009). Although lakes comprise only a small fraction of Earth's surface (~3%) (Downing et al., 2006) their role in transport, transformation, and storage of carbon is significant (Cole et al., 2007; Dean and Gorham, 1998). The consumption and use of greenhouse gases (GHGs) such as carbon dioxide, methane, and nitrous oxide, by lacustrine microorganisms influences the concentration of these gases in the atmosphere, and therefore Earth's heat budget (Tranvik et al., 2009). Changing climatic variables such as temperature and precipitation can magnify the intensity of lacustrine carbon cycling leading to both increased carbon burial and outgassing. As anthropogenic climate change continues, a strong understanding of lacustrine carbon cycling under different climate scenarios is essential.

Arctic aquatic ecosystems are considered especially susceptible to climate change (Hobbie et al., 2000). Although individual system responses may vary, under current anthropogenic climate change, increased temperature and nutrient input are expected to alter primary production within these lakes (Flanagan et al., 2003). The Arctic is particularly vulnerable to climate change because of the effects of polar amplification and is currently undergoing rapid transformations (SWIPA, 2017). Arctic lakes are currently relatively unproductive, but could experience significant increases in productivity associated with climate change (Flanagan et al., 2003; Woelders et al., 2018). Reduced ice cover and increased albedo will likely dramatically change thermal budgets of lakes and increase growing season and solar energy available for algal growth (Flanagan et al.,

2003; Griffiths et al., 2017; Veillette et al., 2010). Additionally, nutrient availability may increase as permafrost thaws, likely creating even more drastic changes in productivity (Ogbebo et al., 2009; Rouse et al., 1997). Examination of primary productivity variations during past climate fluctuations and warm periods help constrain how Arctic lacustrine ecology, primary productivity, and carbon cycling may change in the future.

Currently, there are few long term, high resolution terrestrial climate records from the Arctic due to the repeated, extensive glaciation of this region during the Pleistocene (Miller et al., 2010). However, Lake El'gygytgyn, located in the eastern Russian Arctic, was never glaciated (Glushkova, 2001) and provides a continuous record of terrestrial Arctic climate since its formation 3.6 Ma (Layer, 2000). Previous studies of Lake El'gygytgyn have predominantly used diatom counts and biogenic silica percentages as a proxy for past productivity (Melles et al., 2012; Meyer-Jacob et al., 2014; Snyder et al., 2013). However, in addition to diatoms, green algae, dinoflagellates, and cyanobacteria are all common in Arctic environments (Pienitz et al., 2004). These additional algal classes generally lack rigid morphological structures and do not preserve well in sediments (Pienitz et al., 2004). Organic geochemical analysis of biomarkers for these algal populations can be used to interpret past climate change by constraining their response to climate (e.g. Volkman et al., 1998; Castañeda et al., 2009). Important climatic changes recorded in the productivity of different algal classes can be missed in diatom focused productivity records. Analysis of Lake El'gygytgyn records by Habicht et al. (Chapter 2) emphasizes the different and often dissimilar behavior of proxy signals and highlights the utility of a multiproxy approach for paleoclimate reconstructions.

In this study, we employ several individual molecules and compound classes as biomarkers for various primary producers. Biomarkers are organic compounds preserved in sediments or rocks that can be traced to a specific source organism(s) or process, thereby providing a proxy for climatic or environmental conditions at the time of deposition (Peters et al., 2005). A variety of biomarkers are recognized as effective proxies because of their durability (millions of years) and source specific molecular structures (Eglinton and Hamilton, 1967; Volkman, 1986; Cranwell et al., 1987). Algae are good bio-indicators for environmental conditions and play an important role in the biogeochemical cycle of lakes. They are generally abundant and diverse with rapid dispersal rates and short life cycles, thus responding quickly to environmental changes (Stevenson and Smol, 2003). A previous study incorporating algal and terrestrial biomarkers from Lake El'gygytgyn demonstrated the utility of this approach (D'Anjou et al., 2013b). Here we expand on this study and present an assessment of primary productivity and organic matter preservation changes in Lake El'gygytgyn during glacial-interglacial cycles of the Middle Pleistocene between 800 and 200 ka. In addition to biomarker concentrations, we use bulk sediment stable isotopes to examine organic matter cycling. We find climatically induced changes in the algal community and note periods of enhanced productivity and preservation during glacial and interglacial periods.

## 3.3 Background

### 3.3.1 Regional setting and study site

Lake El'gygytgyn is a meteorite impact crater lake formed 3.6 Ma (Layer, 2000), located 100 km north of the Arctic Circle in the Chukotka Peninsula in far east Russia

(67° 30'N, 172° 5'E) (Figure 3.1). The impact crater has a diameter of 18 km and a catchment area of ~293 $km^2$ (Nolan and Brigham-Grette, 2007). A network of 50 small, highly seasonal streams carries surface runoff and snowmelt into the lake and the Enmyvam River provides an outlet to the Bering Sea (Nolan and Brigham-Grette, 2007). The lake itself is 12km wide and 175m deep, with a total volume of ~14.1 $km^3$ (Nolan and Brigham-Grette, 2007). Today, the lake is monomictic and ultra-oligotrophic, with water temperatures not exceeding 4 °C and annual overturning occurring in late summer (Nolan and Brigham-Grette, 2007). Lake El'gygytgyn is ice covered for much of the year, with lake ice forming by October and persisting until July (Nolan and Brigham-Grette, 2007). In the modern environment, the water column is oxygenated throughout (Nolan and Brigham-Grette, 2007), but previous studies of the paleorecord have noted periods of bottom water anoxia associated with perennial lake ice cover during glacials (Holland et al., 2013; Melles et al., 2007).

Modern air temperatures at the lake range from -46 °C in winter to 26 °C in summer with a mean annual air temperature of -10.3 °C (Nolan and Brigham-Grette, 2007). Permafrost 100-300 m deep surrounds the lake (Nolan and Brigham-Grette, 2007). The catchment area is extremely arid (<200 mm $a^{-1}$) and precipitation in winter and summer is approximately equal (Nolan and Brigham-Grette, 2007). Two atmospheric pressure patterns, the Siberian High and Aleutian Low, dominate the climatology of this region. The locations and strength of these pressure patterns are variable, but create consistent strong winds at the lake (Mock et al., 1998). The winds are either south-easterly or north-westerly (Nolan et al., 2013) and are strongest in winter (Nolan and Brigham-Grette, 2007). Very little algae or aquatic vegetation is visible in the lake today

(Nolan and Brigham-Grette, 2007). The morphology of the lake is such that the sides are steep thereby limiting the area for aquatic macrophyte growth.

### 3.3.2 Biomarkers

#### 3.3.2.1 Aliphatic Hydrocarbons

Aliphatic hydrocarbons (straight chain *n*-alkanes, *n*-alkenes, and *n*-alkanols) are a major component of plant leaf waxes. They are widespread in lacustrine sedimentary archives and may be transported from the terrestrial environment or produced in situ (Didyk et al., 1978; Eglinton and Hamilton, 1967). Principally, the sources of *n*-alkyl lipids in lake sediments are algae and photosynthetic bacteria producing $n\mathrm{C}_{17}$-$n\mathrm{C}_{21}$ compounds (Cranwell et al., 1987; Meyers, 2003), aquatic macrophytes and emergent vegetation ($n\mathrm{C}_{21}$-$n\mathrm{C}_{25}$) (Ficken et al., 2000), and vascular plants ($n\mathrm{C}_{25}$- $n\mathrm{C}_{33}$) (Cranwell et al., 1987; Eglinton and Hamilton, 1967) living around the lake. The distribution and concentration of *n*-alkyl lipids preserved in sediments can indicate relative inputs of autochthonous versus allochthonous organic matter and primary productivity. Here we use the $n\mathrm{C}_{18}$ alkanol as a general algal biomarker, as its presence and concentration was different than that of the other short chain *n*-alkanols ($n\mathrm{C}_{20\text{-}22}$). However, since terrestrial plants and bacteria also produce small amounts of the short chain compounds, we also examined dinosterol, $\mathrm{C}_{28}$-$\mathrm{C}_{30}$ 1, 15 *n*-alkyl diols, and brassicasterol as algal biomarkers.

#### 3.3.2.2 Sterols and stanols

Sterols are compounds present in all eukaryotes and act as membrane rigidifiers, and specific sterols are attributed to different phytoplankton groups (Volkman, 2003; Volkman, 1986). The sterols found in microalgae have a great diversity of structures and

these compounds are commonly used as biomarkers for diatoms and dinoflagellates (Volkman, 1986; Volkman et al., 1998; Volkman, 2003). Dinosterol (4α, 23, 24-trimethyl-5α-cholest-22-en-3β-ol) is found in many, but not all, dinoflagellate species (Volkman, 2003). Many sterols are synthesized by both terrestrial and aquatic plants but dinosterol is not (Volkman et al., 1999), making it useful for assessing changes in dinoflagellate productivity. Several sterols are used as biomarkers for diatoms. One of the most common sterols is the $C_{27}$ sterol cholesterol (cholest-5-en-3β-ol), which is often thought to be an animal sterol but is also highly prevalent in microalgae (Volkman, 2003). Generally the most abundant sterols in diatoms are $C_{28}$ sterols including brassicasterol or diatomsterol (24-methylcholesta-5,22-dien-3β -ol) and fucosterol (24-methylcholesta-5,24(28)-dien-3β-ol) (Rampen et al., 2010; Volkman, 2003). The $C_{29}$ sterols are often attributed to higher plants (Volkman 1986), but are also found in abundance in microalgae (Volkman, 2003). These include the compounds sitosterol, β-sitosterol (24-ethylcholest-5-en-3β-ol), and stigmasterol (Barrett et al., 1995; Rampen et al., 2010; Volkman et al., 1998). These compounds are not unambiguous diatom biomarkers as they can also be produced by other algal groups (Rampen et al., 2010; Volkman, 2003) in addition to terrestrial higher plants (Nishimura and Koyama, 1977).

#### 3.3.2.3 *n*-alkyl diols

Long chain ($C_{28}$- $C_{32}$) 1, 15 *n*-alkyl diols are produced by Eustigmatophyte (yellow-green) algae and are commonly found as constituents of marine sediments (Volkman et al., 1992). Recent research has found the $C_{32}$ 1, 15 *n*-alkyl diol to be exclusively produced in freshwater environments and can be used to track riverine input

to marine environments (de Bar et al., 2016; Lattaud et al., 2017a; Lattaud et al., 2017b). Long chain *n*-alkyl diols have also been noted in many lacustrine environments and are frequently found in high abundance (Castañeda et al., 2009 and references therein). The presence of these compounds in lacustrine settings is thought to indicate input from algae (Rampen et al., 2012), although other producers may exist in lakes (Castañeda and Schouten, 2011). These compounds have successfully been used to reconstruct variability in lacustrine primary productivity tracking climatic and environmental changes (Rampen et al., 2012).

#### 3.3.2.4 Hopanoids

Cyanobacteria are ubiquitous components of freshwater phytoplankton communities. These bacteria have been shown to produce 2-methylhopanoids and other hopanoid compounds bacteriohopanepolyols (BHPs) (Summons et al., 1999; Talbot et al., 2008), which may be applied as biomarkers. Hopanoids are pentacyclic triterpenoids produced by many prokaryotes as cell membrane components, which are thought to serve a rigidifying purpose and regulate the fluidity and permeability of cell membranes, similar to sterols in eukaryotes (Ourisson et al., 1987; Ourisson and Albrecht, 1992). Hopanoids are most abundant in aerobic bacteria (e.g. methanotrophs, heterotrophs, and cyanobacteria), are not found in Archaea, and are rare in eukaryotic organisms, so their presence can be interpreted as a general bacterial biomarker, while some BHPs can provide more specific markers (Talbot et al., 2008).

#### 3.3.2.5 GDGTs

Branched glycerol dialkyl glycerol tetraethers (brGDGTs) are membrane lipids thought to be produced by Acidobacteria (e.g., Sinninghe Damsté et al., 2011; Sinninghe Damsté et al., 2018). These compounds are found globally in soils, peats, and lakes (e.g. Weijers et al., 2007; Peterse et al., 2012; De Jonge et al., 2013; Buckles et al., 2014; De Jonge et al., 2015) and form the basis of the methylation of branched tetraethers (MBT) paleothermometer index (e.g. Weijers et al., 2007; De Jonge et al., 2015). At Lake El'gygytgyn, like other studied lakes (e.g. Miller et al., 2018), the majority of production is thought to occur within the water column. The MBT and MBT'5ME index (De Jonge et al., 2014a; Weijers et al., 2007) has been applied to examine past temperature fluctuations at Lake El'gygytgyn on a variety of timescales (D'Anjou et al., 2013b; de Wet et al., 2016; Holland et al., 2013; Keisling et al., 2016).

## 3.4 Methods

### 3.4.1 Bulk isotopes

802 Lake El'gygytgyn sediment samples were analyzed for bulk stable carbon ($\delta^{13}C$) and nitrogen ($\delta^{15}N$) isotopes of total organic carbon (TOC) and nitrogen (TON) every ~4 cm throughout the drill core. The samples were freeze dried and reacted with sulfurous acid (1 N $H_2SO_3$) remove any carbonates. An aliquot of each sample was weighed into a tin capsule, which was introduced to a Costech ECS140 CHN/S/O elemental analyzer coupled to a Thermo DeltaV+ isotope ratio mass spectrometer at the UMass Stable Isotope Laboratory. In house standards of caffeine and acetanilide were used to calculate values for $\delta^{15}N$ and $\delta^{13}C$. The standard values were calculated relative

to known values of international standards of Vienna Pee Dee Belemnite (VPDB) and ambient air. The combined error for standards and data presented here is 0.38‰ for $\delta^{15}N$ and 0.86‰ for $\delta^{13}C$. The isotopic results are presented in standard delta notation relative to VPDB for carbon and ambient air for nitrogen. Stable isotope analyses were not performed on the same samples as organic geochemical analysis.

### 3.4.2 Organic geochemical analyses

386 sediment samples (~1 to 6 grams dry weight) were selected for organic geochemical analysis at a resolution of ~one sample per 1.5 ka for the 600 kyr study interval. Mean sedimentation rates in Lake El'gygytgyn during the last 1.0 Ma are ~ 4cm $ka^{-1}$ (Nowaczyk et al., 2013), thus each 1 cm sample in this study integrates approximately 250 years. Freeze-dried, homogenized, samples were extracted using a Dionex Accelerated Solvent Extractor (ASE 200) with a mixture of dichloromethane (DCM)/ methanol (MeOH) (9:1, v/v) at a temperature of 100 $^{o}$C. The resulting total lipid extract (TLE) from each sediment sample was separated into apolar (9:1 DCM/hexane v/v) and polar (1:1 DCM/MeOH v/v) fractions using alumina oxide column chromatography. The polar fractions were evenly split into two fractions. One half of each sample was derivatized to their trimethylsilyl-ethers using bistrimethylsilyltrifluoroacetamide (BSTFA) with acenonitrile as a catalyst (1:1, v/v) and heated at 60 $^{o}$C for 30 minutes. The other half was analyzed for brGDGTs via HPLC-MS (Chapter 2).

Compound identification was performed using a Hewlett Packard 6890 series gas chromatograph with a Restek Rtx-5ms column (60 m x 250 μm ID and 0.25 μm film) coupled to an Agilent 5973 mass spectrometer (GC-MS). Mass spectra were measured

from 50 to 600 m/z and compounds were subsequently identified via their characteristic fragmentation patterns and retention times. In many of the samples analyzed for this study, the stanol versions of compounds were found exclusively, or in much higher concentration that the corresponding sterol (e.g. cholestanol vs. cholesterol). As the sediments analyzed are several hundred thousand years old, some slight degradation may have occurred in the form of a lost double bond. We assume the compounds had the same source organism and sum concentrations of sterols/stanols pairs to examine total abundance.

Quantification of compounds was performed on an Agilent 7890A dual gas chromatograph – flame ionization detector (FID) equipped with an Agilent 7693 autosampler and two 5% phenyl methyl siloxane Agilent HP-5 columns (60 m x 320 μm x 0.25 μm). For some samples, helium was used as the carrier gas and in other analyses hydrogen was the carrier gas due to laboratory upgrades that occurred mid-way through this project. Compounds were quantified using an external calibration curve where squalane was injected at multiple concentrations ranging from 2 to 100 ng/μl. $R^2$ values for linearity tests were >0.99. All oven programs are reported in Table 3.1.

Several ratios/indices exist for describing the distribution of *n*-alkyl lipids. Three of these are applied to the *n*-alkanes measured here. The formulas are as follows:

Average Chain Length (ACL)

$$\mathrm{ACL} = \frac{21n\mathrm{C}_{21} + 23n\mathrm{C}_{23} + 25n\mathrm{C}_{25} + 27n\mathrm{C}_{27} + 29n\mathrm{C}_{29} + 31n\mathrm{C}_{31}}{n\mathrm{C}_{21} + n\mathrm{C}_{23} + n\mathrm{C}_{25} + n\mathrm{C}_{27} + n\mathrm{C}_{29} + n\mathrm{C}_{31}}$$

Terrestrial to Aquatic Ratio (TAR)

$$\mathrm{TAR} = \frac{\mathrm{C}_{27} + \mathrm{C}_{29} + \mathrm{C}_{31}}{\mathrm{C}_{19} + \mathrm{C}_{21} + \mathrm{C}_{23}}$$

Carbon Preference Index (CPI)

$$\mathrm{CPI} = \frac{C_{23} + 2 \times (C_{25} + C_{27} + C_{29} + C_{31})}{C_{33} + 2 \times (C_{24} + C_{26} + C_{28} + C_{30} + C_{32})}$$

### 3.4.3 Time Series Analysis

To determine the spectral characteristics of our primary productivity and organic matter preservation records, we used Mann and Lees (1996) robust red noise multi-taper-method (MTM) analysis in the Astrochron R program (Meyers, 2012), which has significant statistical power for identifying frequencies in the obliquity, precession, and eccentricity bands (Meyers, 2012, 2014). As in Chapter 2, time series analysis was carried out in both the depth and age domain in order to avoid circularity with assumptions made in age model development. The data were pre-whitened using the Lowspec method in Astrochron (Meyers, 2012). All data was interpolated to a 2 ka sampling resolution.

## 3.5 Results

### 3.5.1 Bulk sediment carbon, nitrogen, and isotopes

Total organic carbon (TOC) values range from 0.1 to 1.6% with an average of 0.4 (Figure 3.2). Total nitrogen (TN) values range from 0.03 to 0.1% with an average of 0.05% (Figure 3.2). Values for the carbon to nitrogen (C/N) ratio range from 3 to 22 with an average of 8 (Figure 3.2). Unfortunately, after bulk carbon and nitrogen measurements were completed (prior to these authors taking over work on these samples), data for much of the study interval were lost due to computer malfunction and lack of backup. The remaining data, presented here, spans the interval of 800 ka to 588 ka and 441 ka to 424

ka. $\delta^{13}C$ values range from -23‰ to -35‰, with an average of 28‰ (Figure 3.2). $\delta^{15}N$ values range from -1‰ to 5‰, with an average of 3‰ (Figure 3.2).

### 3.5.2 Algal biomarkers

Compounds identified include cholesterol, cholestanol, β-sitosterol, β-sitostanol, sitostanol, sitosterol, $C_{28}$ to $C_{32}$ 1,15 *n*-alkyl diols, 24-methyl cholestanol, dinosterol, dinostanol, brassicasterol and $C_{28}$ and $C_{30}$ hopanols (Figure 3.3). These compounds were present to varying degrees in samples throughout the record. The range of algal lipid concentrations are reported in Table 3.2. Given the microfossil evidence for a diverse and thriving diatom community in Lake El'gygytgyn (Snyder et al., 2013), we searched for diatom biomarkers including diatomsterol, loliolide, isololiolide, gorgesterol, and fucoxanthin, all of which are molecular indicators for diatom species (Rampen et al., 2010). Interestingly, we were unable to identify these diagnostic diatom biomarkers in our samples except for brassicasterol, which was identified in a few samples.

In all samples, the alkanols $nC_{18}$-$C_{30}$ were identified (Figure 3.4). These compounds displayed a strong even-over-odd predominance with the most abundant chain length being the $nC_{26}$ or $nC_{28}$ alkanol, suggesting a predominantly terrestrial source for these compounds. However, the $nC_{18}$ alkanol displayed different variations and was significantly more abundant than the other short chain alkanols. Therefore, we interpret this compound as a general authochthonous productivity biomarker similar to the other algal lipids.

Similarly to the *n*-alkanols in the polar fraction, straight chain *n*-alkanes in the apolar fraction were present in all samples (Figure 3.4). Although a large unresolved

complex mixture was present in some samples obscuring the shorter chain length compounds, $n$C$_{23}$ to $n$C$_{33}$ were resolved in most samples. The alkanes have a strong odd-over-even predominance suggesting a terrestrial source and minimal degradation. CPI values 0.5 to 8. The most abundant *n*-alkane is generally $n$C$_{27}$ or $n$C$_{29}$ and the average chain length (ACL) (C$_{27}$-C$_{33}$) averages 29.4. Variations in ACL between 200 and 800 ka have been attributed to terrestrial vegetation turnover associated with changes in aridity and temperature (Chapter 2). Here, we use *n*-alkane and *n*-alkanol abundances to represent contributions of terrestrial organic matter to Lake El'gygytgyn sediments (Figure 3.4).

Concentrations of branched GDGTs and crenarcheol were measured by Habicht et al. (Chapter 2). These compounds are thought to be primarily produced in the water column at Lake El'gygytgyn and so are reported and interpreted here as autochthonous bacterial markers (Figure 3.3).

### 3.6 Discussion

The ~600 kyr long record presented here spans multiple glacial-interglacial cycles which are diverse and have variations in strength, timing, length, and forcing factors (Lang and Wolff, 2011; Past Interglacials Working Group of PAGES, 2016). Although these cycles are global climate events, their expression varies regionally and can be proxy dependent (Lang and Wolff, 2011; Past Interglacials Working Group of PAGES, 2016). Proxy records of primary productivity are often used to reconstruct paleoclimate variability, with increased production generally associated with warm intervals (Prokopenko et al., 2001). Previous studies of Lake El'gygytgyn have analyzed productivity using the ratio of silica to titanium (Melles et al., 2012), percentage of

biogenic silica (Meyer-Jacob et al., 2014), diatom counts (Snyder et al., 2013), and organic biomarkers (D'Anjou et al., 2013b; Holland et al., 2013). These records provided evidence for significant variability in productivity associated with glacial-interglacial cycles. Highly productive "super interglacials" were identified throughout the Lake El'gygytgyn record but there is also some evidence for high productivity during glacial periods (Holland et al., 2013; Melles et al., 2012, 2007; Meyer-Jacob et al., 2014; Snyder et al., 2013). However, these records primarily focus on diatoms, which are only one of several algal groups that may have been important primary producers in Lake El'gygytgyn. In the following sections we discuss organic matter sources (allochthonous and autochthonous), glacial-interglacial shifts in algal communities, and changes in the production and preservation of organic matter.

### 3.6.1 Ice cover changes

Variations in TOC, TN, the C/N ratio and $\delta^{13}C$ values all record similar patterns, suggesting a shared control/mechanism. TOC values are low due to the oligotrophic nature of the lake, as has been noted by previous measurements of TOC in Lake El'gygytgyn sediments (Melles et al., 2012, 2007). Peaks in TOC occur during both glacial and interglacial periods, suggesting that both preservation and production control this signal (see next section) (Figure 3.2). TN values are generally low, reflecting limited terrigenous and nutrient input(Figure 3.2). The C/N ratio has a wide range and likely records relatively greater or smaller contributions of autochthonous and allochthonous organic matter. Changes in the C/N ratio values are driven by changes in the TOC and TN. These three records change concurrently, with high TOC, TN and C/N occurring simultaneously(Figure 3.2). These patterns are also recorded in the $\delta^{13}C$ record(Figure

3.2). Clear glacial-interglacial variations are lacking from the $\delta^{15}N$ record (Figure 3.2). Depleted and enriched $\delta^{15}N$ values occur during both cold and warm intervals and do not clearly mirror any of the other bulk sediment proxy variations, likely due to the complexity of variables influencing nitrogen isotopes in lakes (e.g. Birks et al., 2012 and references therein).

The mean $\delta^{13}C$ value is 28‰, suggesting a predominant carbon source of terrestrial vegetation (Meyers and Ishiwatari, 1993). This supports the conclusions of Holland et al. (2013) that most of the organic matter preserved in Lake El'gygytgyn sediments has an allochthonous source (discussed below). Negative $\delta^{13}C$ excursions from the mean have previously been interpreted in other Lake El'gygytgyn studies as occurring during periods of extensive perennial ice cover when terrestrial OM input is reduced, the lake becomes stratified, and methanogenesis in anoxic bottom waters is enhanced (Melles et al., 2007). $^{13}C$ depleted values presented here generally correspond to intervals of high TOC% (Figure 3.2). There is not a clear glacial-interglacial pattern of variation, but the most depleted $\delta^{13}C$ values occur during glacial periods. Although methanogenesis associated with water column anoxia is thought to produce the more depleted $\delta^{13}C$ values, little evidence of this process has been found in Lake El'gygytgyn. Holland et al. (2013) found no clear sign of it in their analysis of the last 60 ka, and at least the upper water column likely remained oxygenated for several glacial-interglacial cycles evidenced by the existence of an established salmonid species (Nolan and Brigham-Grette, 2007) and the presence of vivianite nodules (Minyuk et al., 2006). Instead, Holland et al. (2013) suggest continued recycling of $CO_2$ from oxidized and

degraded organic matter back to aquatic primary producers with limited atmospheric $CO_2$ exchange during glacial periods.

Whether or not methanogenesis occurs in the lake and is reflected in the $\delta^{13}C$ record , we interpret the depleted carbon isotope values as periods of perennial lake ice cover. Most of the depleted $\delta^{13}C$ values correspond to the presence of sediment facies A (Figure 3.2), which was interpreted to be deposited during bottom water anoxia under perennial ice cover (Melles et al., 2012). During these periods, terrestrial organic matter input is effectively reduced. This is reflected in the terrestrial to aquatic ratio (TAR) values calculated from *n*-alkane distributions (Figure 3.4). Low TAR values are representative of enhanced aquatic organic matter contributions, while higher values reflect greater contributions from the terrestrial environment. Throughout the record, low TAR values correspond to intervals of depleted $\delta^{13}C$ (Figure 3.4). Holland et al. (2013) also note relative abundances of autochthonous organic matter increased during cold periods. Interestingly, high C/N ratios also occur during intervals of depleted $\delta^{13}C$ (Figure 3.2). This seems counterintuitive as high C/N ratios are generally interpreted to represent high terrestrial OM input. However, the C/N ratio can be influenced by a number of factors and likely in this case is not directly representing autochthonous vs allochthonous contributions to the sediment. The higher C/N ratios may be due to nitrogen limitation under perennial ice cover as algal growth under nitrogen limited conditions can yield C/N ratios as high as 20 (Healey and Hendzel, 1980; Hecky, 1993).

Overall, changes in TOC and TN, the C/N ratio and $\delta^{13}C$ all show similar patterns of variation, whereas the $\delta^{15}N$ record does not. This suggests the former proxies are all

responding to the same climatic forcing or mechanism, e.g. perennial lake ice cover/absence while the latter is driven by something else.

### 3.6.2 Organic matter sources in Lake El'gygytgyn

Organic matter in lake sediments can have varying sources through time due to changes in autochthonous primary production, input from allochthonous sources in the catchment area, as well as the relative amounts of particulate and dissolved material delivered to the lake. Organic matter can also undergo partial and differential degradation as it is incorporated into the lake sediments. Thus, TOC concentration and its stable isotopic composition may reflect a variety of environmental parameters .

TOC concentrations throughout the Pleistocene glacial-interglacial cycles are low, ranging from 1-2%, with peaks noted during both glacial and interglacial periods suggesting a mixed signal of organic matter production and preservation (Melles et al., 2012, 2007) (Figure 3.2). Compound specific stable isotope analysis of Lake El'gygytgyn sediments spanning the last 60 ka suggests most of the organic matter in the lake is of a terrestrial origin, with a secondary aquatic source, and negligible microbial production sources (Holland et al., 2013). Interestingly, this dominance of terrestrial organic matter continues during glacial periods, when the lake was perennially ice covered and terrestrial vegetation productivity was likely limited by the extremely cold and arid climatic conditions. Continual contributions of terrestrial organic matter is also evidenced by the constant presence of pollen in Lake El'gygytgyn sediments throughout glacial intervals (Lozhkin et al., 2007a). However, a mechanism for terrestrial OM input remains

unclear but formation of a shallow ice moat during glacial summers for allochthonous material input has been proposed (Nolan and Brigham-Grette, 2007).

Autochthonous OM sources were found to be consistently secondary to allochthonous OM, but are the greatest during peak glacial conditions (Holland et al., 2013). As previously noted, the TAR of *n*-alkanes suggests increased relative contributions of autochthonous organic matter during periods of perennial ice cover. Increased diatom productivity has also been noted during some glacial periods (Snyder et al., 2013). Our results agree with previous findings, indicating that most of the organic material in Lake El'gygytgyn sediments is of terrestrial origin a(D'Anjou et al., 2013b; Holland et al., 2013)c. Total concentrations of the suites of aliphatic hydrocarbons representing allochthonous OM are often an order of magnitude greater than the autochthonously sourced compounds (Figure 3.4). $\delta^{13}C$ values average 28‰, suggesting a generally terrestrial source carbon. Depleted $\delta^{13}C$ values likely result from organic matter recycling by aquatic primary producers under perennial ice cover limiting atmospheric $CO_2$ exchange (Holland et al., 2013) and limited input of terrestrial organic material. C/N ratios, often used to assess relative contributions of authochthonous and allochthonous organic matter are ambiguous. The C/N ratio is highest (generally suggesting terrestrial OM input) during glacial periods when the lake is thought to be perennially ice covered.

### 3.6.3 Organic matter production and preservation

We find aquatic and terrestrial compound abundances generally correspond to changes in %TOC with higher compound concentrations occurring during intervals of

elevated %TOC during both glacial and interglacial periods (Figure 3.3). Many of the intervals of highest %TOC and aquatic compound concentrations also coincide with intervals of elevated percent biogenic silica (Figure 3.3). This suggests aquatic primary production is recorded by the algal biomarker concentrations. However, high TOC and biomarker concentrations also occur during intervals when biogenic silica is low, suggesting increased preservation is occurring. Indeed, many of the peaks in %TOC (and organic compounds) correspond to intervals of low Mn/Fe, a proxy for bottom water oxygenation (Melles et al., 2012, 2007) (Figure 3.3). Therefore we infer that these peaks in TOC and biomarker concentrations are reflecting enhanced organic matter preservation under anoxic bottom water conditions. Significant aquatic production may also occur during glacial periods under ice cover, as the limiting factor for productivity is not ice thickness, but light limitation due to snow cover (Gore, 1997). Thus, during arid glacials when little snow cover is present, it is hypothesized that aquatic producers were active in Lake El'gygytgyn, whereas during wetter cold periods with more snow, production was limited (Melles et al., 2007).

These patterns are logical but make interpretation of organic matter production versus preservation difficult. The two processes are coupled, in that increased aquatic productivity reduces oxygen in the water column and results in enhanced preservation. For example, we note high TOC and biomarker concentrations during MIS 12 coupled with low Mn/Fe ratios and depleted $\delta^{13}C$ values and low biogenic silica (Figure 3.2 and 3.3). Additionally, MIS 12 is interpreted as a particularly arid glacial period, reflected by high *n*-alkane average chain lengths, (Chapter 2) and snow cover was likely limited. Therefore, some autochthonous productivity under snow-free perennial ice cover and

enhanced preservation under anoxic conditions likely produced the high TOC and biomarker concentrations. As an interglacial example, in MIS 17 high TOC and biomarker concentrations are concurrent with high biogenic silica and high Mn/Fe suggesting a larger component of authochthonous productivity during this interval (Figure 3.2 and 3.3).

### 3.6.4 Productivity response to temperature

Many modern studies of Arctic lakes suggest increased productivity and changes in dominant primary producers associated with warming in recent years (e.g. Veillette et al., 2010; Woelders et al., 2018). However, our data suggest that organic matter production and preservation in the paleorecord at Lake El'gygytgyn is not driven by changes in summer temperature. Concentrations of organic compounds do not show a clear correspondence to temperature (Figure 3.5). Peak abundances occur during glacial and interglacial periods and do not generally seem to respond to temperature fluctuations recorded by the brGDGT paleothermometer, interpreted as relative record for summer temperature, (Chapter 2) measured on the same samples (Figure 3.5). For example, during MIS 7 when brGDGT temperatures are highest, there is little to no change in biomarker concentrations, whereas during MIS 11, when moderate temperatures are reconstructed, there is a large increase in biomarker concentrations (Figure 3.5). There are also high abundances of compounds preserved during MIS 12 when temperatures are relatively cold. This is in contrast to the conclusions of D'Anjou et al. (2013) who note generally higher abundances of algal lipids during warm interglacial periods MIS 11 and 9 but agrees with Holland et al. (2013) who noted high aquatic biomarker concentrations during both interglacials and glacials. Other records of productivity from Lake

El'gygytgyn based on diatoms and biogenic silica have indicated significant increases in productivity associated with ultra-warm "super interglacials", such as MIS 11 (Melles et al., 2012; Meyer-Jacob et al., 2014; Snyder et al., 2013). Although biomarker concentrations are high during MIS 11, it is not outstanding when compared to the rest of the record, nor are reconstructed temperatures particularly high (Chapter 2). Thus, we caution that biogenic silica records should not be interpreted as a proxy for temperature change as has been done by previous studies (e.g. Melles et al., 2007, 2012; Brigham-Grette et al., 2013). Overall, the lack of correspondence between temperature and the biomarker concentrations is an interesting result with implications for what may happen in Arctic lakes under anthropogenic climate warming.

### 3.6.5 Ecological succession in autochthonous primary producers

Previous studies of Lake El'gygytgyn primary producers have focused exclusively on diatoms (Cherapanova et al., 2006; Snyder et al., 2013). Although diatoms are a major component the algal community in Arctic lakes, crysophytes, dinoflagellates, cyanobacteria, green algae, and other aquatic biota are also significant (Pienitz et al., 2004). Here we attempt to identify ecological succession of these different algal classes using biomarker distributions. Unfortunately, diagnostic biomarkers for these different classes were relatively few in our samples. Particularly interesting is the general lack of specific diatom biomarkers. Diatom assemblage analysis indicates turnover in the dominant species of diatoms through time, but suggests they are perpetually present in the lake. It is unclear why their specific diagnostic biomarkers would be absent from the same sediments. Due to the lack of diatom specific biomarkers, we apply

sitosterol/stanol (which was present in most samples) as a more general marker attributed to diatoms

Despite the scarcity of specifically diagnostic biomarkers, we were able to identify at least one biomarker for several biota classes. Sitosterol/stanol and β-sitostanol and brassicasterol/stanol, dinosterol/stanol, long chain $C_{28}$ to $C_{30}$ 1, 15 *n*-alkyl diols, and $C_{28}$ and $C_{30}$ hopane/hopanol were used to represent diatoms, dinoflagellates, green algae, and cyanobacteria respectively. We calculated a fractional abundance of each compound class and infer this to represent the relative contribution of each algal group (Figure 3.6). We note that for the majority of samples (during glacials and interglacials), the diatom biomarkers (dominated by sitosterol/stanol) are the largest autochthonous component, supporting previous studies that found high concentrations of diatoms during glacial and interglacial time periods (Cherapanova et al., 2006; Snyder et al., 2013) (Figure 3.6). The diatom biomarkers are followed in dominance by the long chain diols, suggesting that green algae may have been a dominant primary producer during some periods of Lake El'gygytgyn's history. The next group is the dinoflagellate biomarkers. These markers are present in similar abundance during both glacial and interglacial periods, suggesting they were not responsive to temperature changes or wind driven mixing during ice free conditions (Figure 3.6). Interestingly, the hopanoid biomarkers seem to predominate when other groups are not present, which suggests cyanobacteria may be the dominant producer when other groups are absent or reduced (Figure 3.6). Overall, this analysis indicates turnover in the dominant authochthonous primary producer occurred throughout the study interval. However, it is difficult to discern any clear glacial-interglacial patterns of ecological succession. The changes do not appear to be clearly linked with biogenic

silica, although higher fractional abundances of diatom biomarkers generally occur during high biogenic silica intervals, supporting the important role of diatoms as primary producers at Lake El'gygytgyn (Figure 3.6). Many of the periods when all four types of biomarkers are present occur during intervals of elevated TOC (Figure 3.6). This suggests the apparent changes in diversity/predominance of one producer over another could instead be associated with the degree of organic matter preservation. The lack of strong glacial-interglacial pattern implies that throughout the paleorecord, neither temperature, nor ice cover were responsible for major shifts in the algal community structure. This is interesting, because today, rising temperature and reduced ice cover are thought to have the strongest impact on Arctic algal community structure (Flanagan et al., 2003; Griffiths et al., 2017; Veillette et al., 2010; Woelders et al., 2018). Therefore, we speculate that other factors such as changes in nutrient supply or wind patterns will have a greater impact on autochthonous primary production and algal community composition.

### 3.6.6 Orbital forcing of productivity and preservation

Time series analysis of TOC, biogenic silica, bulk sediment $\delta^{13}C$, the concentration of the long chain $n C_{25}$ to $n C_{33}$ alkanes, and the concentration of the $C_{18}$ *n*-alkanol was performed. These variables were selected to assess orbital forcing controls on organic matter preservation, production, lake ice cover, allochthonous productivity, and autochthonous productivity, respectively.

The time series analysis of the geochemical proxies TOC, biogenic silica, and $\delta^{13}C$ indicates orbital frequencies preserved in each of the records. TOC and $\delta^{13}C$ are predominantly controlled by precession (0.04 cycles/kyr) (19 and 23 kyr), while biogenic silica is influenced by both obliquity (0.02 cycles/kyr) (41 kyr) and precession (Figure

3.7). This suggests that the intensity of Arctic summers (precession) controls the extent of ice cover, organic matter production, and preservation. The length of the summer season (obliquity) also influences authochthonous, specifically diatom, productivity.

Time series analysis of the representative autochthonous and allochthonous productivity biomarkers suggests terrestrial and aquatic productivity respond to different orbital parameters. The concentration of allochthonous biomarkers (long chain *n*-alkanes) is predominantly controlled by obliquity (Figure 3.8). This suggests that the length of the summer season controls the productivity of terrestrial vegetation. The dominant frequency preserved by the autochthonous primary producers, represented by the $nC_{18}$ alkanol concentrations, is precession (Figure 3.8). Interestingly, obliquity is not a strong component of this record despite it being a significant control on the biogenic silica record. Therefore, it seems that for at least some of the algal primary producers, the intensity of the summer season is the sole significant influence.

### 3.7 Conclusions

Algal lipid concentrations and bulk sediment stable isotopes were used to assess changes in autochthonous and allochthonous primary productivity and sedimentary organic matter sources and preservation during the Mid-Pleistocene. Overall, we note that allochthonous sources are the dominant contributor to Lake El'gygytgyn sediments. Biomarkers from autochthonous algal sources were much less abundant, but formed a larger component during glacial periods. Changes in algal community structure occur throughout the record, but are not clearly linked to glacial-interglacial climatic shifts. However, time series analysis suggests the importance of orbital forcing on organic matter production and preservation in the terrestrial Arctic.

### 3.8 Acknowledgements

MHH thanks William Daniels and Addie Rose Holland for helpful conversations. David Finkelstein, Devon Colcord, and Amy Goodman are recognized for their work performing the bulk stable isotope measurements. Jeffrey Salacup is thanked for his technical lab assistance. Julie Chessia and Geoffrey Small are appreciated for their efforts in biogeochemical sample preparation and analysis. Funding support for this study was provided by NSF Grant #1204087 to Brigham-Grette, Castañeda, and Burns. Data from this publication will be archived on the NOAA Paleoclimate Database.

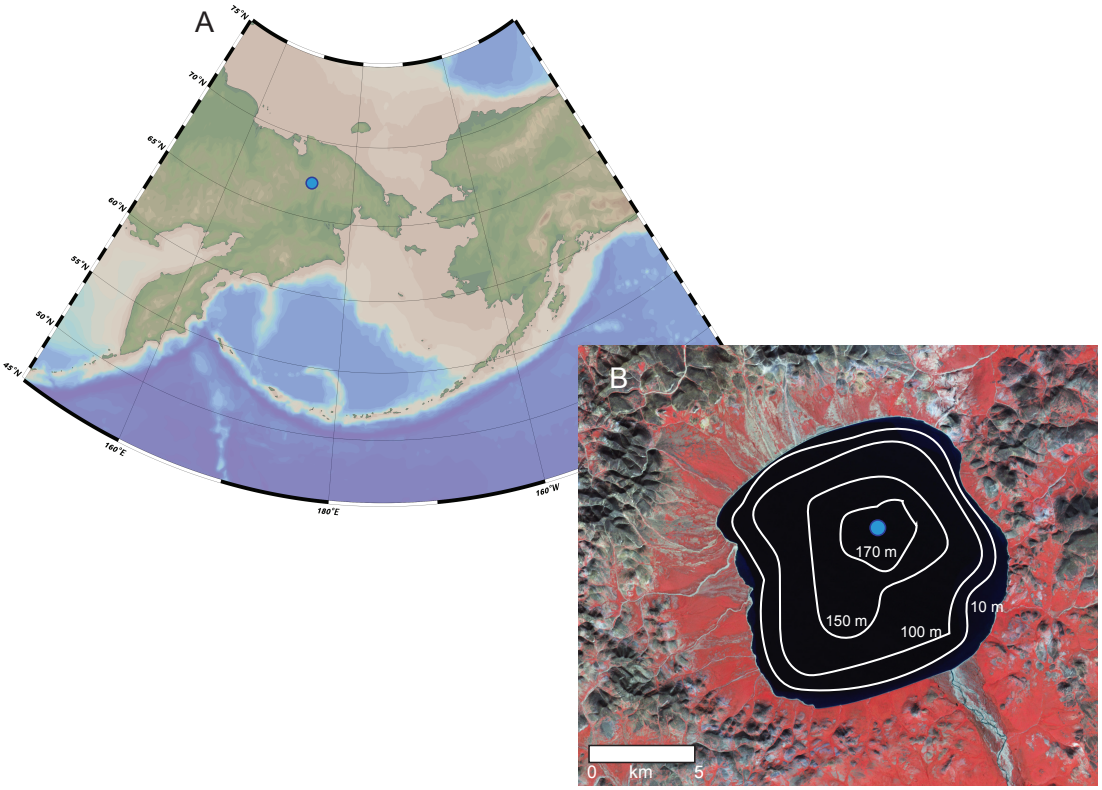


**Figure 3.1 Location of Lake El'gygytgyn. A) Lake El'gygytyn is designated by the blue dot in panel. B) Local topography and bathymetry of Lake El'gygytgyn (NASA, 2008). Core site for ICDP 5011 drilling is designated by the blue dot.**

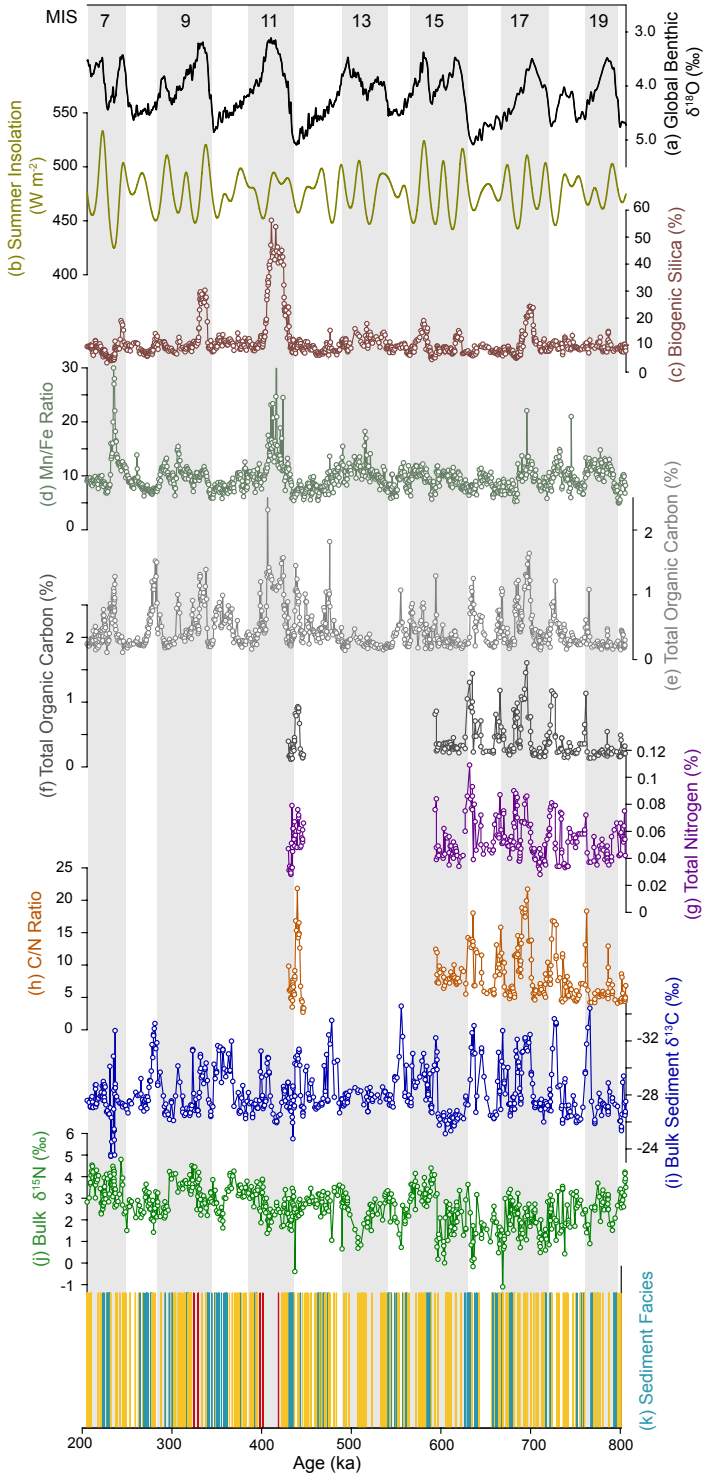
MIS
7
9
11
13
15
17
19
(a) Global Benthic δ18O (‰)
3.0
4.0
5.0
(b) Summer Insolation (W m-2)
550
500
450
400
(c) Biogenic Silica (%)
60
50
40
30
20
10
0
(d) Mn/Fe Ratio
30
20
10
0
(e) Total Organic Carbon (%)
2
1
0
(f) Total Organic Carbon (%)
2
1
0
(g) Total Nitrogen (%)
0.12
0.1
0.08
0.06
0.04
0.02
0
(h) C/N Ratio
25
20
15
10
5
0
(i) Bulk Sediment δ13C (‰)
-32
-28
-24
(j) Bulk δ15N (‰)
6
5
4
3
2
1
0
-1
(k) Sediment Facies
200
300
400
500
600
700
800
Age (ka)

**Figure 3.2 Lake El'gygytgyn bulk sediment stable isotopes and sedimentological properties. A) Global benthic oxygen isotope stack (Lisiecki and Raymo, 2005). B) June insolation at 65 $^{o}$N (Laskar et al., 2004). C) Biogenic silica (Meyer-Jacob et al., 2014). D) Manganese to iron ratio (Melles et al., 2012). E) Total organic carbon (Melles et al., 2012). F) Total organic carbon. G) Total Nitrogen. H) Carbon to nitrogen ratio. I) Bulk sediment $\delta^{13}$C. J) Bulk sediment $\delta^{15}$N. K) Sediment Facies A (blue), B (yellow), and C (red) (Melles et al., 2012).**

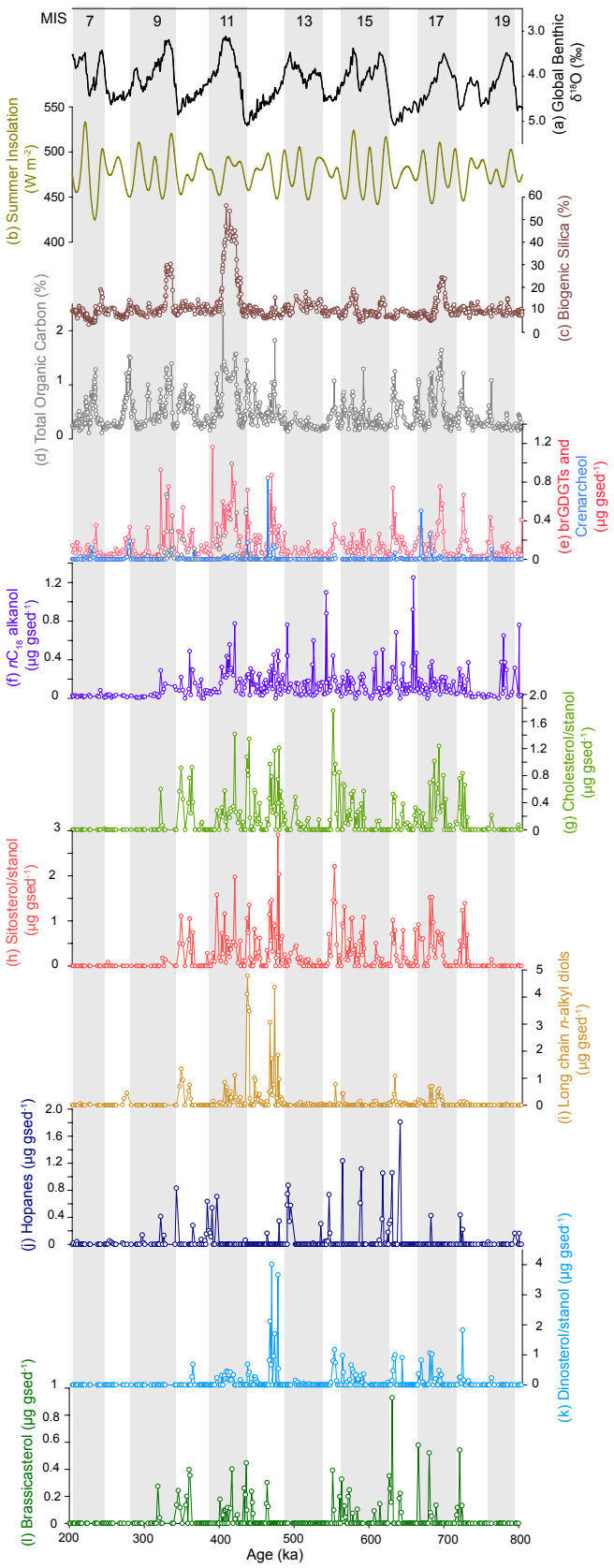
MIS
7
9
11
13
15
17
19
(a) Global Benthic δ18O (‰)
3.0
4.0
5.0
(b) Summer Insolation (W m-2)
550
500
450
400
(c) Biogenic Silica (%)
60
50
40
30
20
10
0
(d) Total Organic Carbon (%)
2
1
0
(e) brGDGTs and Crenarcheol (µg gsed-1)
1.2
0.8
0.4
0
(f) nC18 alkanol (µg gsed-1)
1.2
0.8
0.4
0
(g) Cholesterol/stanol (µg gsed-1)
2.0
1.6
1.2
0.8
0.4
0
(h) Sitosterol/stanol (µg gsed-1)
3
2
1
0
(i) Long chain n-alkyl diols (µg gsed-1)
5
4
3
2
1
0
(j) Hopanes (µg gsed-1)
2.0
1.6
1.2
0.8
0.4
0
(k) Dinosterol/stanol (µg gsed-1)
4
3
2
1
0
(l) Brassicasterol (µg gsed-1)
1
0.8
0.6
0.4
0.2
0
200
300
400
500
600
700
800
Age (ka)

**Figure 3.3 Lake El'gygytgyn aquatic biomarker concentrations. A) Global benthic oxygen isotope stack (Lisiecki and Raymo, 2005). B) June insolation at 65 $^{o}$N (Laskar et al., 2004). C) Biogenic silican (Meyer-Jacob, 2014). D) Total organic carbon (Melles et al., 2012). E) Concentration of total brGDGTs (pink) and isoprenoid GDGT crenarcheol (blue). Grey points come from D'Anjou et al. (2013). F) Concentration of *n*$C_{18}$ alkanol. G) Summed concentrations of cholesterol and cholestenol, H) sitosterol and sitostanol, I) , $C_{28}$ to $C_{32}$, 15 *n*-alkyl diols, J) $C_{28}$ and $C_{30}$ hopane and hopanol, K) dinosterol and dinostanol, L) brassicasterol.**

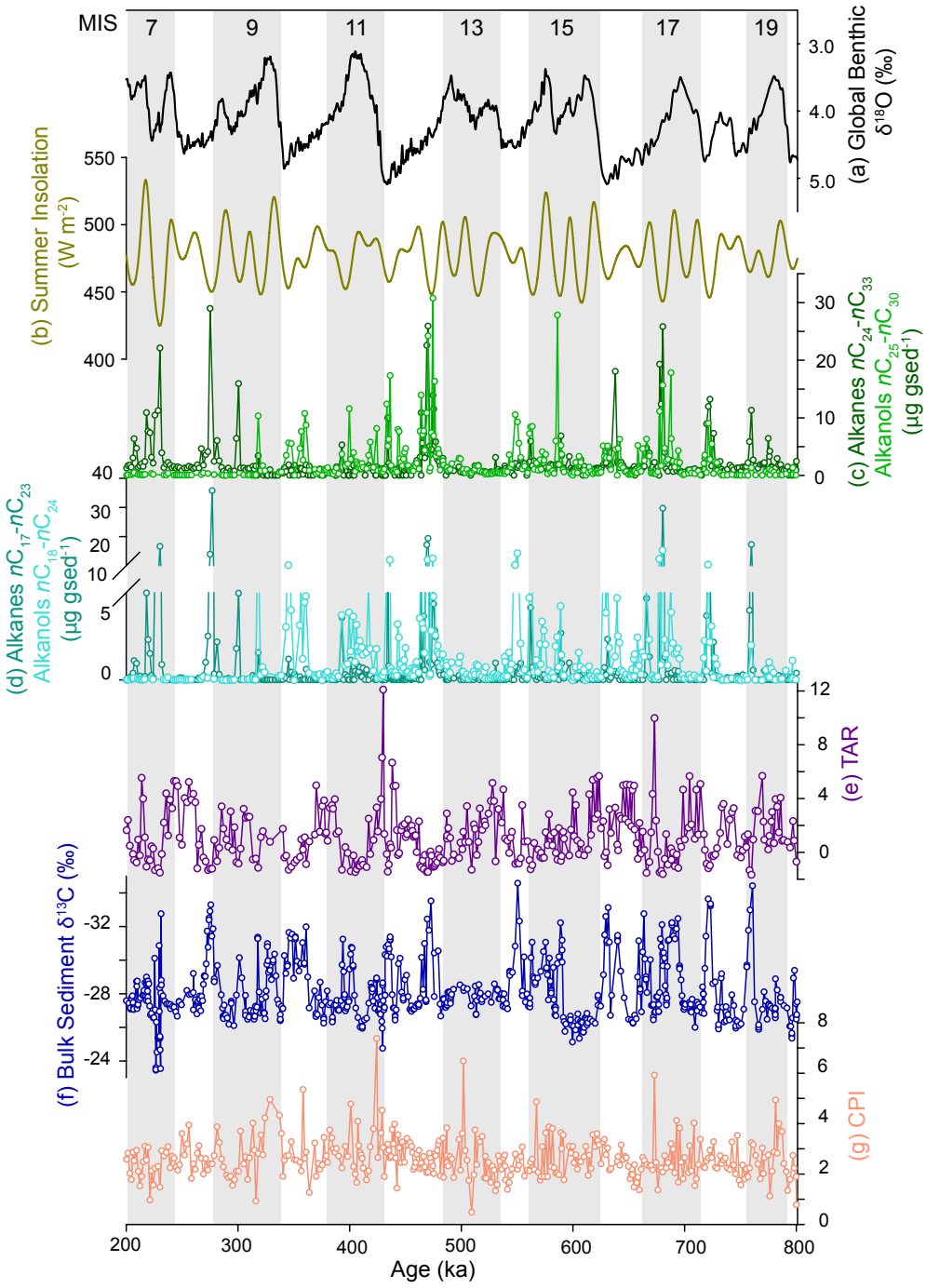
MIS
7
9
11
13
15
17
19
(a) Global Benthic $\delta^{18}O$ (‰)
3.0
4.0
5.0
(b) Summer Insolation (W m$^{-2}$)
550
500
450
400
(c) Alkanes $nC_{24}$-$nC_{33}$
Alkanols $nC_{25}$-$nC_{30}$
(µg gsed$^{-1}$)
30
20
10
0
40
(d) Alkanes $nC_{17}$-$nC_{23}$
Alkanols $nC_{18}$-$nC_{24}$
(µg gsed$^{-1}$)
30
20
10
5
0
(e) TAR
12
8
4
0
(f) Bulk Sediment $\delta^{13}C$ (‰)
-32
-28
-24
(g) CPI
8
6
4
2
0
200
300
400
500
600
700
800
Age (ka)

**Figure 3.4 Lake El'gygytgyn *n*-alkyl lipid biomarker concentrations and ratios. A) Global benthic oxygen isotope stack (Lisiecki and Raymo, 2005). B) June insolation at 65 $^{o}$N (Laskar et al., 2004). C) Concentration of total long chain $n$C$_{24}$-$n$C$_{33}$ alkanes (dark green) and total long chain $n$C$_{25}$-$n$C$_{30}$ alkanols (light green). D) Concentration of total short and mid chain $n$C$_{17}$-$n$C$_{23}$ alkanes (teal) and total short and mid-chain $n$C$_{18}$-$n$C$_{24}$ alkanols (aqua). E) Terrestrial to aquatic ratio of *n*-alkanes. F) Bulk sediment $\delta^{13}$C G) Carbon preference index (CPI) ratio of *n*-alkanes.**

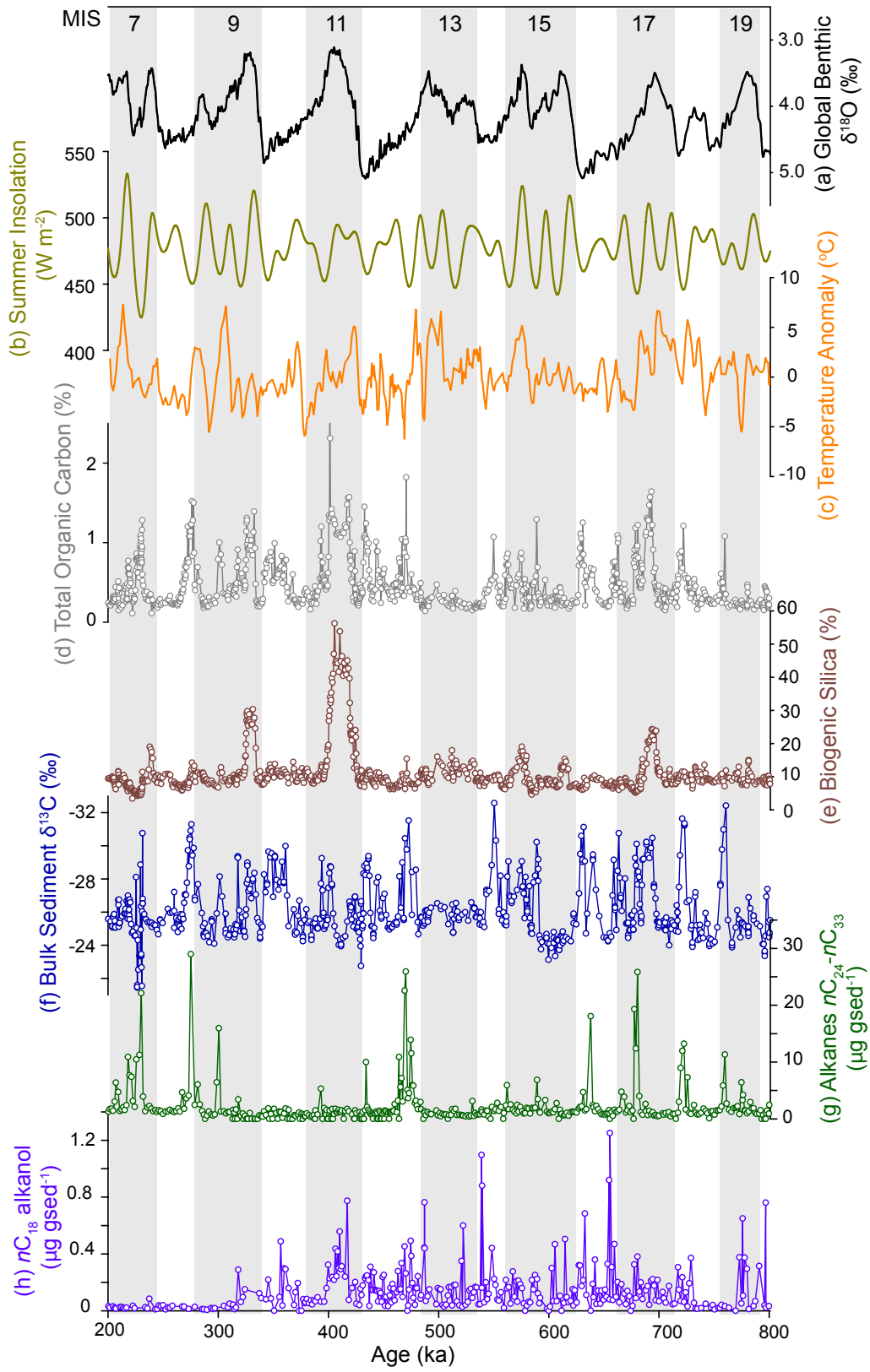
MIS
7
9
11
13
15
17
19
(a) Global Benthic δ18O (‰)
3.0
4.0
5.0
(b) Summer Insolation (W m-2)
550
500
450
400
(c) Temperature Anomaly (°C)
10
5
0
-5
-10
(d) Total Organic Carbon (%)
2
1
0
(e) Biogenic Silica (%)
60
50
40
30
20
10
0
(f) Bulk Sediment δ13C (‰)
-32
-28
-24
(g) Alkanes nC24-nC33 (µg gsed-1)
30
20
10
0
(h) nC18 alkanol (µg gsed-1)
1.2
0.8
0.4
0
200
300
400
500
600
700
800
Age (ka)

**Figure 3.5 Autochthonous and allochthonous biomarkers and sediment geochemistry. A) Global benthic oxygen isotope stack (Lisiecki and Raymo, 2005). B) June Insolation at 65oN (Laskar et al., 2004). C) Temperature anomaly from brGDGTs (Chapter 2). D) Total organic carbon (Melles et al., 2012). E) Biogenic silica (Meyer-Jacob et al., 2014). F) Bulk sediment $\delta^{13}C$. G) Concentration of summed long chain $n$-$C_{24}$-$n$-$C_{33}$ alkanes. H) Concentration of $n$-$C_{18}$ alkanol.**

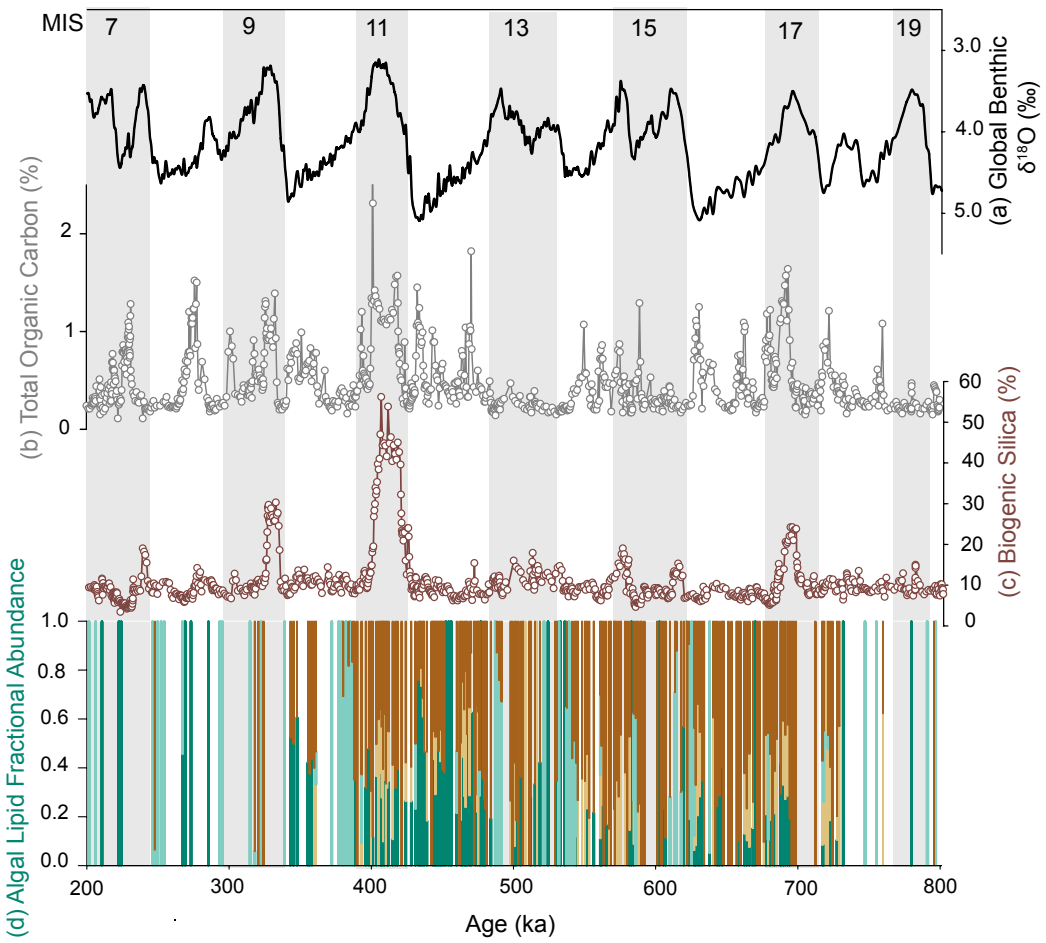


**Figure 3.6 Autochthonous lipid fractional abundances. A) Global benthic oxygen isotope stack (Lisiecki and Raymo, 2005). B) Total organic carbon (Melles et al., 2012). C) Biogenic silica (Meyer-Jacob, 2014). D) Fractional abundance of autochthonous lipids. Long chain $C_{28}$ to $C_{30}$ 1,15 *n*-alkyl diols (teal), dinosterol/stanol (tan), hopane and hopanol (aqua), and brassicasterol/stanol (brown).**

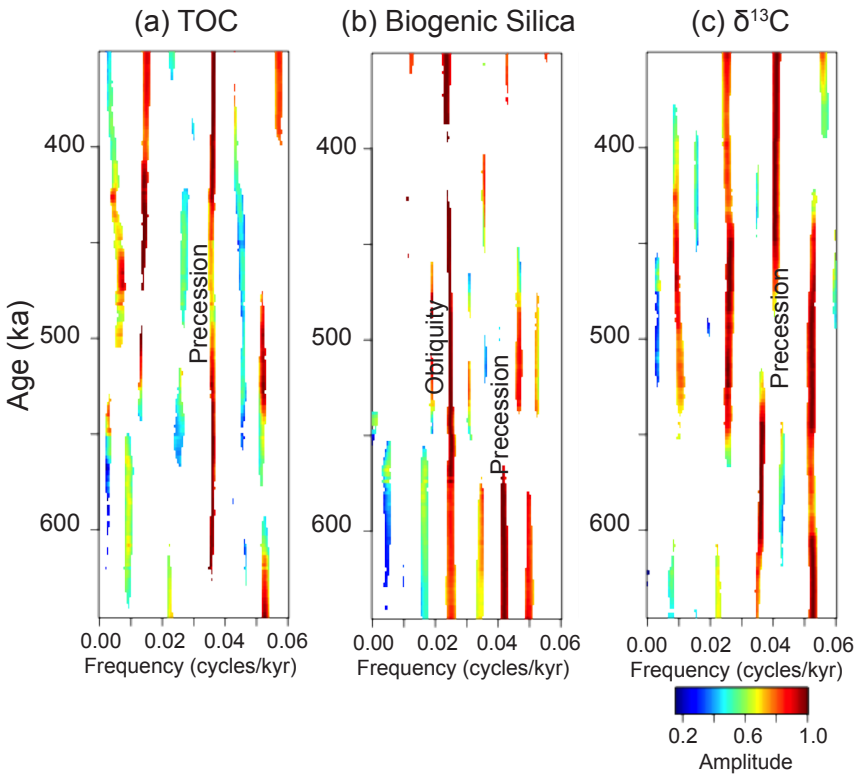


**Figure 3.7 Normalized and filtered amplitude plots of sediment geochemistry. A) Total organic carbon. B) Biogenic silica. C) $\delta^{13}C$. Dominant frequencies for each proxy are labelled with their corresponding astronomical forcing parameter. The white areas indicate no significant frequency.**

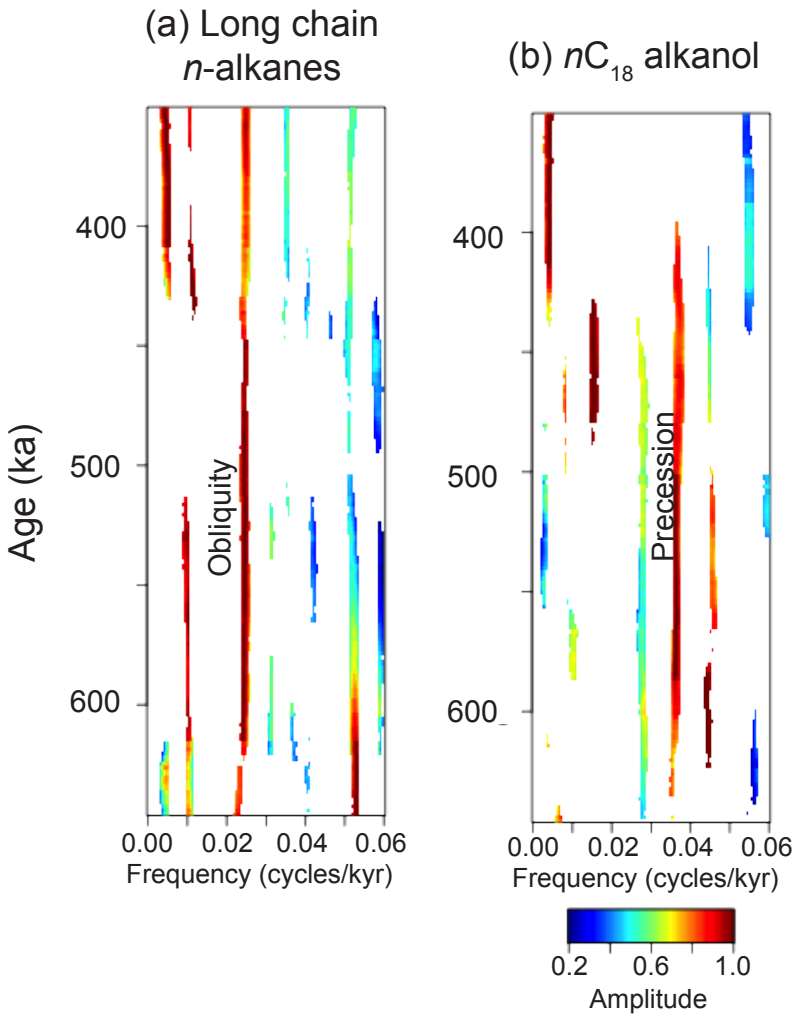


**Figure 3.8 Normalized filtered amplitude of biomarkers. A) Long chain $nC_{25}$ to $nC_{33}$ alkanes. B) $nC_{18}$ alkanol. Dominant frequencies for each proxy are labelled with their corresponding astronomical forcing parameter. The white areas indicate no significant frequency.**

| Instrument | Carrier Gas | Fraction | Temperature Program | Final Temperature Hold (mins) |
|---|---|---|---|---|
| GC-MS | He | Apolar | 70°C to130°C at 20°C $min^{-1}$; then 130°C-320°C at 4°C $min^{-1}$ | 20 |
| GC-FID | He | Apolar | 70°C-130°C at10°C $min^{-1}$; then 130°C-320°C at 4°C $min^{-1}$ | 10 |
| GC-MS | He | Polar | 60°C-130°C at 20°C $min^{-1}$; then 130°C-320°C at 4°C $min^{-1}$ | 15 |
| GC-FID | He | Polar | 70°C-130°C at 20°C $min^{-1}$; then 130°C-320°C at 4°C $min^{-1}$ | 15 |
| GC-FID | H | Polar | 70°C-130°C at 17°C $min^{-1}$; then 130°C-320°C at 7°C $min^{-1}$ | 20 |

**Table 3.1 Oven programming temperatures and rates, and carrier gasses for apolar and polar analysis via GC-MS and GC-FID.**

| Compound | Maximum Concentration (μg gsed$^{-1}$) | Mean Concentration (μg gsed$^{-1}$) | Median Concentration (μg gsed$^{-1}$) |
|---|---|---|---|
| $n$C$_{18}$ alkanol | 1.3 | 0.2 | 0.1 |
| Cholesterol/stanol | 1.8 | 0.2 | 0 |
| Long chain diols | 4.8 | 0.2 | 0 |
| Hopanes | 1.8 | 0.1 | 0 |
| Sitosterol/stanol | 6.2 | 0.3 | 0.1 |
| Dinosterol/stanol | 4.0 | 0.1 | 0 |
| Brassicasterol | 0.9 | 0 | 0 |
| brGDGTs | 1.2 | 0.2 | 0.1 |
| crenarcheol | 0.8 | 0 | 0 |
| Short chain alkanols ($n$C$_{18}$-$n$C$_{24}$) | 15.4 | 1.5 | 0.5 |
| Long chain alkanols ($n$C$_{25}$-$n$C$_{30}$) | 30.8 | 2.3 | 0.9 |
| Short chain alkanes ($n$C$_{17}$-$n$C$_{24}$) | 35.7 | 0.8 | 0.1 |
| Long chain alkanes ($n$C$_{25}$-$n$C$_{33}$) | 28.9 | 2.1 | 1.2 |

**Table 3.2 Concentrations of autochthonous and allochthonous productivity biomarkers. Minimum concentration for all biomarker classes was 0.**

# CHAPTER 4

# MARINE ISOTOPE STAGE 7 WAS STRONGER THAN THE LAST INTERGLACIAL IN THE TERRESTRIAL WESTERN ARCTIC

## 4.1 Abstract

The response of the Arctic climate system to global warming includes increased temperatures, changes in precipitation patterns, as well as reduced sea ice extent, and shifts in dominant atmospheric circulation patterns. Comparing these dramatic changes to the natural variability of the Earth system is difficult because paleoclimate records from the Arctic older than the Greenland ice cores (128 ka) are rare. Here we examine temperature and hydroclimate changes in the terrestrial Arctic throughout the Mid to Late Pleistocene and Holocene (280 ka) using the hydrogen isotopic composition of plant leaf waxes (*n*-alkanes) in sediments from Lake El'gygytgyn, NE Russia. We find significant glacial-interglacial variability in our record. A comparison of interglacial periods indicates Marine isotope stage (MIS) 7 was the strongest interglacial period in the studied interval, followed by MIS 5 and the Holocene. Glacial periods are overall similar but MIS 6 was the strongest of our studied interval. We attribute these differences predominantly to ice-volume associated feedbacks, including sea level and sea ice extent affecting moisture source trajectories to Lake El'gygytgyn. We also invoke temperature variations and the influences of vegetation change as important controls of the leaf wax

hydrogen isotope record. Time series analysis suggests combined forcing of precession and obliquity created long, intense summers during MIS 7. High temperatures and reduced Arctic sea ice likely resulted in the enriched values we observe in this interval. We also find a coherent regional response in the mid- and high latitude marine and terrestrial realms suggesting that MIS 7 was a strong interglacial and deserves further investigation.

## 4.2 Introduction

Future Arctic climate change will likely involve both increased temperature and fluctuations in precipitation amount and seasonality (IPCC, 2013; SWIPA, 2017). Climate change is amplified at the poles, and the Arctic has been warming at twice the rate of the global average over recent decades (SWIPA, 2017). These shifts will likely induce major perturbations to the ocean-atmosphere system, such as variability in atmospheric circulation (e.g. Overland et al., 2012), as well as ecosystem disturbance including vegetation turnover and tundra greening (e.g. Post et al., 2009). However, it is unclear how these transformations compare to the broader history of Arctic climate variability. A strong understanding of the natural extent of Arctic climate fluctuations is essential because the region plays a key role in global climate due to strong feedbacks associated with oceanic, atmospheric, cryosphere, and terrestrial processes (IPCC, 2013; SWIPA, 2017).

Currently, relatively little is known about terrestrial Arctic climate variability, especially during past interglacial periods, beyond the extent of the Greenland ice cores (NGRIP and NEEM Members et al., 2013, 2004), which span the past 128,000 yrs (Yau et al., 2016). Long, continuous sedimentary records of Arctic climate are rare due to the

repeated, extensive glaciation of the high northern latitudes (Miller et al., 2010). Therefore, our best knowledge of interglacial climate in the terrestrial Arctic is largely limited to the Holocene (e.g. Brooks et al., 2015; Kaufman et al., 2016; Sundqvist et al., 2014) and some discontinuous sedimentary sequences including the last interglacial (e.g. Anderson et al., 2006; Axford et al., 2009; McFarlin et al., 2018). Additionally, many proxy records from these intervals infer summer biased temperature, while very few assess precipitation or atmospheric circulation changes (Sundqvist et al., 2014; Thomas et al., 2018). Thus, our understanding of the natural variability of coupled temperature and hydrologic change on long timescales is hindered, as is our knowledge of the spatial climate variability over vast swaths of the Arctic (e.g. McKay et al., 2018).

The study of past climate change, particularly warm intervals, can help us better contextualize the impacts of current anthropogenic warming on the Arctic. The characterization of Mid-and Late-Pleistocene interglacials is an area of active research and studies note diversity associated with proxy systematics and regional climate dynamics (Lang and Wolff, 2011; Past Interglacials Working Group of PAGES, 2016). Globally, the warmest climate conditions of the last 800 ka occurred during the last interglacial, Marine Isotope Stage (MIS) 5, especially MIS 5e or the Eemian (Lang and Wolff, 2011; Past Interglacials Working Group of PAGES, 2016). During this interval, global ice volume was similar to or smaller than today (Lisiecki and Raymo, 2005), producing comparable, or higher global sea level (Dutton et al., 2015; Rohling et al., 2014). Earth's orbital parameters combined to produce a strong positive Northern Hemisphere summer insolation anomaly relative to other interglacials (Laskar et al., 2004), producing global temperatures 0-2 $^{o}$C above present while circum-Arctic

temperatures are estimated to have been 4-5 $^{o}$C higher than today (Anderson et al., 2006). Global climate records of MIS 7, the penultimate interglacial, are more variable as in some records it is expressed as a strong interglacial, and in others it is much weaker (Lang and Wolff, 2011; Past Interglacials Working Group of PAGES, 2016). The maximum northern hemisphere summer insolation of the past one million years is achieved during MIS 7c (Laskar et al., 2004). While most paleoclimate records indicate MIS 5e as the strongest substage of the last interglacial, records from MIS 7 indicate more heterogeneity with various records indicating that stages 7a, 7c or 7e were the strongest (Lang and Wolff, 2011; Past Interglacials Working Group of PAGES, 2016). New work suggesting an age of 203 ka for the Old Crow Tephra could mean that many interglacial sites across western Beringia are, in fact, correlative to MIS 7 and not MIS 5e as previously thought (Hamilton and Brigham-Grette, 1991; Burgess et al. 2019). What was the magnitude of warming during MIS 5 and MIS 7 in the continental Arctic and how does this compare to early Holocene conditions? How does warming during MIS 7c, which is characterized by the highest insolation at 65 oN of the past 1.1Ma, compare to MIS 5? Our study addresses these outstanding questions.

One area of the Arctic not impacted by large scale continental ice sheets (Glushkova, 2001; Glushkova and Smirnov, 2006) is Beringia, the large land bridge stretching from the Kolyma to MacKenzie rivers and including the Bering and Chukchi seas. Sediment cores from Lake El'gygytgyn, in western Beringia, provide a remarkable archive of Arctic climate change from the Pliocene to Holocene (Brigham-Grette et al., 2013; Melles et al., 2012, 2011). Lakes are excellent recorders of climate-sensitive environmental changes as their sediments accumulate terrestrial and aquatic organic

matter, thus providing a signal of lake catchment and regional processes. Arctic lakes are particularly effective paleoclimate indicators due to the sensitivity of the region to global climate fluctuations (polar amplification). Additionally, since summer temperatures throughout the Arctic are near freezing, small climate changes can induce large environmental responses (Vincent et al., 2012). Organic biomarkers and their isotopic composition are useful tools to reconstruct paleoclimate (e.g. Castañeda and Schouten, 2011). Previous analysis of organic biomarkers and stable isotopes in Lake El'gygytgyn sediments has yielded several records of terrestrial Arctic temperature and environmental change for the Plio-Pleistocene transition, Marine Isotope Stage 31 (around 1.1 Ma), the Mid-Pleistocene, and from MIS 3 to 1 (D'Anjou et al., 2013b; de Wet et al., 2016; Holland et al., 2013; Keisling et al., 2016). Here we present a unique plant leaf wax (n-alkane) hydrogen isotope record from the continental arctic spanning the interval from 0 to 280 ka. This record provides novel insights into terrestrial Arctic temperature and hydroclimate changes over multiple glacial-interglacial cycles.

## 4.3 Regional Setting and Background

### 4.3.1 Regional Climate

The modern climate of Beringia is controlled predominantly by the position and relative strength of the Siberian High and Aleutian Low atmospheric pressure systems (Mock et al., 1998). Analysis of synoptic weather patterns in the region (from 1961 to 2009) indicates a strong seasonality with summer weather predominantly characterized by weak low pressure over the Arctic Ocean or Siberia, while winter weather is characterized by strong high pressure in the Arctic and strong low pressure over the

North Pacific (Nolan et al., 2013). Wind patterns at Lake El'gygytgyn are generally bidirectional and change on a seasonal basis; northwest winds are dominant during winter and southeast winds during summer (Nolan et al., 2013; Nolan and Brigham-Grette, 2007). Thus, advected air and moisture is generally sourced from the Arctic Ocean in winter and the North Pacific during summer (Wilkie et al., 2013). Modern air temperature at the lake ranges from extremes of -40 ºC in winter to 26 ºC in summer, with an annual average of -10 ºC (Nolan and Brigham-Grette, 2007), with winters driving the mean annual climate signal due to the extreme cold temperatures (Nolan et al., 2013). Average annual precipitation is ~20 cm water equivalent, with a bias toward more winter precipitation (Nolan and Brigham-Grette, 2007). Relative humidity (RH) at Lake El'gygytgyn averages approximately 80% in summer as the higher air temperatures allow the air to hold more moisture (Nolan, 2013). During the winter, the air is never fully saturated (Nolan, 2013). There is significant variability in the summer with a wide range of RH values, while the winter is more stable (Nolan, 2013).

### 4.3.2 Regional Influences on Precipitation Isotopes

Modern hydrology and isotope systematics at the lake were studied by Wilkie et al. (2013). The authors found that precipitation isotopes at Lake El'gygytgyn fall close to the Global Meteoric Water Line (GMWL)(Craig, 1961), similar to previous observations from Lake El'gygytgyn (Schwamborn et al., 2006) and throughout Siberia (e.g. Kurita et al., 2004; Opel et al., 2011; Sugimoto et al., 2003). Wilkie et al. (2013) also found a strong correlation of precipitation isotopes to temperature with heavy isotope (deuterium) depletion occurring in the winter resulting in more negative isotopic values, and the opposite pattern in summer, as has been observed throughout the high northern latitudes

(Daniels et al., 2017a; Porter et al., 2016). Seasonal variations in precipitation isotopes at Lake El'gygytgyn are also associated with moisture source changes, with winter precipitation derived from the north and east while summer precipitation has a southwesterly source (Wilkie et al., 2013)(Figure 4.1). Modern winter precipitation amounts are higher than summer (Nolan and Brigham-Grette, 2007) so northern and eastern (e.g. Arctic Ocean and Chukchi Sea) moisture sources may play a more significant role in determining precipitation isotopes at Lake El'gygytgyn today. Arctic Ocean and North Pacific Ocean surface waters have an approximate difference in hydrogen isotope composition of up to 15‰, with Arctic waters being more deuterium depleted (NASA GISS, 2018), thus changing moisture sources, or changing the relative amount of moisture from the two sources, would have a notable impact on precipitation isotopes at Lake El'gygytgyn.

### 4.3.3 Sedimentary Leaf Wax Biomarkers

Plant leaf waxes (*n*-alkanes) are widespread and generally abundant compounds in lacustrine sediments and may be transported to lacustrine settings by wind and water erosion or produced in lakes by aquatic plants (Didyk et al., 1978; Eglinton and Hamilton, 1967). Long-chain *n*-alkanes ($C_{27}$ to $C_{33}$) are generally characteristic of higher terrestrial plants (Cranwell et al., 1987; Eglinton and Hamilton, 1967), and synthesized as part of their epicuticular waxes to maintain moisture. Previous work suggests long-chain lengths, specifically $C_{25}$ to $C_{31}$ *n*-alkanes and $C_{28}$ *n*-alkanoic acids, in Lake El'gygytgyn sediments are derived from higher terrestrial plants in the catchment (Holland et al., 2013; Wilkie et al., 2013). We use the hydrogen isotope composition ($\delta^2H$) of the long-chain ($C_{27}$ to $C_{31}$) *n*-alkanes to examine past variability in the isotopic composition of

precipitation. The composition of short chain lengths was measured to examine the isotopic composition of lake water; a dual isotopic approach (e.g. Rach et al., 2017) can be used to examine past changes in relative humidity or evaporation. The short chain-length data are included in the supplement.

The $\delta^2H$ value of terrestrial plant leaf waxes ($\delta^2H_{wax}$) reflects the $\delta^2H$ of precipitation ($\delta^2H_{precip}$), which is dependent on the degree of Rayleigh distillation of a water mass (Dansgaard, 1964). At high latitudes, $\delta^2H_{precip}$ is strongly correlated with mean annual air temperature (Rozanski et al., 2013). Plants incorporate hydrogen from meteoric water into their epicuticular waxes (Gat, 1996) so, changes in $\delta^2H_{wax}$ values preserved in the sedimentary record reflect changes in the isotopic composition of the source water ($\delta^2H_{precip}$) (e.g. Sauer et al., 2001; Sachse et al., 2006; Smith and Freeman, 2006; Sachse et al., 2012). For terrestrial plants the source water is local precipitation while for aquatic plants the hydrogen source is lake water. However, other factors, including evapotranspiration from leaves and soil, biosynthetic fractionation during *n*-alkane synthesis, and plant type (e.g. tree vs grass) can also be strong influences (Craig and Gordon, 1965; Hou et al., 2008; Liu and Yang, 2008; McInerney et al., 2011; Rach et al., 2017; Smith and Freeman, 2006). Previous work has shown that plants at Lake El'gygytgyn predominantly source their water from spring snow melt, resulting in a winter biased signal preserved in their waxes (Wilkie et al., 2013). Because of the extreme cold, winters also dominate the mean annual air temperatures (MAAT) at the site, and so along with the shoulder seasons likely drive much of the variation recorded in paleo-proxy records of MAAT (Nolan et al., 2013). Therefore, we interpret our leaf wax $\delta^2H$ record as likely reflecting a mean annual to slightly winter-biased signal. Additional

details regarding the many possible controls on the $\delta^2H_{wax}$ signal are included in the discussion and supplementary materials.

Due to the uncertainties associated with plant-type dependent biosynthetic fractionation (e.g. Daniels et al., 2017; Sachse et al., 2012; Wilkie et al., 2013) and the effects of moisture source changes (e.g. Dansgaard, 1964; Keisling et al., 2016; Wilkie et al., 2013) that may change over long time scales, we do not attempt to convert our measured $\delta^2H_{wax}$ values to $\delta^2H_{precip}$ or quantify temperature change. Instead, we discuss $\delta^2H_{wax}$ values as likely recording $\delta^2H_{precip}$ and attribute variations to relative temperature and shifts in moisture source. Throughout the study interval, changes in moisture source and trajectory (e.g. Keisling et al., 2016; Thomas et al., 2018) driven by sea level fluctuations, sea ice, and ice sheets likely influence our $\delta^2H_{wax}$ record. Changes in the orbital parameters of obliquity and precession affect insolation and significantly impact high-latitude climate by modulating the length and intensity of the seasons respectively (Huybers, 2011), and therefore influence the $\delta^2H_{wax}$ record at Lake El'gygytgyn.

### 4.3.4 Study Site

Lake El'gygytgyn is located 100 km north of the Arctic Circle in NE Russia (67.5$^o$ N, 172.08$^o$ E) (Figure 4.1). The lake lies within an 18-km-wide meteorite impact crater formed 3.6 Ma (Layer, 2000). Today, Lake El'gygytgyn is 12 km wide and 175 m deep. The catchment area is covered by tundra vegetation (Lozhkin et al., 2007) and is located in a zone of continuous permafrost up to 350 m deep (Mottaghy et al., 2013). Despite the cold climate of the region, the catchment area was never glaciated during Quaternary ice ages because of the relative aridity of the region (Glushkova and Smirnov, 2006). The lake is monomictic and oligotrophic, remaining ice covered for 10 months of

the year, surface water temperatures do not exceed 4 ºC except in shallow nearshore shelf areas (Nolan and Brigham-Grette, 2007).

## 4.4 Methods

### 4.4.1 Core Chronology

Sediment samples used in this and previous studies of Lake El'gygytgyn come from two cores: a pilot core, LZ1024 taken in 2003 (Juschus et al., 2009, 2007) and a composite drill core 5011 taken in 2009 (Melles et al., 2011). Together these cores span the last 3.6 Myrs. The Lake El'gygytgyn age model was developed using magnetostratigraphy and tuning various parameters from core scanning to the global benthic oxygen isotope stack (Lisiecki and Raymo, 2005) and local insolation (Laskar et al., 2004) (Nowaczyk et al., 2013). All Lake El'gygytgyn data are plotted using the previously published age model (Nowaczyk et al., 2013) with supplementary age constraints for core Lz1024 (Juschus et al., 2007).

### 4.4.2 Organic and Stable Isotope Geochemistry

For this study, 138 samples from core sections between 0 and 280 ka were analyzed. Lipids were extracted from freeze dried and homogenized samples using an Accelerated Solvent Extractor (ASE 200 with a mixture of dichloromethane (DCM)/ methanol (MeOH) (9:1, v/v). For samples from core LZ-1024 the total lipid extract (TLE) was separated into neutral and acid fractions on a solid phase extraction (SPE) column (Wilkie, 2012) and the neutral fraction was subsequently separated into apolar and polar fractions via alumina oxide column chromatography. For samples from core 5011, the TLE was immediately subjected to alumina chromatography for apolar and

polar fraction separation. For all samples, apolar and polar fractions were separated using an organic solvent mixtures of 9:1 DCM/hexane v/v (apolar) and 1:1 DCM/MeOH v/v (polar). *n*-Alkanes present in the apolar fraction were identified and quantified using the methods detailed in Habicht et al. (in review). If numerous co-eluting or close-eluting peaks were present in the samples, purification was performed using silver nitrate impregnated silica gel columns.

$\delta^2$H values of *n*-alkanes ($C_{23}$-$C_{31}$) were measured at both the University of Massachusetts Amherst Stable Isotope Laboratory, and the University at Buffalo Organic and Stable Isotope Biogeochemistry Laboratory. Fifteen samples were measured in both labs to check interlaboratory analytical reproducibility: all samples were duplicated within error. Samples measured at the University of Massachusetts were run on a Thermo Delta V isotope ratio mass spectrometer (irMS) coupled to Thermo Trace GC via a ConFlo IV interface. Samples measured at the University at Buffalo were run on a Thermo Delta V Plus irMS coupled to a Thermo Trace 1310 GC equipped with a TriPlus RSH autosampler via an Isolink II and ConFlo IV interface. The GC columns for both instruments were 30 m Agilent HP-1MS columns with an inner diameter of 0.25mm and a 0.25um film thickness. The split/splitless injector was held at 250 $^{o}$C and began in split mode for 0.75 minutes with a flow of 14 mL/min, and was then splitless for the remainder of the injection. Helium was used as the carrier gas with column flow held constant at 1.50 mL min$^{-1}$. The GC oven began at a temperature of 70 $^{o}$C and held for one minute before increasing to 230 $^{o}$C at 27 $^{o}$C min$^{-1}$ with no hold. A second increase of 6 $^{o}$C min$^{-1}$ occurred to 315 $^{o}$C where the final temperature was held for 10 minutes. The pyrolysis reactor was held constant at 1420 $^{o}$C. All samples were run in duplicate with

brackets of three $H_2$ reference gas injections. Lab standards of known isotopic composition were run between each sample and three times at the beginning and end of each instrument run to track linearity and drift.

Molecular deuterium/hydrogen ratios are reported in standard delta notation relative to the Vienna Standard Mean Ocean Water (VSMOW). All samples measured at University of Massachusetts Amherst were measured in duplicate. Uncertainty for these samples was calculated following Polissar and D'Andrea (2014). Full propagation of the uncertainty of each reported $\delta^2H$ value was determined using the pooled standard deviation approach detailed by Polissar and D'Andrea (2014) and includes both the uncertainty of the reference $H_2$ gas $\delta^2H$, as determined by the standards, and the measurement uncertainty for each analyzed compound of interest. For samples measured at University at Buffalo, $H^{3+}$ factor was determined every other day and was 2.44±0.37 to 2.61±0.22, with a mean of 2.50±1.44. Three samples were run at a later date after a source cleaning and filament replacement when the $H^{3+}$ factor was 4.21±0.80. Five of the 105 samples were injected in duplicate while the rest were injected in triplicate. For each run a suite of standards with known isotopic composition (A. Schimmelmann, Indiana University) was included to check for instrument drift ($C_{22}$ , $C_{25}$ , and $C_{35}$ *n*-alkanes) and peak size linearity ($C_{27}$ and $C_{31}$ *n*-alkanes) and to normalize measured values to VSMOW. Total random and analytical uncertainty expressed as the standard error of the mean averaged 1.8‰ for $C_{31}$ and 2.4‰ for $C_{29}$ and 1.9‰ for $C_{27}$.

### 4.4.3 Correction for Global Ice Volume

We correct our measured leaf wax $\delta^2H$ values for the effect of global ice volume changes on meteoric water $\delta^2H$ values (Collins et al., 2013; Niedermeyer et al., 2010).

We calculate the ice volume $\delta^2H$ correction for each sample based on the sample age and a sea level and temperature corrected benthic oxygen isotope curve (Waelbroeck et al., 2002). The benthic $\delta^{18}O$ record (Waelbroeck et al., 2002) was interpolated to each Lake El'gygytgyn $\delta^2H$ sample age and converted to $\delta^2H$ values using the global meteoric water line (Craig, 1961). This correction assumes that sea water $\delta^2H$ changes were uniform throughout Lake El'gygytgyn's moisture source regions.

### 4.4.4 Time Series Analysis

To determine the spectral characteristics of our leaf wax $\delta^2H$ record, we applied the Mann and Lees (1996) robust red noise multi-taper method (MTM) in the Astrochron R program (Meyers, 2012), which has significant statistical power for identifying frequencies at the precession, obliquity, and eccentricity bands (Meyers, 2012, 2014). As the record only contains two eccentricity cycles, data were pre-whitened to suppress 100-ka background noise. We also filtered the data using Analyseries to identify dominant frequencies within the record.

## 4.5 Results

### 4.5.1 Composition and source of sedimentary alkanes

Alkanes preserved in Lake El'gygytgyn sediments show strong odd over even predominance. The Carbon Preference Index (CPI) measures the relative abundance of odd over even carbon chain lengths, with values >1 indicating a terrestrial plant source and thermal immaturity of the source rock or sediment (Bray and Evans, 1961; Eglinton and Hamilton, 1967). CPI values for Lake El'gygytgyn samples measured for hydrogen isotopes range from 1.0 to 4.7 (median = 2.9). Long chain compounds are generally more

abundant than shorter homologues as indicated by Average Chain Length (ACL) values. ACL is a weighted average of a set of carbon chain lengths (Poynter and Eglinton, 1990). For samples included in this study, the ACL of odd carbon number *n*-alkanes ($C_{21\text{-}31}$) ranged from 24.1 to 28.9 (median = 26.8). Generally, the most abundant homologue in Lake El'gygytgyn samples is $n$C$_{27}$, followed by $n$C$_{29}$ and $n$C$_{25}$. Average concentrations for $n$C$_{27}$, $n$C$_{29}$, and $n$C$_{31}$ are 802, 549, and 471 ng g dry sediment$^{-1}$ respectively. Equations used for CPI and ACL are as follows:

$$\mathrm{CPI} = \frac{\mathrm{C}_{23} + 2 \times (\mathrm{C}_{25} + \mathrm{C}_{27} + \mathrm{C}_{29} + \mathrm{C}_{31})}{\mathrm{C}_{33} + 2 \times (\mathrm{C}_{24} + \mathrm{C}_{26} + \mathrm{C}_{28} + \mathrm{C}_{30} + \mathrm{C}_{32})}$$

Bray and Evans (1961)

$$\mathrm{ACL} = \frac{21n\mathrm{C}_{21} + 23n\mathrm{C}_{23} + 25n\mathrm{C}_{25} + 27n\mathrm{C}_{27} + 29n\mathrm{C}_{29} + 31n\mathrm{C}_{31}}{n\mathrm{C}_{21} + n\mathrm{C}_{23} + n\mathrm{C}_{25} + n\mathrm{C}_{27} + n\mathrm{C}_{29} + n\mathrm{C}_{31}}$$

### 4.5.2 $\delta^2$H of Sedimentary Alkanes

Lake El'gygytgyn $\delta^2$H wax isotope values measured over the interval of 0 to 280 ka range from -224‰ to -292‰, -234‰ to -291‰, and -222‰ to -298‰ for $n$C$_{27}$, $n$C$_{29}$, and $n$C$_{31}$ alkanes respectively (Figure 4.2). Total uncertainty for each sample ranged from 0.1‰ to 9.3‰ with an average of 2.4‰. For all three long-chain compounds, generally more enriched $\delta^2$H values (median=-264‰) occur during interglacials MIS 7, 5, and 1, while more depleted $\delta^2$H values (median=-277‰) occur during glacial periods MIS 6, 4, and 2 (Figure 4.2). Application of the ice volume correction results in an increased deuterium depletion of up to 8‰ for rainfall during glacial periods (Figure 4.2). Overall, similar glacial-interglacial patterns are recorded in all three chain lengths (Figure 4.2).

However, there are some differences between the amplitude of change in $\delta^2H_{wax}$ values of each chain length, particularly between the $C_{31}$ and $C_{29}$ during MIS 7c-a (Figure 4.2). It is possible that the different *n*-alkane chain lengths had varying sources during this interval, but it is unclear why the patterns would otherwise be so similar. We base our discussion and interpretation primarily on the $nC_{29}$ alkane as it is more abundant in our samples than the $nC_{31}$ homologue, and previous work at Lake El'gygytgyn has shown it has a terrestrial source. Unless otherwise specified, hereafter, discussion of the Lake El'gygytgyn $\delta^2H_{wax}$ record refers to the $nC_{29}$ record.

Isotopic analysis of shorter homologues ($nC_{25}$ and $nC_{23}$) was also performed. Despite purification steps, the presence of co-eluting compounds prevented reliable isotopic analysis for short chain compounds in many of the samples, leading to a lower resolution record. $\delta^2H$ values for $C_{25}$ range from -231‰ to -295‰ (median = -272‰) while values for $C_{23}$ range from -217‰ to -299‰ (median = -271‰).

The $\delta^2H_{wax}$ record from Lake El'gygytgyn shows significant variability in $\delta^2H$ values both within each climatic cycle and when comparing the intensity of glacials and interglacials throughout the study interval. The interglacial periods with the most enriched $\delta D_{wax}$ values are MIS 7e, 7a, and 5e (Figure 4.2). The periods with the most depleted $\delta^2H_{wax}$ values are glacial stages MIS 6e, 6a, 4, and interstadial MIS 7d (Figure 4.2).

Overall, the $\delta^2H_{wax}$ record strongly resembles the global benthic oxygen isotope stack (Lisiecki and Raymo, 2005), a record for global ice volume and deep water temperature. This relationship suggests western Arctic precipitation isotopes are strongly influenced by changes in global ice volume and associated feedbacks. The $\delta^2H_{wax}$ record

also seems influenced by local insolation. Enriched $\delta^2H_{wax}$ occur during some insolation maxima, but not others. Interestingly, the most depleted isotope values do occur when insolation is low.

### 4.6 Discussion

Relatively few Arctic records have used $\delta^2H_{wax}$ to reconstruct paleoenvironmental changes (Balascio et al., 2013, 2017; Keisling et al., 2016; McFarlin et al., 2018; Moossen et al., 2015; Pagani et al., 2006; Pautler et al., 2014; Porter et al., 2016; Shanahan et al., 2013a; Thomas et al., 2012, 2016a, 2018). These records vary in their studied timescale and the interpretation of $\delta^2H$ value changes, which reflects the varying response of lake catchments to climatic change and highlights our limited understanding of the biological and environmental mechanisms influencing the hydrogen isotopic composition of leaf waxes, particularly in the high latitudes. The record presented here provides novel insight into Arctic temperature and hydroclimate variations with linkages to global and regional ice volume over the last 280 ka.

Although $\delta^2H_{wax}$ primarily reflects patterns of change in $\delta^2H_{precip}$, $\delta^2H_{wax}$ is depleted by a fractionation factor due to a number of processes occurring between leaf wax formation and deposition (e.g. Sachse et al., 2012). Many studies from temperate and tropical regions have studied apparent fractionation in modern systems, and found a general range of -100 to -130‰ (Hou et al., 2008; Kahmen et al., 2013b; Sachse et al., 2004; Smith and Freeman, 2006). However, studies from the high latitudes have yielded dramatically different results with apparent fractionations ranging from -61 to -135‰ (Daniels et al., 2017a; Porter et al., 2016; Sachse et al., 2004; Shanahan et al., 2013a; Wilkie et al., 2013). Therefore, attempted conversion of $\delta^2H_{wax}$ to $\delta^2H_{precip}$ has a large

uncertainty. $\delta^2H_{wax}$ analysis and assessment of apparent fractionations at high latitude sites is further complicated by the dramatic seasonal differences in day length, which some studies have suggested results in small apparent fractionations (Porter et al., 2016; Shanahan et al., 2013a; Yang et al., 2011) and others have indicated is a small or negligible impact (Daniels et al., 2018). Regardless, over long timescales the annual cycle of day length is approximately constant. Therefore, day length is not a key factor in the interpretation of sedimentary $\delta^2H_{wax}$ records at a given location.

Dominant plant type and vegetation changes over long timescales can also bias $\delta^2H_{wax}$ reconstructions. Apparent fractionation varies significantly by species at the individual plant level (Chikaraishi and Naraoka, 2003; Hou et al., 2008; Liu and Huang, 2005), particularly at arid sites (Feakins and Sessions, 2010). This variation has also been linked to plant life form (e.g., tree vs grass) (Liu and Yang, 2008; Sachse et al., 2012). Thus, paleoclimate reconstructions may be biased due to climate-driven vegetation changes. Some authors suggest interspecies differences may be temporally and spatial integrated into the sedimentary record at a catchment scale, allowing accurate reconstructions of regional climate variations (Feakins and Sessions, 2010; Hou et al., 2008; Sachse et al., 2004), while other studies suggest it is necessary to account and correct for the effect of vegetation changes in the paleo record (Daniels et al., 2017a).

Previous work at Lake El'gygytgyn by Wilkie et al. (2013) assessed modern hydrology stable isotopes and controls on plant leaf wax $\delta^2H$ signatures as well as vegetation chain length distributions of *n*-alkanoic acids. In their survey of terrestrial vegetation, Wilkie et al. (2013) note a large interspecies variation in compound distributions, with some terrestrial species producing relatively large amounts of short-

chain compounds, creating an average chain length for terrestrial plant species of 24 to 27. Carbon isotope analysis of *n*-alkanoic acids in the sedimentary record suggests only $nC_{30}$ and longer homologues are attributable solely to higher terrestrial plants, while alkanes $nC_{25}$ and longer have a terrestrial signature (Holland et al., 2013). Isotopic offsets between *n*-alkanoic homologues were also noted for some species (Wilkie et al., 2013). Isotopic analysis of fractionation between different chain lengths and source waters defined an average net fractionation between plants and mean annual precipitation of -107 +/- 12 ‰ (Wilkie et al., 2013). Unfortunately, this analysis was not performed for *n*-alkanes, so we cannot apply this apparent fractionation to reconstruct precipitation isotope values here.

### 4.6.1 Influences on $\delta^2H_{precip}$ and $\delta^2H_{wax}$

Disentangling the controls on $\delta^2H_{precip}$ and $\delta^2H_{wax}$ is complex. A modeled hierarchical framework suggests that $\delta^2H_{precip}$ is the predominant control on plant leaf wax $\delta^2H$ (e.g. Collins et al., 2013; Huang et al., 2002; Liu and Yang, 2008; Sachse et al., 2012, 2006, 2004) but plant type (e.g. Berke et al., 2018; Daniels et al., 2017; Feakins, 2013; Sachse et al., 2012) and evapotranspiration (e.g. Feakins and Sessions, 2010; Smith and Freeman, 2006) as well as other parameters can also play a significant role (Liu and An, 2018). Multiple factors likely influence the $\delta^2H$ values recorded at Lake El'gygytgyn and are discussed in detail below. These include temperature, global ice volume changes and associated sea level and sea ice feedbacks that influence moisture source area, vegetation change, and evaporative enrichment.

#### 4.6.1.1 Temperature

Temperature has a strong effect on $\delta^2H_{precip}$ at the high latitudes, because air temperature controls the availability of atmospheric moisture (Dansgaard, 1964). Assuming a similar degree of rainout, decreased air temperature results in more depleted deuterium values while increased temperature results in deuterium enrichment. It follows that the glacial-interglacial cycles in the Lake El'gygytgyn $\delta^2H_{wax}$ record are strongly modulated by temperature fluctuations. Pollen assemblage climate reconstructions from Lake El'gygytgyn spanning MIS 1-8 suggest a maximum glacial-interglacial change of 10 $^oC$ and 5 $^oC$ for summer and winter, respectively (Lozhkin et al., 2007). Application of an annual mean precipitation isotope to temperature conversion for Russia by Kurita et al. (2004) suggests these glacial-interglacial fluctuations in seasonal temperature could account for a 52‰ (summer) and 26.5‰ (winter) change in the $\delta^2H_{precip}$. The range of measured $\delta^2H_{wax}$ values for $n$-$C_{29}$ alkane is 57‰, thus we infer that a large portion of the variability in this record could be attributed to temperature.

Summer insolation exerts a dominant control on Arctic temperature. If insolation were the main driver of temperature changes here, we could expect to see concurrent changes between insolation and $\delta^2H_{wax}$. Although there are several periods when the two covary (Figure 4.3), insolation does not appear to be the only dominant control throughout much of the record. For example, deuterium depleted values occur when insolation is low during MIS 7d and 6a, while enriched deuterium values are out of phase with peak insolation at MIS 7c (Figure 4.3). Interestingly, previous temperature reconstructions from Lake El'gygytgyn based on branched glycerol dialkyl glycerol tetraethers, suggested that temperature fluctuations at the lake were predominantly

influenced by summer insolation (Chapter 2). For the interval when both records are available, the leaf waxes and brGDGTs exhibit significant differences (Figure 4.3). The most enriched $\delta^2H_{wax}$ values preserved occur during MIS 7e, while the warmest brGDGT reconstructed temperatures are during MIS 7c, and coincide with peak summer insolation at 65 $^oN$ (Chapter 2)(Figure 4.3). The strong correspondence of the brGDGT record to insolation highlights the dominance of precessional forcing on high latitude summer temperatures. Analysis of modern conditions at Lake El'gygytgyn suggests the hydrogen isotopic composition of leaf waxes incorporates a mean annual/winter biased $\delta^2H_{precip}$ signal (Wilkie et al., 2013) whereas brGDGTs are thought to be strongly summer biased (de Wet et al., 2016; Keisling et al., 2016; Chapter 2 and references therein). Therefore, the difference in proxy seasonality may account for some of the discrepancy between the records.

The $\delta^2H_{wax}$ record strongly resembles the global benthic oxygen isotope stack (Lisiecki and Raymo, 2005), a record for ice volume and deep water temperature. This suggests the changes recorded by $\delta^2H_{wax}$ (winter/mean annual temperature and precipitation $\delta^2H$) may have been predominantly driven by temperature and atmospheric circulation changes in the Arctic caused by the growth and decay of Northern Hemisphere ice sheets and associated feedbacks, specifically sea level and sea ice extent (next section). Previous work incorporating brGDGTs and leaf wax hydrogen isotopes at Lake El'gygytgyn during the Plio-Pleistocene transition noted an overall decoupling of the two proxy records and invoked changing moisture sources to account for discrepancies between the records (Keisling et al., 2016). Given the lack of

correspondence between summer insolation and the $\delta^2H_{wax}$ record, there is likely another strong influence on the record during our study interval as well.

#### 4.6.1.2 Moisture Source Changes Driven by Ice Volume

Changes in global ice volume on glacial-interglacial cycles effect fluctuations in the isotopic composition of ocean water and therefore precipitation. These changes (on the order of 8 to 10‰) are smaller than the glacial-interglacial ranges we observe in our record $\delta^2H_{wax}$ record. Therefore, ice-volume driven isotopic changes in source water are not the main source of variations we observe. We have corrected our $\delta^2H_{wax}$ to account for changes in source water composition, resulting in an ~8‰ deuterium depletion during glacial periods and no overall change to the structure of the record. However, we invoke feedbacks associated with global ice volume including sea level and sea ice extent to account for some of the variability in our record.

The region of Beringia is extremely sensitive to changes in global sea level. The Bering Strait and large expanses of the continental shelf are shallow and have a present depth of ~50m (Figure 4.1). Assuming little influence of dynamic topography or isostatic adjustment (Milne and Mitrovica; 2008), Pleistocene sea level changes likely drove repeated exposure and submersion of the Bering Land Bridge during glacials and interglacials respectively (Rohling et al., 2014; Dutton et al., 2015). These fluctuations dramatically influence the continentality and therefore regional climate of Beringia and Lake El'gygytgyn (Bartlein et al., 2015). Changes in continentality influence the distance moisture must travel from the source to Lake El'gygytgyn and therefore the degree of rain out. Greater continentality during glacial periods would produce lower $\delta^2H_{precip}$

values whereas during interglacial periods, moisture sources to Lake El'gygytgyn were more proximal, leading to higher $\delta^2H_{precip}$ (Figure 4.1).

Sea ice extent also likely played a role in determining precipitation isotopes at Lake El'gygytgyn. Recent reductions in sea ice have been linked to increased precipitation throughout the Arctic (Kopec et al., 2016) and fluctuations in sea ice extent associated with global climate changes likely also influenced Arctic precipitation in the past. For example, sea ice extent in Baffin Bay during the Holocene has been invoked as a mechanism driving precipitation isotopes in Western Greenland (Thomas et al., 2016a). During glacial periods, the Arctic Ocean was likely perennially ice covered (Cronin et al., 2010) and extensive perennial and seasonal sea ice was also present in the Bering Sea and Northwest Pacific respectively (Takahashi et al., 2011; Vaughn and Caissie, 2017). Sea ice would have effectively inhibited the Arctic Ocean as a moisture source and decreased the proximity of North Pacific or Bering Sea moisture sources during glacial periods, likely causing precipitation at Lake El'gygytgyn to be derived from much more distal sources (Figure 4.1). Sea ice-driven changes in moisture source from predominantly Arctic Ocean and Chukchi Sea to primarily Bering Sea and North Pacific could double the distance traveled by precipitating water masses. Although North Pacific waters are more enriched than the Arctic Ocean, this enrichment is generally not large, on the order of 10‰ (NASA GISS). More importantly, the source would have been more distal during glacial periods, and air masses and moisture arriving from the North Pacific source would have experienced greater rain out leading to more deuterium depleted precipitation isotope values at the lake (e.g. Gagliotti et al., 2017).

The significant influence of moisture source on high latitude precipitation is well demonstrated (Bowen et al., 2005; Kopec et al., 2016; Noone, 2008; Sodemann et al., 2008; Werner et al., 2001). Isotope enabled modeling for the high latitudes has indicated that changing moisture source and the Rayleigh distillation of air masses moving inland across landmasses is the dominant control on precipitation isotopes (Sime et al., 2013; Werner et al., 2001). Thus, temperature is an apparent control caused by seasonal changes in moisture source. This relationship can be applied to glacial-interglacial timescales in the same way. Changing the dominant moisture source and increasing the degree of rain out (e.g. from proximal Arctic source to more distal Pacific source) causes an apparent temperature dependence because the isotope shift occurs in the same direction (from more enriched to more depleted values). This interpretation of high latitude precipitation isotope records has been applied in several recent studies (Keisling et al., 2016; Thomas et al., 2016a, 2018).

Changes in the seasonality of precipitation falling at Lake El'gygytgyn could also result in isotopic shifts in the $\delta^2H_{wax}$ record (Keisling et al., 2016). If the amount of winter precipitation decreased and summer precipitation increased, we would expect more deuterium enriched $\delta^2H_{wax}$ values, even during glacial periods. Additionally, increased seasonality would likely change the amplitude of glacial-interglacial $\delta^2H$ changes. Glacial-interglacial shifts in precipitation seasonality at Lake El'gygytgyn are particularly difficult to constrain without additional records of temperature and aridity from this time interval. However, we can infer that precipitation isotope seasonality shifts toward summer during glacial periods because Arctic (winter) moisture sources are effectively shut off by perennial sea ice.

#### 4.6.1.3 Vegetation

Another factor in interpretation of the plant leaf wax hydrogen isotope record is vegetation. Modern vegetation at the lake is characterized as tundra, with lichen and herbaceous taxa dominating, while the closest modern forest is composed of conifers and lies ~150 km south west of the lake (Lozhkin et al., 2007a). However, major shifts in plant type and the dominant vegetation at Lake El'gygytgyn occurred in the past. Pollen assemblages indicate that trees and shrubs were abundant around the lake during MIS 5, whereas during glacial periods herbs and forbs are dominant (Lozhkin et al., 2007b; Lozhkin and Anderson, 2013)(Figure 4.3). Plant type has been shown to have a significant impact on apparent isotopic fractionation, although there are wide ranges in apparent fractionation within each category (Sachse et al., 2012). In the Arctic, $\delta^2H$ values for woody plants are 10 to 20‰ more depleted than grasses measured at the same site (Daniels et al., 2017a; Yang et al., 2011). At Lake El'gygytgyn, analysis of modern vegetation indicates less negative apparent fractionation in *n*-alkanoic acids for woody plants than grasses, suggesting the potential for shifts in the dominant vegetation to affect the $\delta^2H_{wax}$ signal across major climatic shifts (Wilkie et al., 2013). Therefore, one component of the leaf wax $\delta^2H$ record may be significant changes in vegetation type that occurs on glacial-interglacial cycles, with a predominance of woody plants contributing to isotopic enrichment during interglacials, and grasses contributing to a more depleted glacial signature (Figure 4.3). Measured apparent fractionations for $nC_{29}$ alkanes from Alaska and mean annual precipitation indicate a 23‰ higher apparent fractionation for woody plants compared to grasses (Daniels et al., 2017). Thus, a complete glacial-interglacial vegetation turnover from herbs and grasses to trees and shrubs could result in

an amplification of the $\delta^2H_{wax}$ signal by up to 23‰. However, a complete turnover in vegetation is unlikely, so this is a maximum estimate. Due to the low resolution of the Lake El'gygytgyn pollen record and lack of site-specific apparent fractionation data for *n*-alkanes we do not attempt to apply a correction for vegetation here, but recognize that vegetation changes likely account for some of the variability we observe (Figure 4.3).

#### 4.6.1.4 Evaporative Enrichment

The isotopic composition of plant leaf waxes has been shown to be influenced by evaporative enrichment from soil and leaf water (e.g. Kahmen et al., 2013b, 2013a; Sachse et al., 2012). This effect is particularly important under arid conditions (Feakins and Sessions, 2010; Hou et al., 2008; Kahmen et al., 2013a; Polissar and Freeman, 2010; Smith and Freeman, 2006). The evaporative enrichment of leaf water is biome dependent, and ranges from 40-100‰ in arid environments (Kahmen et al., 2013a). Increased aridity during glacial periods likely caused enhanced evaporative enrichment, whereas wetter conditions during interglacials would have lessened this effect at Lake El'gygytgyn. Therefore, the $\delta^2H_{wax}$ values during glacial periods may be preferentially enriched.

### 4.6.2 Record Interpretation

The individual factors discussed above (temperature, sea ice and sea level feedbacks, and vegetation) all act in concert to drive changes recorded in the Lake El'gygytgyn $\delta^2H_{wax}$ record. We note that despite temperature being the apparent dominant control on isotope systematics at the high latitudes (Dansgaard, 1964), the $\delta^2H_{wax}$ record is not purely a temperature signal. We suggest extensive sea ice in the Arctic Ocean, Bering Sea and North Pacific (Cronin et al., 2010; Takahashi et al., 2011;

Vaughn and Caissie, 2017), as well as increased continentality due to lowered sea level, coupled with lower temperatures likely drove depleted $\delta^2H_{wax}$ values at Lake El'gygytgyn during glacial periods by limiting atmospheric moisture, decreasing the proximity to moisture source, and increasing the degree of rain out. Whereas, higher temperatures, coupled with proximal and mixed Arctic and North Pacific moisture sources resulted in more deuterium enriched precipitation at Lake El'gygytgyn. These factors act in tandem to influence the precipitation isotopes in the terrestrial Arctic. Glacial-interglacial vegetation changes and associated shifts in apparent fractionation may have resulted in an amplified $\delta^2H_{wax}$ signal although this is difficult to constrain. Overall, the $\delta^2H_{wax}$ record presented here is interpreted as a moisture source signal amplified by temperature and vegetation changes.

### 4.6.3 Time Series Analysis

To elucidate orbital forcings of the $\delta^2H_{wax}$ record, we performed time series analysis. LOWSPEC analysis of the dataset indicates the dominant frequencies are 0.025 and 0.044 equating to 39 ka and 23 ka or obliquity and precession respectively as well as a heterodyne of obliquity and precession at 0.03 equating to 30 ka. Evaluative Harmonic Analysis (EHA) indicates that precession and obliquity both have strong influence on the record prior to 150 ka (Figure 4.4). After 150 ka, there is a combined forcing from both orbital parameters in a 30 ka heterodyne and there is also a significant eccentricity signal at this time (Figure 4.4). These patterns can also be seen in the filtered signal. Enriched $\delta^2H_{wax}$ values during MIS 7e and 7a occur when obliquity and precession are in phase, while more depleted values occur when the two are out of phase (Figure 4.4). Peaks during MIS 6 are associated with precession, but out of phase with obliquity (Figure 4.4).

At MIS 5e, the precession and obliquity are somewhat in phase again to produce more enriched values (Figure 4.4). After MIS 5e, the amplitude of the two frequencies is much lower and approximately equal (Figure 4.4). This time series analysis suggests that the enriched $\delta^2H_{wax}$ values during MIS 7 (and to a lesser extent during 5e and the Holocene) are a result of long (obliquity) and intense (precession) summers (Figure 4.4 and 4.5). These conditions would have influenced the $\delta^2H_{wax}$ values and resulted in enrichment in two ways: 1) by causing significant warming and 2) by reducing Arctic sea ice and providing a more continuous proximal moisture source to the lake.

### 4.6.4 Interglacials

One interesting feature of the record is the variability in $\delta^2H_{wax}$ values during interglacials. Generally, interglacial $\delta^2H_{wax}$ values are deuterium-enriched, but there is significant variability both within and between each interglacial period. Overall, the $\delta^2H_{wax}$ values during interglacials seem to steadily decrease through time, from strong MIS 7e and 7a, the most deuterium-enriched interglacials, followed by MIS 5e, and finally the least deuterium-enriched interglacial values during the Holocene (Figure 4.6). This result is somewhat surprising as in many global climate record comparisons, MIS 5e stands out as a particularly strong (warm) interglacial, while MIS 7 is much weaker (cooler), and MIS 5 is the warmest interglacial period of this studied interval throughout the globe (Lang and Wolff, 2011; Past Interglacials Working Group of PAGES, 2016). Not only is MIS 7 the most deuterium-enriched interglacial in our record, it also displays the greatest amplitude of change (Figure 4.6). Precession is the primary determinant of high latitude seasonal intensity. The peaks in the $\delta^2H_{wax}$ record during MIS 7 are coincident with summer insolation at 240 ka (MIS 7e) and 190 ka (MIS 7a), but are

'missing' at 220 ka during MIS 7c (Figure 4.6). Enriched $\delta^2H_{wax}$ also corresponds to peaks in insolation during warm intervals at MIS 5e, 3a, and the Holocene. Interestingly, the most deuterium depleted $\delta^2H_{wax}$ values also correspond to insolation lows during stadials and interstadials such as MIS 7d 6e, 4, and 2 but there are 'missing' troughs at 110 ka during MIS 5d, and at 90 ka during MIS 5b. This suggests summer insolation (temperature) is not always the dominant control on precipitation isotopes at Lake El'gygytgyn and another parameter (perhaps sea level/sea ice extent) is a strong control. Our time series analysis suggests the combination of obliquity and precessional forcing are necessary to produce the most enriched $\delta^2H_{wax}$ values, i.e. long intense summers causing warmth and sea ice reduction. Whereas intense, but short summers result in somewhat enriched values. Perhaps during the insolation lows, such as MIS 7d, when $\delta^2H_{wax}$ values are particularly depleted, perennial sea ice may have formed in the Arctic.

A potential cause for the especially enriched values during MIS 7a and e is reduced Arctic sea ice. The Arctic Paleo Index (API), a record of Arctic Ocean productivity and sea ice cover, indicates drastically reduced Arctic sea ice (high API values) during MIS 7e and 7a, but not MIS 7c (Marzen et al., 2016) (Figure 4.6). These periods of reduced sea ice are concurrent with intervals of enriched $\delta^2H_{wax}$ at Lake El'gygytgyn (Figure 4.6). Reduced sea ice would have enabled the Arctic Ocean to act as a more significant and proximal moisture source to Lake El'gygytgyn, resulting in more enriched $\delta^2H_{wax}$ values. Conversely, during MIS 7c, the API values indicate no reduction in Arctic sea ice, and thus precipitation would have been sourced from the more distal North Pacific resulting in the depleted $\delta^2H_{wax}$ values (Figure 4.6). The high amplitude variations recorded in the $\delta^2H_{wax}$ are also mirrored in the API values. These abrupt and

frequent oscillations during MIS 7 correspond to insolation and highlight the rapid response of the Arctic to orbital forcing and the precessional frequency (Figure 4.6). A record of sea ice extent in the Sea of Okhotsk also suggests high frequency precession-induced changes in sea ice during the last 130 ka (Figure 4.6). However, the pattern of rapid, high amplitude transitions is not preserved throughout the entire $\delta^2H_{wax}$ record and stops after MIS 5e, after which more gradual climate transitions occur. Time series analysis of the $\delta^2H_{wax}$ record supports this as the early portion of the record is controlled by precession and obliquity, whereas a heterodyne of the two occurs later (Figure 4.4).

Records of sea surface temperatures (SSTs) in the North Pacific, Bering Sea and, and Arctic are few. However, a record from the Sea of Okhotsk spanning the last 180 ka (Lattaud et al., 2018; Lo et al., 2018) bears a remarkable resemblance to the leaf wax $\delta^2H$ record (Figure 4.6). A record of North Pacific SSTs from site ODP 882 (Martínez-Garcia et al., 2010) also shows some similar patterns of variation throughout the study interval, as does a record of planktic $\delta^{18}O$ from the Sea of Okhotsk (Nürnberg et al., 2011) (Figure 4.6). The strong connection between warming in the North Pacific and climate conditions at Lake El'gygytgyn has been noted in previous studies (Brigham-Grette et al., 2013; de Wet et al., 2016; Keisling et al., 2016; Melles et al., 2012). Warming and stratification in the North Pacific likely contributed to warmer conditions at Lake El'gygytgyn by affecting the dominant atmospheric circulation at the site and contributing to the highly deuterium-enriched values we observe. Teleconnections through the Pacific between the Arctic and Antarctic have been noted in previous studies from Lake El'gygytgyn (Brigham-Grette et al., 2013; Melles et al., 2012), where reductions in Antarctic bottom water (AABW) formation under reduced ice sheet/shelf extent modify thermohaline

circulation and lead to warming and stratification in the North Pacific. Indeed, MIS 7 is a period when modeling studies suggest the West Antarctic Ice Sheet (WAIS) may have collapsed (Pollard and DeConto, 2009) although proxy evidence for this WAIS collapse is currently lacking. Records of Greenland Ice Sheet (GIS) collapse during MIS 7 are ambiguous. Yet MIS 7 is not considered among the super interglacials recognized more widely at Lake El'gygytgyn (Melles, et al., 2012). Interestingly, the amplitude of glacial-interglacial $\delta^2H$ variations recorded in Antarctic ice cores (Jouzel et al., 2007) is approximately the same as those recorded in $\delta^2H_{wax}$ at Lake El'gygytgyn, ~60‰.

Terrestrial records from the region also show similar climate patterns to those observed in the $\delta^2H_{wax}$ record. At Lake El'gygytgyn, summer temperature pollen biome reconstructions agree with the $\delta^2H_{wax}$ record indicating MIS 5e was warmer than the Holocene (Melles et al., 2012) (Figure 4.3). The amount of annual precipitation at Lake El'gygytgyn follows a similar pattern, with MIS 5e being greater than the Holocene (Melles et al., 2012) (Figure 4.3), although the isotopic 'amount effect' is unlikely to play a major role at the high latitudes as they lack the deep atmospheric convection that occurs in the tropics. Unfortunately, the pollen biome data is unavailable for MIS 7. Interestingly, percent biogenic silica from Lake El'gygytgyn does not indicate particularly warm conditions. However, the validity of interpreting biogenic silica as a temperature proxy at Lake El'gygytgyn has been questioned (Chapter 2 and 3).These comparisons in timing and intensity of glacial-interglacial changes in temperature and precipitation, highlight the conclusions of Chapter 2, noting significant variations in inter-proxy response to changing climatic conditions.

Temperature records from Lake Weinan (Tang et al., 2017) and the Chinese Loess Plateau (Peterse et al., 2014) indicate greater warmth during MIS 5 than the Holocene and capture significant temperature fluctuations during MIS 4 and 3 likely associated with insolation changes (Figure 4.7). The record from Lake Weinan extends back to MIS 8 and bears a striking similarity to the Lake El'gygytgyn $\delta^2H_{wax}$ throughout, suggesting regionally cohesive temperature fluctuations and atmospheric drivers (Figure 4.7). The Weinan and El'gygytgyn records suggest high amplitude fluctuations occurred during MIS 7, with MIS 7e being the warmest interval (Figure 4.7). Both records also indicate MIS 7 was significantly warmer than MIS 5 and show strong correspondence to insolation lows during cool periods (ex. MIS 6e and 4) with less of a response during warm intervals (ex. MIS 7c) (Figure 4.7). The biogenic silica record from Lake Baikal also records a strong response to precessional forcing but suggests MIS 5e was the strongest interglacial instead of MIS 7e (Figure 4.7).

Records of precipitation and monsoon strength from China also include some similarities during throughout the study interval (Beck et al., 2018; Thomas et al., 2014) (Figure 4.7). The same structure is present during MIS 7, with MIS 7e being the strongest followed by a significant decrease during MIS 7d and recovery through MIS 7c-a (Figure 4.7). This coupling of temperature and precipitation/monsoon variability suggests a strong interdependence between the high latitudes, mid-latitudes and tropics as has been noted by (Beck et al., 2018; Sun et al., 2012). We suggest that orbital forcing influencing the length and intensity of the summer season may have played a role in determining temperature and precipitation variability across the region.

Numerous sites throughout the Arctic which were initially identified as last interglacial (Hamilton and Brigham-Grette, 1991) and which have formed the interpretation that MIS 5e was the warmest interglacial in the Arctic (e.g. Miller et al., 2010) have recently been reassigned to MIS 7 as a result of improved dating and chronology of the Old Crow Tephra (Burgess et al., 2019). Furthermore, the cohesive regional response we find during MIS 7 suggests that further investigation into this interval as a particularly strong interglacial in the mid- and high latitudes is warranted.

### 4.6.5 Glacial Variations

Strongly depleted $\delta^2H_{wax}$ values occur throughout the record during glacial periods. Overall, the glacial periods are relatively similar (within ~10‰). However, the most depleted $\delta D_{wax}$ values occur during MIS 6, suggesting that this may have been a colder glacial period in the Arctic. Although it is not globally expressed as outstandingly cold (Lang and Wolff, 2011), it is thought that MIS 6 may have been strong in the high latitudes and that an ice shelf was present in the Arctic Ocean during MIS 6 (e.g. Colleoni et al., 2016; Gasson et al., 2018). It is also possible that the extent of the Eurasian ice sheet may have strongly influenced climate in Beringia, as it is thought to have been at its largest Mid to Late Pleistocene extent during MIS 6 (Svendsen et al., 2004). Depleted $\delta^2H_{wax}$ values also occur during MIS 8, 4, and 2. None of these periods are thought to have had an Arctic ice shelf, but perennial Arctic and North Pacific sea ice likely contributed to moisture source/trajectory changes during these glacials as well (Figure 4.1). It is likely that an ice shelf and sea ice in the Arctic would affect the precipitation $\delta^2H$ in much the same way. Sedimentological characteristics of Lake El'gygytgyn sediments suggest MIS 4, 6a, 7d, and 8 were periods of cold and wet conditions, while

MIS 2 was much more arid (Melles et al., 2007). During cold and wet glacial periods, elevated regional precipitation allowed for up to 40% glacial ice cover in eastern Siberia (Glushkova et al., 1994). More pronounced glaciation during MIS 4 than MIS 2 is also noted in central Siberia (Stauch and Lehmkuhl, 2010; Svendsen et al., 1999). Overall, the glacial intervals reconstructed in the $\delta D_{wax}$ record are similar and wetter/drier conditions or more extreme cold and distal moisture sources are difficult to distinguish.

### 4.7 Conclusions

Leaf wax hydrogen isotopes from Lake El'gygytgyn, Russia were used to examine terrestrial Arctic climate changes over the past 280 ka. This unique record provides new insights into terrestrial Arctic temperature and hydroclimate changes over several glacial-interglacial cycles. The $\delta^2H_{wax}$ record is interpreted to predominantly reflect temperature and moisture source changes caused by sea level and sea ice fluctuations. We find the most enriched values during MIS 7 when precession and obliquity forcing are significant, followed in strength by MIS 5e and the Holocene, respectively. New evidence revising the age of the Old Crow Tephra from 130 ka to 203 ka (Burgess et al., 2019) means that many warm interglacial sites once thought correlated to MIS 5 are now recording very warm conditions during MIS 7 across eastern Beringia consistent with the results we present from the Lake El'gygytgyn record. Several other regional records also indicate MIS 7 was a stronger interglacial than MIS 5. More research should be performed to investigate MIS 7 as a particularly strong interglacial in the mid- to high latitudes.

## 4.8 Acknowledgements

MHH thanks Benjamin Keisling, William C. Daniels, and Jeffrey M. Salacup for insightful discussions. Owen Cowling is recognized for his technical lab assistance and expertise. University of Massachusetts undergraduate researchers Julie Chessia, Joanne Johnson, Stephen Lukas, Victoria Phu, and Geoffrey Small are appreciated for their assistance in sample extraction and preparation. We also thank Lake E Team members working with Martin Melles, University of Cologne and Pavel Minyuk, NEISRI Magadan for their continuing collaboration. Support for this research was provided by NSF grant #1204087 to Brigham-Grette, Castañeda, and Burns, and the University of Massachusetts Dissertation Fieldwork Grant to Habicht. Data from this publication will be archived on the NOAA Paleoclimate Database.

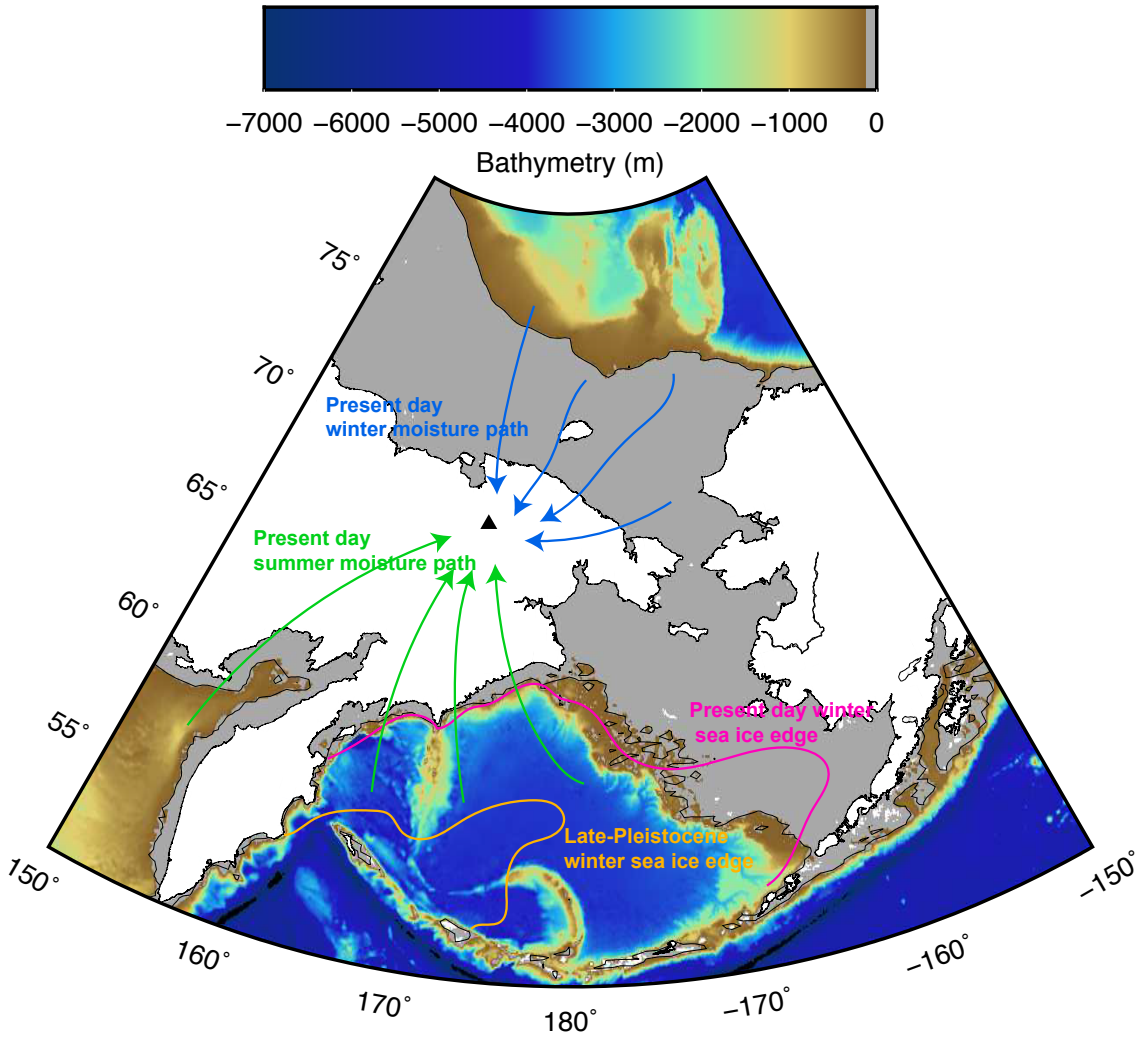


**Figure 4.1 Lake El'gygytgyn in northeast Arctic Russia (triangle). Exposed Bering Land Bridge at 125m below present sea level (grey). Location of present day winter sea ice extent (pink). Late Pleistocene glacial winter sea ice-extent (orange) (Detlef et al., 2018). Present day seasonal moisture source directions for winter (blue) and summer (green).**

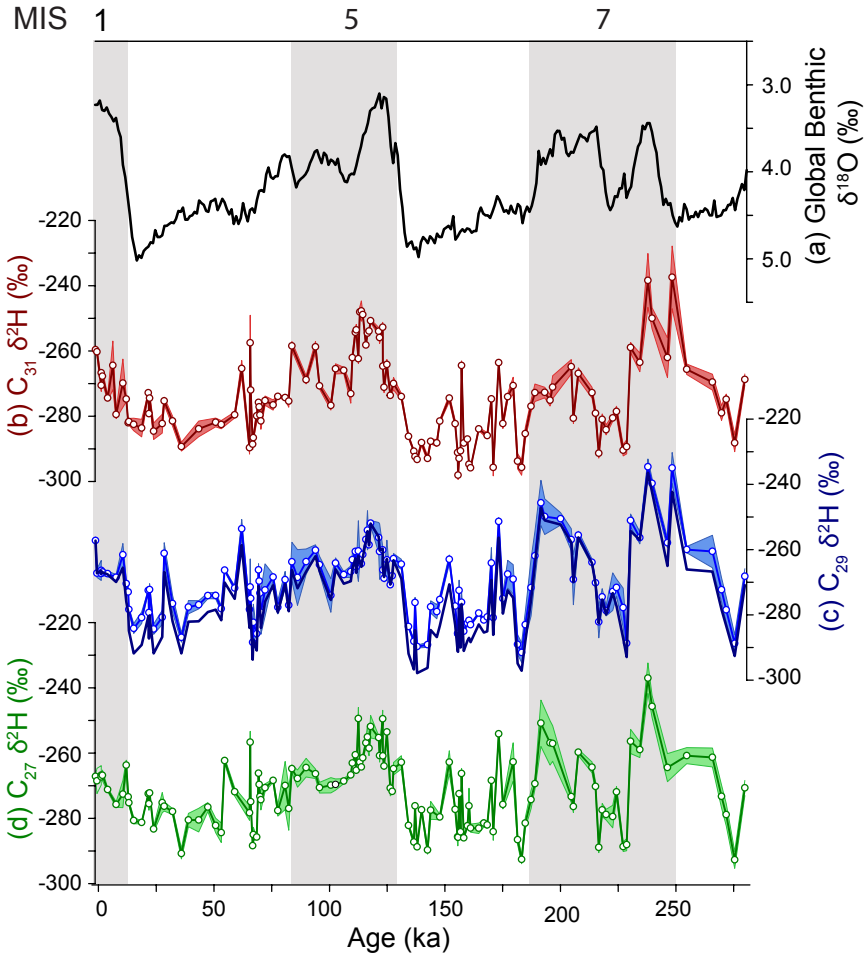


**Figure 4.2 $\delta^2H_{wax}$ values of $n$C$_{27}$-C$_{31}$. A) Global benthic oxygen isotope stack (Lisiecki and Raymo, 2005). B) $\delta^2H_{wax}$ values of C$_{31}$ *n*-alkanes. C) $\delta^2H_{wax}$ values of C$_{29}$ *n*-alkanes. The thicker dark blue line shows the record with an ice volume correction applied. D) $\delta^2H_{wax}$ values of C$_{27}$ *n*-alkanes. In plots B-D the circles represent raw measurements and the colored envelopes represent error associated with each measurement. Ice volume correction was not applied to $\delta^2H_{wax}$ of C$_{27}$ or C$_{31}$.**

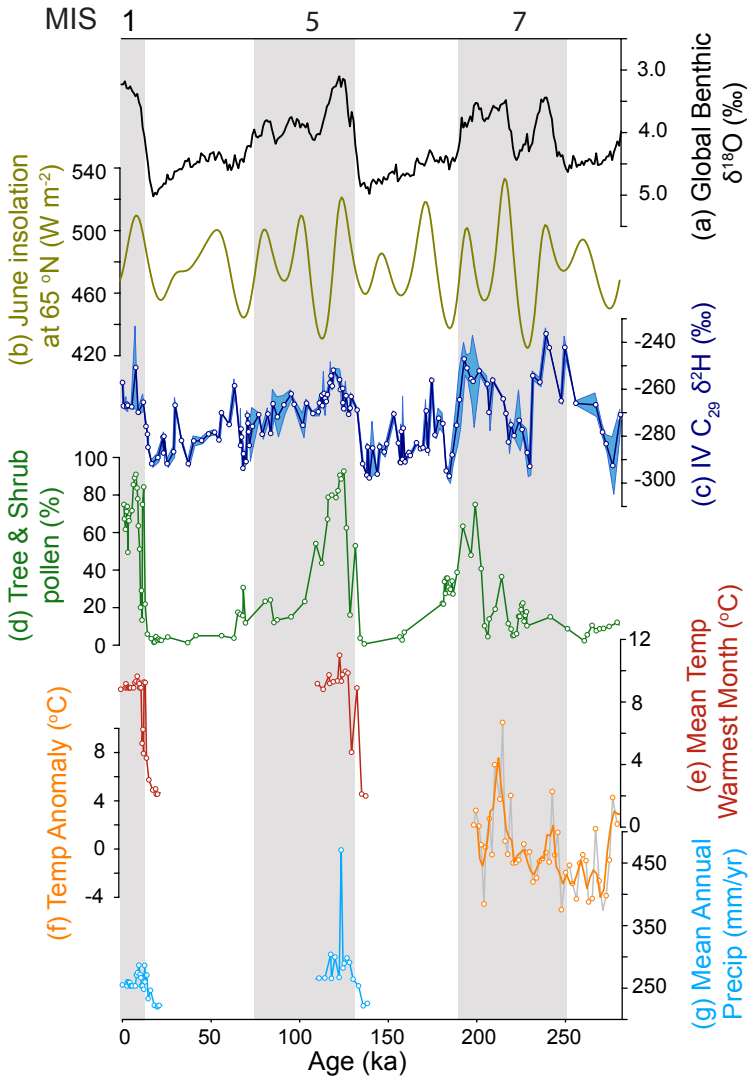


**Figure 4.3 Lake El'gygytgyn proxy records. A) Global benthic oxygen isotope stack (Lisiecki and Raymo, 2005). B) June insolation at 65 °N (Laskar et al., 2004), C) Ice volume corrected $\delta^2H_{wax}$ values of $C_{29}$ *n*-alkanes. Points represent values and blue envelope represents associated error for each point. D) Percent tree and shrub pollen in Lake El'gygytgyn sediments (Lozhkin et al., 2007a). E) Mean temperature of the warmest month pollen biome reconstruction from Lake El'gygytgyn (Melles et al., 2012). F) Lake El'gygytgyn temperature anomaly based on brGDGTs (Habicht et al., in review). G) Mean annual precipitation pollen biome reconstruction from Lake El'gygytgyn (Melles et al., 2012).**

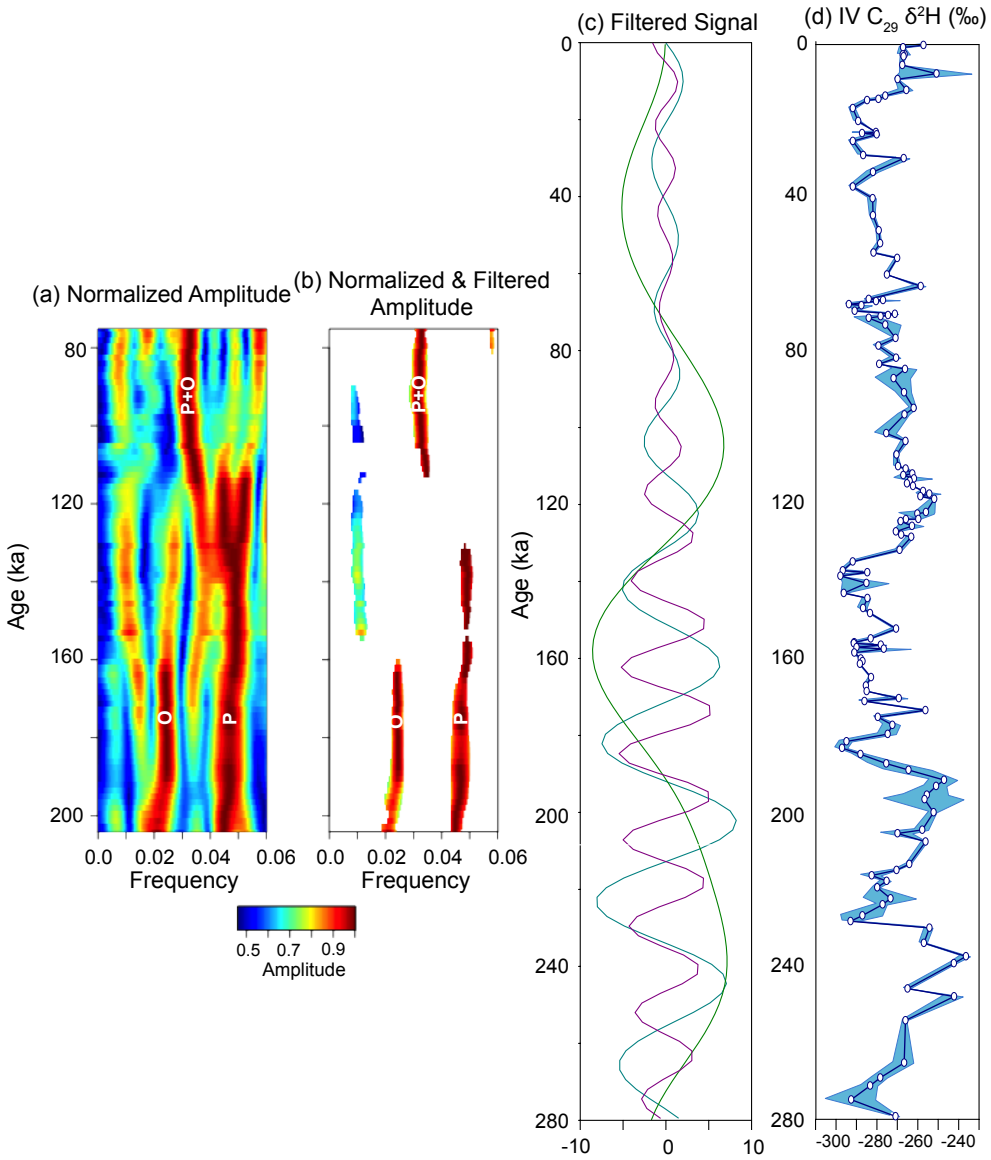


**Figure 4.4 Evaluative Harmonic Analysis diagrams of Lake El'gygytgyn $\delta^2H_{wax}$ record and filtered frequencies. A) Normalized amplitude shows the presence of obliquity and precessional forcing prior to 150 ka and a combined heterodyne of the two after 150 ka. B) Normalized and filtered amplitude demonstrates the significance of each orbital frequency through time at 90% confidence. C) Filtered record for eccentricity, frequency of 0.00857, bandwidth 0.005 (green), obliquity, frequency of 0.025, bandwidth 0.005 (aqua), and precession, frequency of 0.04357, bandwidth 0.005 (purple). D) Ice volume corrected $nC_{29}$ $\delta^2H_{wax}$ record.**

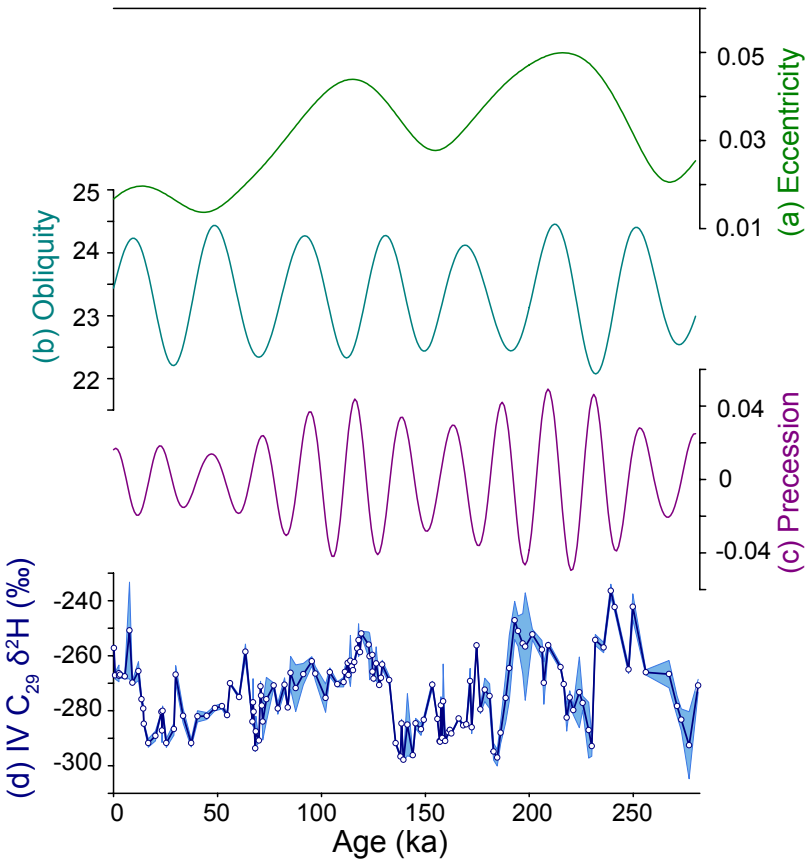


**Figure 4.5 Lake El'gygytgyn $\delta^2H_{wax}$ record and orbital parameters. A) Eccentricity. B) Obliquity. C) Precession. D) Ice volume corrected $\delta^2H_{wax}$.**

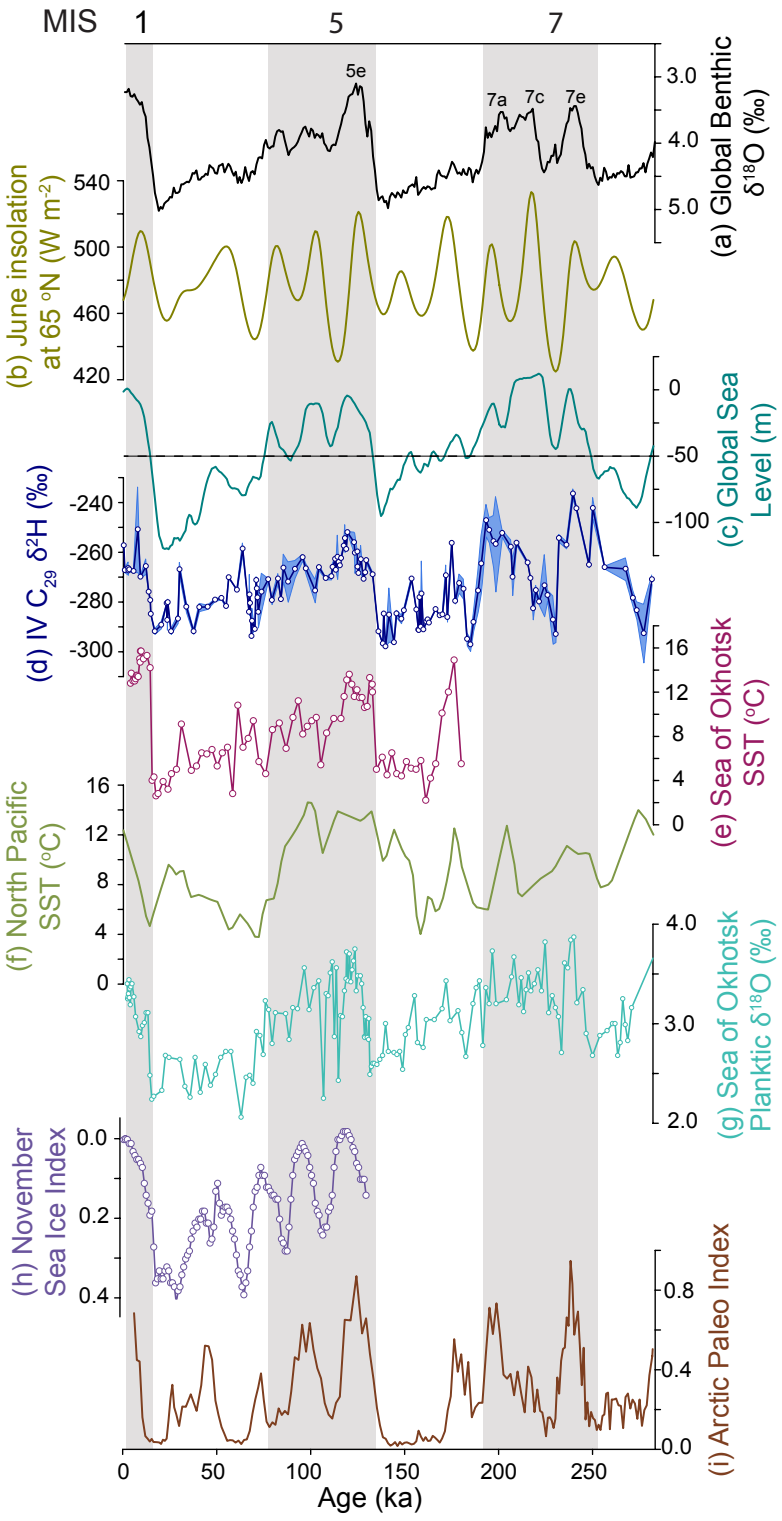
MIS
1
5
7
5e
7a
7c
7e
(a) Global Benthic δ18O (‰)
(b) June insolation at 65 °N (W m-2)
(c) Global Sea Level (m)
(d) IV C29 δ2H (‰)
(e) Sea of Okhotsk SST (°C)
(f) North Pacific SST (°C)
(g) Sea of Okhotsk Planktic δ18O (‰)
(h) November Sea Ice Index
(i) Arctic Paleo Index
Age (ka)

**Figure 4.6 North Pacific and Arctic Ocean paleoclimate records. A) Global benthic oxygen isotope stack (Lisiecki and Raymo, 2005). B) June insolation at 65 °N (Laskar et al., 2004). C) Global sea level (Rohling et al., 2014). Dotted line at 50 m represents threshold for opening and closing Bering Strait. D) Ice volume corrected $\delta^2H_{wax}$ values of $C_{29}$ *n*-alkanes. Points represent values and blue envelope represents associated error for each point. E) $TEX_{86}$ sea surface temperatures from the Sea of Okhotsk (Lattaud et al., 2018; Lo et al., 2018). F) $Uk_{37}$ sea surface temperatures from the North Pacific (Martínez-Garcia et al., 2010). G) Planktic oxygen isotope record from the Sea of Okhotsk (Nürnberg et al., 2011). H) November sea ice index from the Sea of Okhotsk (Lo et al., 2018). I) Arctic Paleo Index from the Arctic Ocean (Marzen et al., 2016).**

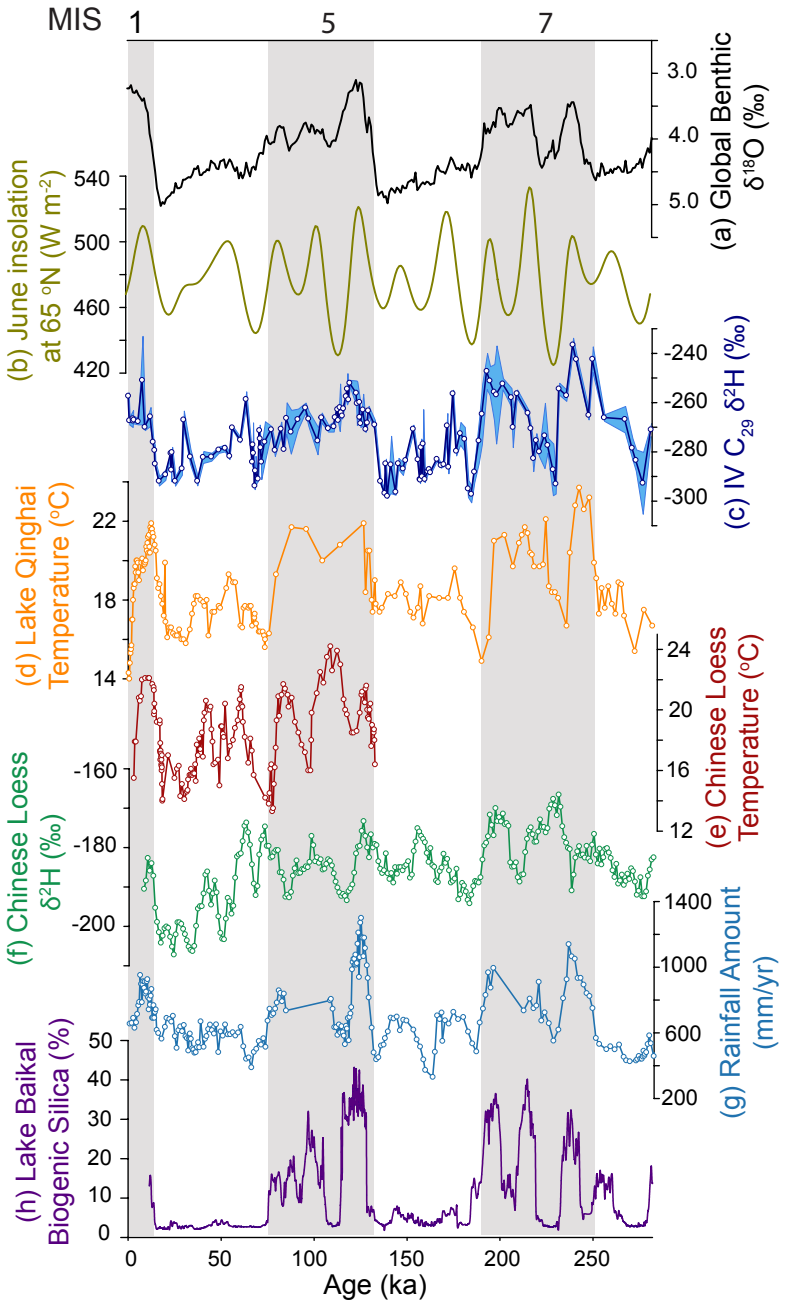


**Figure 4.7 Regional terrestrial paleoclimate records. A) Global benthic oxygen isotope stack (Lisiecki and Raymo, 2005). B) June insolation at 65 ºN (Laskar et al., 2004). C) Ice volume corrected $\delta^2H_{wax}$ values of $C_{29}$ *n*-alkanes. Points represent values and blue envelope represents associated error for each point. D) Temperature reconstruction based on brGDGTs from Lake Weinan (Tang et al., 2017). E) Temperature reconstruction based on brGDGTs from Chinese Loess Plateau (Peterse et al., 2014). F) $\delta^2H$ from Chinese Loess Plateau (Thomas et al., 2016b). G) Annual rainfall amount from Chinese loess (Beck et al., 2018). H) Lake Baikal biogenic silica (Prokopenko et al., 2006).**

# CHAPTER 5

# A COMPARISON OF THE HYDROGEN ISOTOPIC COMPOSITION OF PLANT LEAF WAX *N*-ALKANES AND *N*-ALKANOIC ACIDS FROM LAKE EL'GYGYTGYN (RUSSIA) DURING THE PAST 120,000 YEARS

## 5.1 Abstract

The hydrogen isotope composition of *n*-alkyl lipids is a common paleoclimate proxy. However, many uncertainties regarding proxy interpretation remain. It is often assumed that long-chain *n*-alkanes and *n*-alkanoic acids, ostensibly produced by terrestrial plants, will yield similar downcore trends, but few studies have tested this. Furthermore, the ideal chain length for analyzing terrestrial plant leaf wax isotopes is debated. Here, we address these issues by analyzing paired compound specific hydrogen isotopes of *n*-alkanes ($C_{23}$-$C_{29}$) and *n*-alkanoic acids ($C_{24}$-$C_{30}$) from Lake El'gygytgyn, Arctic Russia since the last full interglacial. Our results show that the choice of compound-class and chain-length can significantly influence isotope records and paleoclimate/paleoenvironmental interpretations.

## 5.2 Introduction

Long-chain *n*-alkanes and *n*-alkanoic acids, synthesized by terrestrial plants as part of their epicuticular leaf waxes, are widely used as plant biomarkers. These waxes exhibit strong odd-over-even and even-over-odd predominance for alkanes and acids respectively, and two to three predominant chain lengths (or homologues) (Eglinton and

Hamilton, 1967; Eglinton and Eglinton, 1963). They are geostable molecules that can survive in the sedimentary record for tens of millions of years and form a large portion of preserved organic matter in many geologic samples (Eglinton and Logan, 1991; Peters et al., 2005). Long-chain *n*-alkanes and their *n*-alkanoic acid counterparts ($C_{27}/C_{28}$ to $C_{33}/C_{34}$) are generally characteristic of higher terrestrial plants (Cranwell et al., 1987; Eglinton and Hamilton, 1967), while short chain homologues ($C_{15}/C_{16}$ to $C_{21}/C_{22}$) are attributed to algae and photosynthetic bacteria (Cranwell et al., 1987; Meyers, 2003). Submerged and emergent aquatic plants are the main producers of mid-chain homologues ($C_{23}/C_{24}$ and $C_{25}/C_{26}$) (Ficken et al., 2000).

The hydrogen isotope composition of plant leaf waxes ($\delta^2H_{wax}$) is a powerful tool for paleoclimate reconstruction (e.g. Tierney et al., 2008; Rach et al., 2014; Keisling et al., 2016; Thomas et al., 2018). Plants incorporate hydrogen from meteoric water into their epicuticular waxes (Gat, 1996), thus changes in $\delta^2H_{wax}$ reflect changes in the isotopic composition of precipitation ($\delta^2H_{precip}$) modified to some degree by fractionation during biosynthetic processes (e.g. Sauer et al., 2001; Sachse et al., 2006; Smith and Freeman, 2006; Sachse et al., 2012). $\delta^2H_{precip}$ is dependent on the degree of Rayleigh distillation of a water mass and influenced by the source water $\delta^2H$, moisture transport path, and temperature (Dansgaard, 1964). Therefore, $\delta^2H_{wax}$ or $\delta^2H_{precip}$ records yield hydrologic information (e.g. Hou et al., 2008; Castañeda et al., 2009; Feakins, 2013; Tierney and deMenocal, 2013; Thomas et al., 2014) with interpretation largely dependent on regional proxy systematics. Despite widespread utilization, numerous uncertainties remain regarding proxy application and interpretation, including differences in biosynthetic fractionation between plant types ($C_3$ vs. $C_4$ vegetation) (e.g. Smith and

Freeman, 2006), plant species (e.g. Hou et al., 2007; Wilkie et al., 2013; Liu et al., 2016; Daniels et al., 2017), and compound classes (e.g. *n*-alkanes and *n*-alkanoic acids) (e.g. Chikaraishi and Naraoka, 2007).

Few modern calibration studies have included data for both *n*-alkanes and *n*-alkanoic acids (e.g. Sauer et al., 2001; Chikaraishi and Naraoka, 2007; Hou et al., 2007; Feakins et al., 2016; Daniels et al., 2017, 2018), and even fewer have analyzed multiple compound classes in the paleorecord (e.g. Yang and Huang, 2003; Li et al., 2009). It is often assumed that long-chain *n*-alkanes and *n*-alkanoic acids (or *n*-alkanols) will yield similar downcore records (e.g. Sachse et al., 2012) but this assumption requires further testing. Furthermore, the ideal homologue for analyzing terrestrial plant leaf waxes is debated. For example, studies analyzing *n*-alkanoic acids commonly measure isotopes of the $nC_{28}$ acid because it is often the most abundant and is assumed to derive from terrestrial higher plants, yet some studies suggest this homologue is primarily produced in the water column (e.g. Holland et al., 2013; van Bree et al., 2018). Here, we present compound specific hydrogen isotope results of paired plant leaf wax *n*-alkane ($\delta^2H_{alkane}$; $nC_{23}$ to $C_{29}$) and *n*-alkanoic acid ($\delta^2H_{acid}$; $nC_{24}$ to $C_{30}$) samples (Wilkie, 2012) from a Lake El'gygytgyn (Arctic Russia) sediment core over the interval of 120 ka to present (Figure 5.1). Our results emphasize that the choice of compound-class and chain-length can significantly influence isotope records and thus paleoclimate/paleoenvironmental interpretations.

### 5.3 Study Site

Lake El'gygytgyn is a meteorite impact crater lake formed 3.6 Ma (Layer, 2000). The lake is 12 km wide and 175 m deep and lies 100 km north of the Arctic Circle in

Chukotka, Russia (Figure 5.1). The site is cold and arid with mean annual air temperature of -10 $^{o}$C and mean annual precipitation of ~200 mm per year (Nolan and Brigham-Grette, 2007). Numerous studies of Lake El'gygytgyn sediments have utilized plant leaf wax distributions and stable isotopes to reconstruct paleoclimatic changes on a variety of timescales (Wilkie, 2012; Holland et al., 2013; Keisling et al., 2016; Habicht et al., Chapters 2-4) as well as modern vegetation and isotope systematics (Wilkie et al., 2013).

## 5.4 Materials and Methods

We analyzed samples from Lake El'gygytgyn piston core LZ 1024 taken in 2003 (Juschus et al., 2009, 2007). The age is based on magnetostratigraphy, tuning of core scanning data to the global benthic oxygen isotope stack (Lisiecki and Raymo, 2005) and local insolation (Laskar et al., 2004), and supplementary age constraints from Juschus et al. (2007) (Nowaczyk et al., 2013).

Initial sample preparation and analysis of *n*-alkanoic acids was performed by Wilkie (2012). We further separated a subset of 48 neutral fractions from Wilkie (2012) into apolar and polar fractions via alumina oxide column chromatography using 9:1 DCM/hexane (v/v; apolar) and 1:1 DCM/MeOH (v/v; polar). *n*-Alkanes were identified and quantified using the methods detailed in Habicht et al. (Chapter 4). $\delta^2H_{alkane}$ values ($C_{23}$-$C_{31}$) were measured in the University of Massachusetts Amherst Stable Isotope Laboratory and the University at Buffalo Stable Isotope and Biogeochemistry Laboratory. Fifteen samples were analyzed in both labs to insure reproducibility within error. Sample analysis and data treatment are detailed in Habicht et al. (Chapter 4). To more easily compare the two compound classes with different ranges, the measured

$\delta^2H_{alkane}$ and $\delta^2H_{acid}$ values were normalized to a value between 0 and 1. Each isotope value for each homologue was normalized using the following equation.

$$\text{Normalized } X = (X\text{-}X_{min})/(X_{max}\text{-}X_{min})$$

## 5.5 Results and Discussion

In plants, long chain alkyl lipids are synthesized via the addition of two carbon acid groups to form long chain *n*-alkyl acyl-ACP with carbon chain length *x*, forming even chain length *n*-alkanoic acids with length *x*, and *n*-alkanes of length *x*-1 (Chikaraishi and Naraoka, 2007; Zhou et al., 2010). Therefore, throughout the discussion we compare pairs of $C_x$ *n*-alkanoic acids and $C_{x-1}$ *n*-alkanes to assess compound class offsets.

### 5.5.1 Sources of n-alkyl lipids

Carbon isotope analysis of *n*-alkanes and *n*-alkanoic acids in Lake El'gygytgyn sediments from 0-60 ka suggests that *n*-alkanes $\geq C_{25}$, and the $C_{30}$ *n*-alkanoic acid, have a terrestrial source (Holland et al., 2013). All shorter chain lengths ($nC_{24}$ to $nC_{28}$) are of mixed terrestrial and aquatic sources (Holland et al., 2013) complicating their use as isotopic proxies. Mixed sources of *n*-alkyl lipids are not ideal for isotopic reconstruction as they incorporate hydrogen from different pools (e.g. precipitation and lake water), potentially complicating the proxy signal. However, two end member chain lengths, one terrestrial (e.g. $nC_{29}$ alkane) and one aquatic (e.g. $nC_{21}$ alkane), can be utilized to reconstruct hydroclimate changes such as relative humidity (e.g. Balascio et al., 2017; Rach et al., 2017; Thomas et al., 2018).

### 5.5.2 Comparison of n-alkane and n-alkanoic acid concentrations

The concentrations of *n*-alkanes and *n*-alkanoic acids in our samples are highly variable. The most abundant *n*-alkane is $C_{27} > C_{29} > C_{25}$, while the most abundant *n*-alkanoic acid is $C_{26} > C_{28} > C_{24}$ (Figure 5.2 and 5.3). The *n*-alkanoic acids are almost always more abundant than the *n*-alkanes, with concentrations up to an order of magnitude higher (Figure 5.2 and 5.3). In general, concentration changes are coincident between the two compound classes, although this is not always the case (Figure 5.2 and 5.3). If the same source is assumed, differences in *n*-alkane vs. *n*-acid abundance may be associated with the relative amounts synthesized by plants. Several studies of modern plants have noted differences in *n*-alkane vs. *n*-alkanoic acid concentration, although the dominant compound class varies by plant type and study site (e.g. Chikaraishi and Naraoka, 2007; Feakins et al., 2016; Daniels et al., 2017). Differences in concentration may also be related to varying compound sources and/or better packaging/preservation of *n*-alkanoic acids in sediments. This pattern has recently been demonstrated in the modern environment (Wu et al., 2019). Analysis of *n*-alkanoic acids in modern plants at Lake El'gygytgyn indicates large interspecies variations in concentration and distribution of compounds with an average chain length ($ACL=\Sigma(C_n*n)/=\Sigma C_n$ , where *n*= 20, 22, 24, 26, 28, 30) ranging from 24 to 27 as well as significant variations in $\delta^2H_{wax}$ (Wilkie et al., 2013). Their study also found that concentration and distribution of *n*-alkanoic acids varies throughout the water column, but is relatively consistent in lake surface sediments (Wilkie et al., 2013).

### 5.5.3 Comparison of $\delta^2H_{alkane}$ and $\delta^2H_{acid}$

The isotopic values for long chain *n*-alkanoic acids $nC_{30}$ and $nC_{28}$ consistently have a greater range (46-78‰) than the *n*-alkanes $nC_{29}$ and $nC_{27}$ (35-41‰) (Figure 5.4B and C) whereas the $\delta^2H$ values for the mid-chain lengths $nC_{23}$ – $nC_{26}$ have generally similar ranges (35-53‰) (Figure 5.4D and E). In general, the $\delta^2H_{alkane}$ values are more depleted than the $\delta^2H_{acid}$ values, consistent with modern plant studies (Chikaraishi and Naraoka, 2007; Daniels et al., 2017b; Feakins et al., 2016; Hou et al., 2007) (Figure 5.4). However, the homologues lack a consistent offset that has been noted in some modern calibration studies (Chikaraishi and Naraoka, 2007; Hou et al., 2007) (Figure 5.4). There are also intervals when the alkanes are more enriched, indicated by a negative normalized difference (Figure 5.4F-J). Despite these differences, long chain *n*-alkanes and *n*-alkanoic acids seem to capture similar trends (Figure 5.4B and C). Comparison of the mid-chain length compounds is complicated by the lower resolution of the $C_{25}$ and $C_{23}$ *n*-alkane records (Figure 5.4D and E).

The trends recorded by the shorter chain aquatic/mixed sourced compounds are somewhat ambiguous. The $\delta^2H_{acid}$ values for $nC_{28}$ and $nC_{26}$ are more enriched and have a smaller range of variability than the $nC_{30}$ (Figure 5.4B-D). However, the range of $\delta^2H_{acid}$ values unexpectedly increases again for $nC_{24}$ (Figure 5.4E). Interestingly, the range of variability of $\delta^2H_{alkane}$ values increases with decreasing chain length (Figure 5.4). However, the significance of this trend may be questionable, as the $nC_{25}$ and $nC_{23}$ records have a lower resolution and it is difficult to determine whether all of the variations are robust (Figure 5.4D and E).

A cross plot of normalized $\delta^2H_{alkane}$ and $\delta^2H_{acid}$ values indicates that the most similar homologues are the $C_{30}$ *n*-alkanoic acid and $C_{29}$ *n*-alkane (Figure 5.5A). As the chain lengths decrease, so do the correlations between compound classes (Figure 5.5A-D) likely due to changing compound sources. This is consistent with carbon isotope results suggesting the $nC_{30}$ acid and $nC_{29}$ alkane are the only pair of terrestrially derived chain lengths (Holland et al., 2013) reflecting the same hydrogen source, precipitation.

### 5.5.4 Paleoclimate Implications

Overall, the $\delta^2H_{wax}$ of long chain terrestrially sourced compounds agrees well with the global benthic oxygen isotope stack, a record of global temperature and ice volume (Lisiecki and Raymo, 2005) (Figure 5.4A), suggesting that $\delta^2H_{wax}$ of these compounds is responding directly to local climate and is not likely complicated by changes in compound source or the mixing of compound sources (Figure 5.4B). A detailed discussion and paleoclimate interpretation of these records is included in Habicht et al. (Chapter 4) and Wilkie (2012). Despite the overall similarity of the long chain $\delta^2H_{alkane}$ and $\delta^2H_{acid}$ records, there are two intriguing deviations. First, is the difference in proxy response during MIS 5, when $\delta^2H_{alkane}$ is more enriched than during the Holocene, but $\delta^2H_{acid}$ is more depleted than during the Holocene (Figure 5.4B). MIS 5 is often reconstructed as a strong interglacial (Lang and Wolff, 2011; Past Interglacials Working Group of PAGES, 2016), and previous results from Lake El'gygytgyn suggest it was 2-4 $^oC$ warmer than the Holocene (Melles et al., 2012) suggesting the $\delta^2H_{alkane}$ record more accurately reflects relative temperature at Lake El'gygytgyn. Second, is during the Holocene when $\delta^2H_{alkane}$ becomes more depleted after an early peak while the $\delta^2H_{acid}$ record becomes more enriched to peak during the middle Holocene (Figure 5.4B). These

trends are also present in the homologue concentrations (Figure 5.2). These differences suggest two different warming scenarios, with the $\delta^2H_{acid}$ values indicating peak conditions at the Middle Holocene, and $\delta^2H_{alkane}$ ratios suggesting a peak in the early Holocene. These findings highlight how the targeted compound class and homologue can significantly influence paleoclimate conclusions drawn from the record.

## 5.6 Conclusion

This study compares $\delta^2H_{wax}$ measurements of a range of *n*-alkane and *n*-alkanoic acid chain lengths measured on the same samples from a lake in the terrestrial Arctic. The isotopic results suggest that long chain $\delta^2H_{alkane}$ and $\delta^2H_{acid}$ record similar climatic trends during the last 120 ka while shorter chain lengths are more variable. However, there are important differences in the response of the $\delta^2H_{alkane}$ and $\delta^2H_{acid}$ records that have significant implications for specific paleoclimate interpretations, such as climatic variations during the Holocene and MIS 5.

The data do not explicitly support the use of *n*-alkanes vs. *n*-alkanoic acids in paleoclimate studies, but suggest trade-offs associated with compound choice. For example, *n*-alkanoic acids are more abundant, but may also reflect a mixed source signal and therefore comprise a more complicated record to deconvolve. We suggest the choice of compound class and target chain length may be constrained by compound abundance and examination of sources throughout the study interval. Consideration of modern vegetation and isotope systematics at the study site may also aid in decision-making. We support a multi-proxy approach to paleoclimate studies and note that analysis of multiple *n*-alkyl chain lengths and compound classes can yield valuable paleoclimate information.

## 5.7 Acknowledgements

MHH thanks Benjamin Keisling and William Daniels for their thoughtful discussion and input. Owen Cowling is recognized for his laboratory assistance. University of Massachusetts undergraduate researchers Joanne Johnson, Stephen Lukas, and Victoria Phu are appreciated for their assistance in sample preparation. Support for this research was provided by NSF grant #1204087 to Brigham-Grette, Castañeda, and Burns and the University of Massachusetts Dissertation Fieldwork Grant to Habicht. Data from this publication will be archived on the NOAA Paleoclimate Database.

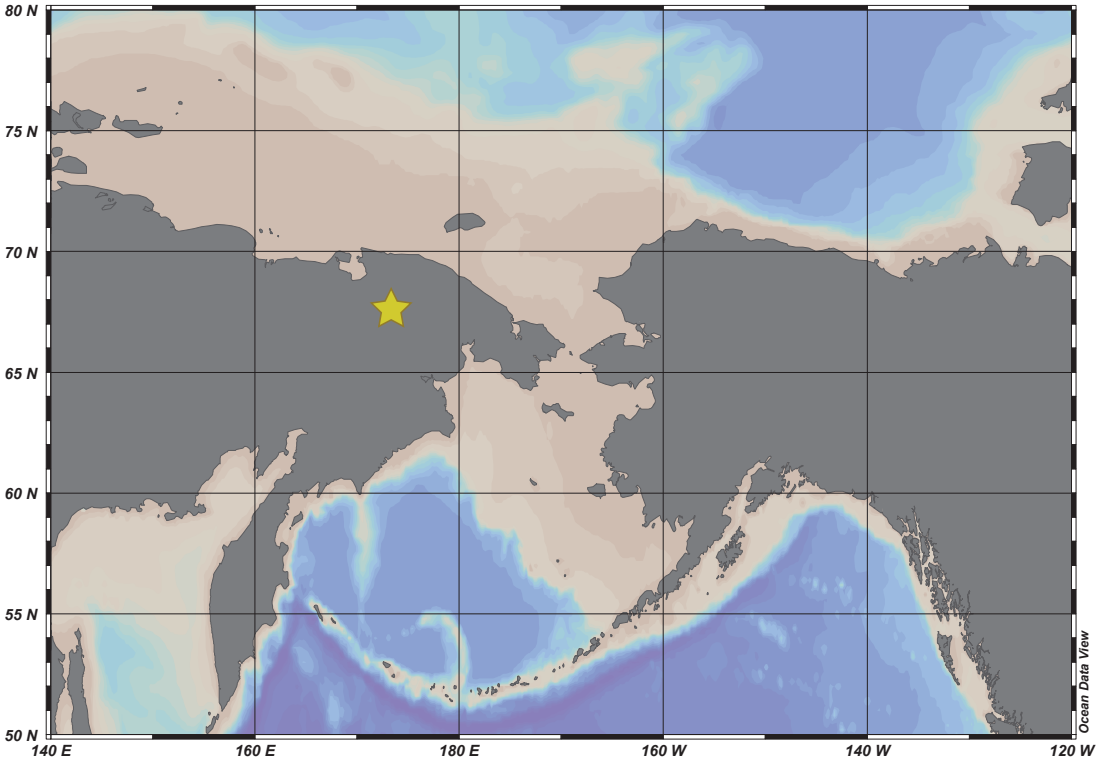


**Figure 5.1 Location of Lake El'gygytgyn in Arctic Russia. Location denoted by the yellow star.**

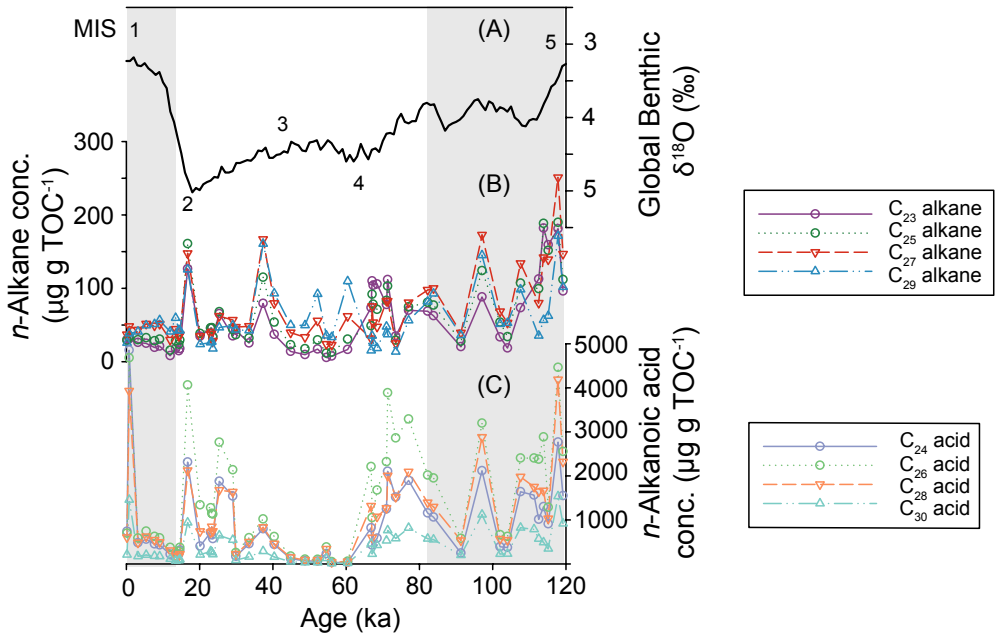


**Figure 5.2 Concentrations of *n*-alkane and *n*-acid homologues down core. A) Global benthic oxygen isotope stack (Lisiecki and Raymo, 2005). Marine Isotope Stages are labeled and grey bars highlight interglacial periods MIS 5 and the Holocene. B) *n*-Alkane concentrations. C) *n*-Alkanoic acids concentrations (Wilkie, 2012). The keys indicate colors and patterns for each homologue.**

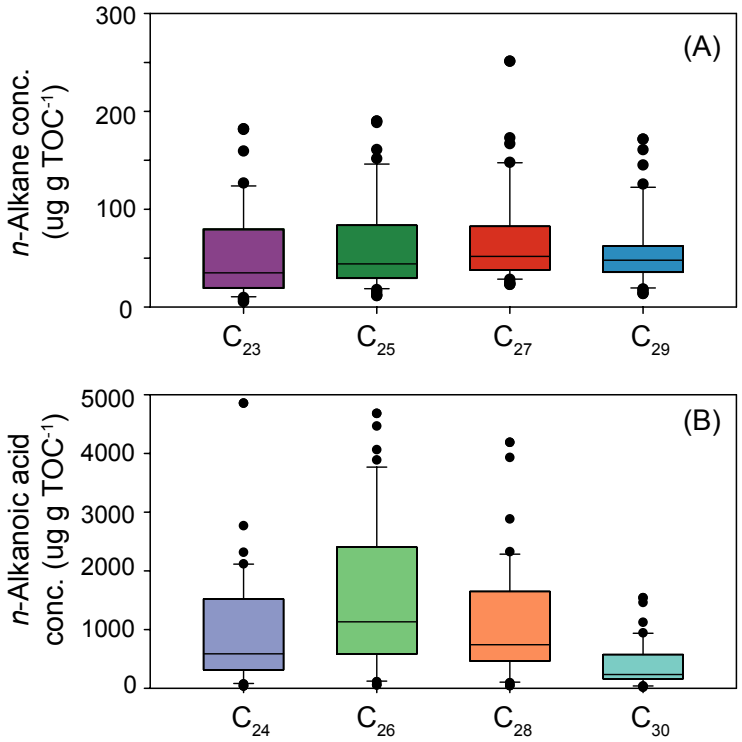


**Figure 5.3 Box and whisker plots of *n*-alkane and *n*-alkanoic acid concentrations. In all plots the bottom and top of the box indicate the first and third quartiles and the middle line inside the box indicates the median. The tips of the whiskers represent the smallest and largest values that are not more than 1.5 times the interquartile range above or below the median. The dots represent outliers.A) *n*-alkane concentrations. B) *n*-alkanoic acid concentrations (Wilkie, 2012).**

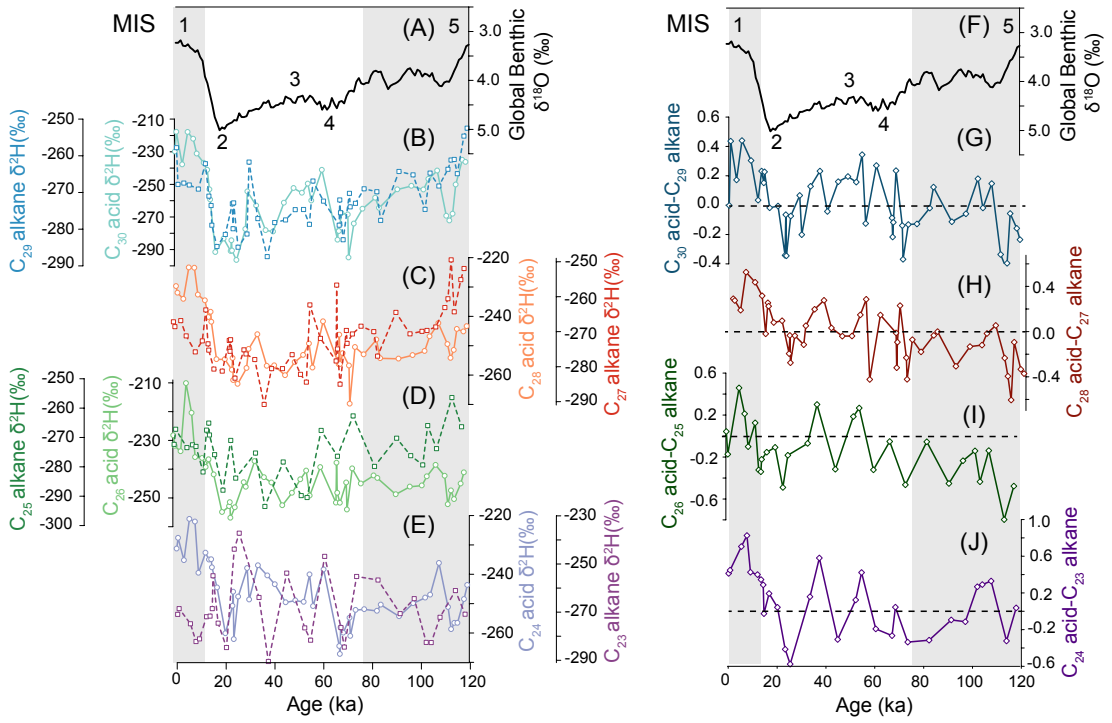


**Figure 5.4 $\delta^2H$ values and normalized difference of *n*-alkanes and *n*-alkanoic acids in Lake El'gygytgyn sediments over the last 120 ka. A) Global benthic oxygen isotope stack (Lisiecki and Raymo, 2005). B) $\delta^2H$ values of $C_{29}$ *n*-alkane (blue) and $C_{30}$ *n*-alkanoic acid (aqua). C) $\delta^2H_{wax}$ values of $C_{27}$ *n*-alkane (red) and $C_{28}$ *n*-alkanoic acid (orange). D) $\delta^2H_{wax}$ values of $C_{25}$ *n*-alkane (green) and $C_{26}$ *n*-alkanoic acid (light green). E) $\delta^2H_{wax}$ values of $C_{23}$ *n*-alkane (purple) and $C_{24}$ *n*-alkanoic acid (lavender). In each panel the circles and continuous lines represent the *n*-alkanoic acids while the squares and dashed lines represent the *n*-alkanes. F) Global benthic oxygen isotope stack (Lisiecki and Raymo, 2005). G) Normalized difference between $C_{30}$ *n*-alkanoic acid and $C_{29}$ *n*-alkane $\delta^2H$ values. H) Normalized difference between $C_{28}$ *n*-alkanoic acid and $C_{27}$ *n*-alkane $\delta^2H$ values. I) Normalized difference between $C_{26}$ *n*-alkanoic acid and $C_{25}$ *n*-alkane $\delta^2H$ values. J) Normalized difference between $C_{24}$ *n*-alkanoic acid and $C_{23}$ *n*-alkane $\delta^2H$ values. Dashed lines indicate a normalized difference of 0. Grey bars denote interglacials. Marine isotope stages are labeled. All isotopic measurements of *n*-alkanoic acids are from Wilkie (2012).**

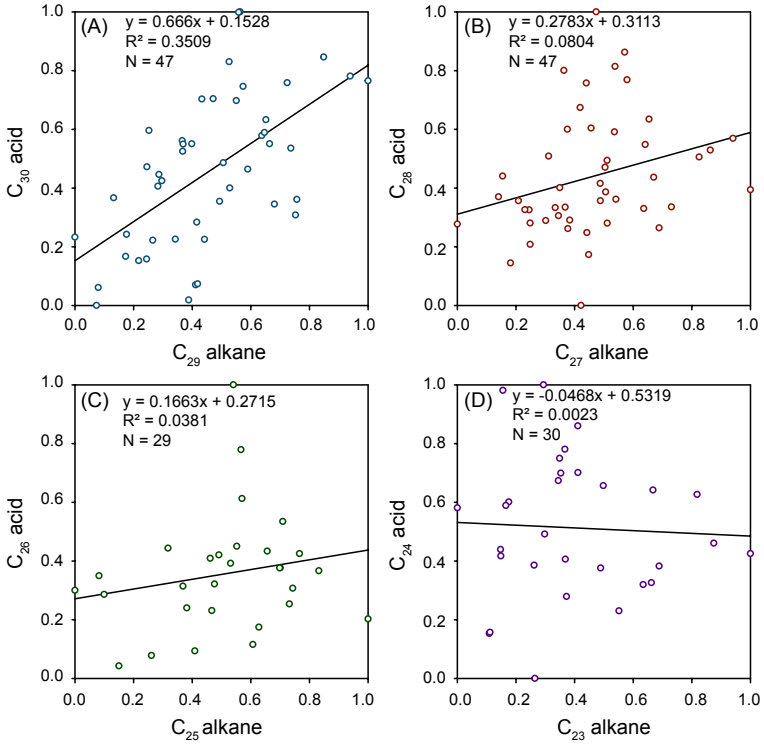


**Figure 5.5 Correlation of acids and alkanes. A) $C_{29}$ alkane and $C_{30}$ acid. B) $C_{27}$ alkane and $C_{28}$ acid. C) $C_{25}$ alkane and $C_{26}$ acid. D) $C_{23}$ alkane and $C_{24}$ acid. Linear regressions are plotted through each data comparison. The equation for the linear regression and the $R^2$ value are listed at the top of each plot.**

# CHAPTER 6

# CONCLUSIONS AND FUTURE WORK

This dissertation includes a variety of organic and stable isotope biogeochemistry methods and studies of different time intervals to address questions surrounding the past 800 ka of Arctic climate change. These techniques are applied to sediments from Lake El'gygytgyn, Russia, a meteorite crater lake providing the longest continuous record from the terrestrial Arctic (3.6 Ma). Overall, the chapters of this thesis provide novel information about Arctic paleoclimate and further promote the use of biomarkers to analyze Lake El'gygytgyn sediments in future studies.

Branched glycerol dialkyl glycerol tetraethers and plant leaf wax *n*-alkanes are employed in Chapter 2 to reconstruct changes in relative temperature and aridity, respectively, from 200-800 ka. These, and previously published data from Lake El'gygytgyn are used to assess individual proxy response to glacial-interglacial changes throughout the Middle-Pleistocene and examine a global climatic transition called the Mid-Brunhes Event. Time series analysis of the new organic geochemical data sets was performed and indicates the importance of orbital forcing on high latitude climate, particularly the intensity of summer insolation (precession) and length of the summer season (obliquity). In future work, these paired organic geochemical analyses should be applied to provide a comprehensive look at temperature and aridity induced vegetation change at Lake El'gygytgyn throughout the entire record. Furthermore, time series analysis of these and the other proxies can be used to assess changes in astronomical forcing over the last 3.6 Ma and individual proxy responses. This can provide valuable insight about the climate system and forcing mechanisms of Arctic climate change,

particularly across intervals of interest such as the Mid-Pleistocene Transition (MPT). Additionally, the temperature data may be applied as a forcing to model melting and exposure histories of the Greenland ice sheet and potentially assess the validity of an Arctic ice cap during past glacial periods. BrGDGTs can only currently provide a record of relative temperature change in the Arctic. Development of new site-specific or regional brGDGT calibration would improve the accuracy of reconstructed temperature variations.

In Chapter 3, concentrations of autochthonous and allochthonous biomarkers measured on the same samples used in Chapter 2, along with stable carbon and nitrogen isotope measurements are used to assess primary productivity and changes in organic matter production and preservation throughout the glacial-interglacial cycles of the Middle Pleistocene. We find that terrestrial organic matter forms the largest component of sedimentary organic content in Lake El'gygytgyn. The concentrations of all biomarker types mirror patterns of total organic carbon fluctuations. These are influenced by both perennial ice cover during glacial periods and enhanced production during interglacials. Although concentrations of source specific algal biomarkers were low, the $n$C$_{18}$ alkanol, a general biomarker for aquatic algae, was abundant in nearly every sample. This could be a good target compound for hydrogen isotope analyses as an aquatic plant endmember in future studies. The difference between long and short chain plant leaf wax hydrogen isotope values is emerging as a proxy to reconstruct relative humidity and evaporation changes. This technique discussed in Chapters 4 and 5. Reconstructing changes in these variables at Lake El'gygytgyn would be an informative counterpart to the temperature and moisture source change records included in Chapters 2 and 4.

Chapter 4 presents a record of temperature and moisture source variations recorded by plant leaf wax hydrogen isotopes from 0-280 ka. Where *n*-alkanes are abundant enough throughout the record, this analysis should be performed. Super interglacials and strong glacial periods should be targeted to identify the full range of hydrogen isotope variability. As noted in Chapter 4, the proxy incorporates a number of climatic and environmental signals. Isotope enabled modeling of multiple glacial-interglacial cycles would be a useful way to assess moisture source changes to Lake El'gygytgyn.

In Chapter 5, the hydrogen isotopic composition of two plant leaf wax compound classes are measured on the same samples from the last 120 ka. This technique is rare for for a paleo record, particularly of this length. The results highlight that compound class choice for analysis is important and may influence paleoclimate interpretations. In the future, comparisons between records from different compound classes should be interpreted with caution.

## REFERENCES


Alonso-Garcia, M., Sierro, F.J., Flores, J.A., 2011. Arctic front shifts in the subpolar North Atlantic during the Mid-Pleistocene (800–400 ka) and their implications for ocean circulation. Palaeogeogr. Palaeoclimatol. Palaeoecol. 311, 268–280. https://doi.org/10.1016/j.palaeo.2011.09.004

Andersen, K.K., Azuma, N., Barnola, J.-M., Bigler, M., Biscaye, P., Caillon, N., Chappellaz, J., Clausen, H.B., Dahl-Jensen, D., Fischer, H., Flückiger, J., Fritzsche, D., Fujii, Y., Goto-Azuma, K., Grønvold, K., Gundestrup, N.S., Hansson, M., Huber, C., Hvidberg, C.S., Johnsen, S.J., Jonsell, U., Jouzel, J., Kipfstuhl, S., Landais, A., Leuenberger, M., Lorrain, R., Masson-Delmotte, V., Miller, H., Motoyama, H., Narita, H., Popp, T., Rasmussen, S.O., Raynaud, D., Rothlisberger, R., Ruth, U., Samyn, D., Schwander, J., Shoji, H., Siggard-Andersen, M.-L., Steffensen, J.P., Stocker, T., Sveinbjörnsdóttir, A.E., Svensson, A., Takata, M., Tison, J.-L., Thorsteinsson, T., Watanabe, O., Wilhelms, F., White, J.W.C., 2004. High-resolution record of Northern Hemisphere climate extending into the last interglacial period. Nature 431, 147–151. https://doi.org/10.1038/nature02805

Anderson, P., Bennike, O., Bigelow, N., Brigham-Grette, J., Duvall, M., Edwards, M., Fréchette, B., Funder, S., Johnsen, S., Knies, J., Koerner, R., Lozhkin, A., Marshall, S., Matthiessen, J., Macdonald, G., Miller, G., Montoya, M., Muhs, D., Otto-Bliesner, B., Overpeck, J., Reeh, N., Sejrup, H.P., Spielhagen, R., Turner, C., Velichko, A., 2006. Last Interglacial Arctic warmth confirms polar amplification of climate change. Quat. Sci. Rev. 25, 1383–1400. https://doi.org/10.1016/j.quascirev.2006.01.033

Andersson, R.A., Kuhry, P., Meyers, P., Zebühr, Y., Crill, P., Mörth, M., 2011. Impacts of paleohydrological changes on n-alkane biomarker compositions of a Holocene peat sequence in the eastern European Russian Arctic. Org. Geochem. 42, 1065–1075. https://doi.org/10.1016/j.orggeochem.2011.06.020

Augustin, L., Barbante, C., Barnes, P.R., Barnola, J.M., Bigler, M., Castellano, E., Cattani, O., Chappellaz, J., Dahl-Jensen, D., Delmonte, B., others, 2004. Eight glacial cycles from an Antarctic ice core. Nature 429, 623–628.

Axford, Y., Briner, J.P., Cooke, C.A., Francis, D.R., Michelutti, N., Miller, G.H., Smol, J.P., Thomas, E.K., Wilson, C.R., Wolfe, A.P., 2009. Recent changes in a remote Arctic lake are unique within the past 200,000 years. Proc. Natl. Acad. Sci. 106, 18443–18446. https://doi.org/10.1073/pnas.0907094106

Balascio, N.L., D'Andrea, W.J., Bradley, R.S., Perren, B.B., 2013. Biogeochemical evidence for hydrologic changes during the Holocene in a lake sediment record from southeast Greenland. The Holocene 23, 1428–1439. https://doi.org/10.1177/0959683613493938

Balascio, N.L., D'Andrea, W.J., Gjerde, M., Bakke, J., 2017. Hydroclimate variability of High Arctic Svalbard during the Holocene inferred from hydrogen isotopes of leaf waxes. Quat. Sci. Rev. https://doi.org/10.1016/j.quascirev.2016.11.036

Barrett, S.M., Volkman, J.K., Dunstan, G.A., LeRoi, J.-M., 1995. Sterols of 14 Species of Marine Diatoms (bacillariophyta)1. J. Phycol. 31, 360–369. https://doi.org/10.1111/j.0022-3646.1995.00360.x

Bartlein, P.J., Edwards, M.E., Hostetler, S.W., Shafer, S.L., Anderson, P.M., Brubaker, L.B., Lozhkin, A.V., 2015. Early-Holocene warming in Beringia and its mediation by sea-level and vegetation changes. Clim Past 11, 1197–1222. https://doi.org/10.5194/cp-11-1197-2015

Bechtel, A., Smittenberg, R.H., Bernasconi, S.M., Schubert, C.J., 2010. Distribution of branched and isoprenoid tetraether lipids in an oligotrophic and a eutrophic Swiss lake: Insights into sources and GDGT-based proxies. Org. Geochem. 41, 822–832. https://doi.org/10.1016/j.orggeochem.2010.04.022

Beck, J.W., Zhou, W., Li, C., Wu, Z., White, L., Xian, F., Kong, X., An, Z., 2018. A 550,000-year record of East Asian monsoon rainfall from 10Be in loess 6.

Berger, A., Yin, Q., 2012. Modelling the Past and Future Interglacials in Response to Astronomical and Greenhouse Gas Forcing, in: The Future of the World's Climate. Elsevier, pp. 437–462.

Berke, M.A., Cartagena Sierra, A., Bush, R., Cheah, D., O'Connor, K., 2018. Controls on Leaf Wax Fractionation and δ2H Values in Tundra Vascular Plants from Western Greenland. Geochim. Cosmochim. Acta. https://doi.org/10.1016/j.gca.2018.10.020

Birks, H.J.B., Lotter, A.F., Juggins, S., Smol, J.P. (Eds.), 2012. Tracking Environmental Change Using Lake Sediments, Developments in Paleoenvironmental Research. Springer Netherlands, Dordrecht. https://doi.org/10.1007/978-94-007-2745-8

Bischoff, J., Mangelsdorf, K., Schwamborn, G., Wagner, D., 2014. Impact of Lake-Level and Climate Changes on Microbial Communities in a Terrestrial Permafrost Sequence of the El'gygytgyn Crater, Far East Russian Arctic: Impact of Lake-Level and Climate Changes on Microbial Communities. Permafr. Periglac. Process. 25, 107–116. https://doi.org/10.1002/ppp.1807

Blaga, C.I., Reichart, G.-J., Heiri, O., Damsté, J.S.S., 2008. Tetraether membrane lipid distributions in water-column particulate matter and sediments: a study of 47 European lakes along a north–south transect. J. Paleolimnol. 41, 523–540. https://doi.org/10.1007/s10933-008-9242-2

Bowen, G.J., Wassenaar, L.I., Hobson, K.A., 2005. Global application of stable hydrogen and oxygen isotopes to wildlife forensics. Oecologia 143, 337–348. https://doi.org/10.1007/s00442-004-1813-y

Brigham-Grette, J., Melles, M., Minyuk, P., Andreev, A., Tarasov, P., DeConto, R., Koenig, S., Nowaczyk, N., Wennrich, V., Rosen, P., Haltia, E., Cook, T., Gebhardt, C., Meyer-Jacob, C., Snyder, J., Herzschuh, U., 2013. Pliocene Warmth, Polar Amplification, and Stepped Pleistocene Cooling Recorded in NE Arctic Russia. Science 340, 1421–1427. https://doi.org/10.1126/science.1233137

Brooks, S.J., Diekmann, B., Jones, V.J., Hammarlund, D., 2015. Holocene environmental change in Kamchatka: A synopsis. Glob. Planet. Change, Holocene environmental change in Kamchatka 134, 166–174. https://doi.org/10.1016/j.gloplacha.2015.09.004

Buckles, L.K., Weijers, J.W.H., Verschuren, D., Sinninghe Damsté, J.S., 2014. Sources of core and intact branched tetraether membrane lipids in the lacustrine environment: Anatomy of Lake Challa and its catchment, equatorial East Africa. Geochim. Cosmochim. Acta 140, 106–126. https://doi.org/10.1016/j.gca.2014.04.042

Burgess, S.D., Coble, M.A., Vazquez, J.A., Coombs, M.L., Wallace, K.L., 2019. On the eruption age and provenance of the Old Crow tephra. Quat. Sci. Rev. 207, 64–79. https://doi.org/10.1016/j.quascirev.2018.12.026

Bush, R.T., McInerney, F.A., 2015. Influence of temperature and C4 abundance on n-alkane chain length distributions across the central USA. Org. Geochem. 79, 65–73. https://doi.org/10.1016/j.orggeochem.2014.12.003

Caissie, B.E., Brigham-Grette, J., Cook, M.S., Colmenero-Hidalgo, E., 2016. Bering Sea surface water conditions during Marine Isotope Stages 12 to 10 at Navarin Canyon (IODP Site U1345). Clim Past 12, 1739–1763. https://doi.org/10.5194/cp-12-1739-2016

Candy, I., Coope, G.R., Lee, J.R., Parfitt, S.A., Preece, R.C., Rose, J., Schreve, D.C., 2010. Pronounced warmth during early Middle Pleistocene interglacials: Investigating the Mid-Brunhes Event in the British terrestrial sequence. Earth-Sci. Rev. 103, 183–196. https://doi.org/10.1016/j.earscirev.2010.09.007

Candy, I., McClymont, E.L., 2013. Interglacial intensity in the North Atlantic over the last 800 000 years: investigating the complexity of the mid-Brunhes Event: INTERGLACIAL INTENSITY IN THE NORTH ATLANTIC. J. Quat. Sci. 28, 343–348. https://doi.org/10.1002/jqs.2632

Castañeda, I.S., Caley, T., Dupont, L., Kim, J.-H., Malaizé, B., Schouten, S., 2016. Middle to Late Pleistocene vegetation and climate change in subtropical southern East Africa. Earth Planet. Sci. Lett. 450, 306–316. https://doi.org/10.1016/j.epsl.2016.06.049

Castañeda, I.S., Schouten, S., 2011. A review of molecular organic proxies for examining modern and ancient lacustrine environments. Quat. Sci. Rev. 30, 2851–2891. https://doi.org/10.1016/j.quascirev.2011.07.009

Castañeda, I.S., Werne, J.P., Johnson, T.C., Filley, T.R., 2009a. Late Quaternary vegetation history of southeast Africa: The molecular isotopic record from Lake Malawi. Palaeogeogr. Palaeoclimatol. Palaeoecol. 275, 100–112. https://doi.org/10.1016/j.palaeo.2009.02.008

Castañeda, I.S., Werne, J.P., Johnsona, T.C., 2009b. Influence of climate change on algal community structure and primary productivity of Lake Malawi (East Africa) from the Last Glacial Maximum to present. Limnol. Oceanogr. 54, 2431–2447.

Cherapanova, M.V., Snyder, J.A., Brigham-Grette, J., 2006. Diatom stratigraphy of the last 250 ka at Lake El'gygytgyn, northeast Siberia. J. Paleolimnol. 37, 155–162. https://doi.org/10.1007/s10933-006-9019-4

Chikaraishi, Y., Naraoka, H., 2007. δ13C and δD relationships among three n-alkyl compound classes (n-alkanoic acid, n-alkane and n-alkanol) of terrestrial higher plants. Org. Geochem. 38, 198–215. https://doi.org/10.1016/j.orggeochem.2006.10.003

Chikaraishi, Y., Naraoka, H., 2003. Compound-specific δD–δ13C analyses of n-alkanes extracted from terrestrial and aquatic plants. Phytochemistry 63, 361–371. https://doi.org/10.1016/S0031-9422(02)00749-5

Clark, J., Mitrovica, J.X., Alder, J., 2014. Coastal paleogeography of the California–Oregon–Washington and Bering Sea continental shelves during the latest Pleistocene and Holocene: implications for the archaeological record. J. Archaeol. Sci. 52, 12–23. https://doi.org/10.1016/j.jas.2014.07.030

Cole, J.J., Prairie, Y.T., Caraco, N.F., McDowell, W.H., Tranvik, L.J., Striegl, R.G., Duarte, C.M., Kortelainen, P., Downing, J.A., Middelburg, J.J., Melack, J., 2007. Plumbing the Global Carbon Cycle: Integrating Inland Waters into the Terrestrial Carbon Budget. Ecosystems 10, 172–185. https://doi.org/10.1007/s10021-006-9013-8

Colleoni, F., Kirchner, N., Niessen, F., Quiquet, A., Liakka, J., 2016. An East Siberian ice shelf during the Late Pleistocene glaciations: Numerical reconstructions. Quat. Sci. Rev., Special Issue: PAST Gateways (Palaeo-Arctic Spatial and Temporal Gateways) 147, 148–163. https://doi.org/10.1016/j.quascirev.2015.12.023

Collins, J.A., Schefuß, E., Mulitza, S., Prange, M., Werner, M., Tharammal, T., Paul, A., Wefer, G., 2013. Estimating the hydrogen isotopic composition of past precipitation using leaf-waxes from western Africa. Quat. Sci. Rev. 65, 88–101. https://doi.org/10.1016/j.quascirev.2013.01.007

Craig, Gordon, 1965. CraigGordon1965_Noone_small3.pdf [WWW Document]. URL http://climate.colorado.edu/research/CG/CraigGordon1965_Noone_small3.pdf (accessed 12.18.16).

Craig, H., 1961. Isotopic Variations in Meteoric Waters. Science 133, 1702–1703. https://doi.org/10.1126/science.133.3465.1702

Cranwell, P.A., Eglinton, G., Robinson, N., 1987. Lipids of aquatic organisms as potential contributors to lacustrine sediments—II. Org. Geochem. 11, 513–527. https://doi.org/10.1016/0146-6380(87)90007-6

Cronin, T.M., DeNinno, L.H., Polyak, L., Caverly, E.K., Poore, R.Z., Brenner, A., Rodriguez-Lazaro, J., Marzen, R.E., 2014. Quaternary ostracode and foraminiferal biostratigraphy and paleoceanography in the western Arctic Ocean. Mar. Micropaleontol. 111, 118–133. https://doi.org/10.1016/j.marmicro.2014.05.001

Cronin, T.M., Gemery, L., Briggs, W.M., Jakobsson, M., Polyak, L., Brouwers, E.M., 2010. Quaternary Sea-ice history in the Arctic Ocean based on a new Ostracode sea-ice proxy. Quat. Sci. Rev., APEX: Arctic Palaeoclimate and its Extremes 29, 3415–3429. https://doi.org/10.1016/j.quascirev.2010.05.024

Daniels, W.C., Huang, Y., Russell, J.M., Giblin, A.E., 2018. Effect of continuous light on leaf wax isotope ratios in Betula nana and Eriophorum vaginatum: implications for Arctic paleoclimate reconstructions. Org. Geochem. 125, 70–81. https://doi.org/10.1016/j.orggeochem.2018.08.008

Daniels, W.C., Russell, J.M., Giblin, A.E., Welker, J.M., Klein, E.S., Huang, Y., 2017a. Hydrogen isotope fractionation in leaf waxes in the Alaskan Arctic tundra. Geochim. Cosmochim. Acta 213, 216–236. https://doi.org/10.1016/j.gca.2017.06.028

Daniels, W.C., Russell, J.M., Giblin, A.E., Welker, J.M., Klein, E.S., Huang, Y., 2017b. Hydrogen isotope fractionation in leaf waxes in the Alaskan Arctic tundra. Geochim. Cosmochim. Acta 213, 216–236. https://doi.org/10.1016/j.gca.2017.06.028

D'Anjou, R.M., Wei, J.H., Castañeda, I.S., Brigham-Grette, J., Petsch, S.T., Finkelstein, D.B., 2013a. High-latitude environmental change during MIS 9 and 11: biogeochemical evidence from Lake El'gygytgyn, Far East Russia. Clim. Past 9, 567–581. https://doi.org/10.5194/cp-9-567-2013

D'Anjou, R.M., Wei, J.H., Castañeda, I.S., Brigham-Grette, J., Petsch, S.T., Finkelstein, D.B., 2013b. High-latitude environmental change during MIS 9 and 11: biogeochemical evidence from Lake El'gygytgyn, Far East Russia. Clim. Past 9, 567–581. https://doi.org/10.5194/cp-9-567-2013

Dansgaard, W., 1964. Stable isotopes in precipitation. Tellus A 16. https://doi.org/10.3402/tellusa.v16i4.8993

de Bar, M.W., Dorhout, D.J.C., Hopmans, E.C., Rampen, S.W., Sinninghe Damsté, J.S., Schouten, S., 2016. Constraints on the application of long chain diol proxies in the Iberian Atlantic margin. Org. Geochem. 101, 184–195. https://doi.org/10.1016/j.orggeochem.2016.09.005

De Jonge, C., Hopmans, E.C., Stadnitskaia, A., Rijpstra, W.I.C., Hofland, R., Tegelaar, E., Sinninghe Damsté, J.S., 2013. Identification of novel penta- and hexamethylated branched glycerol dialkyl glycerol tetraethers in peat using HPLC–MS2, GC–MS and GC–SMB-MS. Org. Geochem. 54, 78–82. https://doi.org/10.1016/j.orggeochem.2012.10.004

De Jonge, C., Hopmans, E.C., Zell, C.I., Kim, J.-H., Schouten, S., Sinninghe Damsté, J.S., 2014a. Occurrence and abundance of 6-methyl branched glycerol dialkyl glycerol tetraethers in soils: Implications for palaeoclimate reconstruction. Geochim. Cosmochim. Acta 141, 97–112. https://doi.org/10.1016/j.gca.2014.06.013

De Jonge, C., Stadnitskaia, A., Hopmans, E.C., Cherkashov, G., Fedotov, A., Sinninghe Damsté, J.S., 2014b. In situ produced branched glycerol dialkyl glycerol tetraethers in suspended particulate matter from the Yenisei River, Eastern Siberia. Geochim. Cosmochim. Acta 125, 476–491. https://doi.org/10.1016/j.gca.2013.10.031

De Jonge, C., Stadnitskaia, A., Hopmans, E.C., Cherkashov, G., Fedotov, A., Streletskaya, I.D., Vasiliev, A.A., Sinninghe Damsté, J.S., 2015. Drastic changes in the distribution of branched tetraether lipids in suspended matter and sediments from the Yenisei River and Kara Sea (Siberia): Implications for the use of brGDGT-based proxies in coastal marine sediments. Geochim. Cosmochim. Acta 165, 200–225. https://doi.org/10.1016/j.gca.2015.05.044

de Wet, G.A., Castañeda, I.S., DeConto, R.M., Brigham-Grette, J., 2016. A high-resolution mid-Pleistocene temperature record from Arctic Lake El'gygytgyn: a 50 kyr super interglacial from MIS 33 to MIS 31? Earth Planet. Sci. Lett. 436, 56–63. https://doi.org/10.1016/j.epsl.2015.12.021

Dean, W.E., Gorham, E., 1998. Magnitude and significance of carbon burial in lakes, reservoirs, and peatlands. Geology 26, 535–538. https://doi.org/10.1130/0091-7613(1998)026<0535:MASOCB>2.3.CO;2

Detlef, H., Belt, S.T., Sosdian, S.M., Smik, L., Lear, C.H., Hall, I.R., Cabedo-Sanz, P., Husum, K., Kender, S., 2018. Sea ice dynamics across the Mid-Pleistocene transition in the Bering Sea. Nat. Commun. 9, 941. https://doi.org/10.1038/s41467-018-02845-5

Didyk, B.M., Simoneit, B.R.T., Brassell, S.C., Eglinton, G., 1978. Organic geochemical indicators of palaeoenvironmental conditions of sedimentation. Nature 272, 216–222. https://doi.org/10.1038/272216a0

Downing, J.A., Prairie, Y.T., Cole, J.J., Duarte, C.M., Tranvik, L.J., Striegl, R.G., McDowell, W.H., Kortelainen, P., Caraco, N.F., Melack, J.M., Middelburg, J.J., 2006. The global abundance and size distribution of lakes, ponds, and impoundments. Limnol. Oceanogr. 51, 2388–2397. https://doi.org/10.4319/lo.2006.51.5.2388

Dutton, A., Carlson, A.E., Long, A.J., Milne, G.A., Clark, P.U., DeConto, R., Horton, B.P., Rahmstorf, S., Raymo, M.E., 2015. Sea-level rise due to polar ice-sheet mass loss during past warm periods. Science 349, aaa4019–aaa4019. https://doi.org/10.1126/science.aaa4019

Eglinton, G., Hamilton, R.J., 1967. Leaf Epicuticular Waxes. Science 156, 1322–1335. https://doi.org/10.1126/science.156.3780.1322

Eglinton, G., Logan, G.A., 1991. Molecular preservation. Phil Trans R Soc Lond B 333, 315–328. https://doi.org/10.1098/rstb.1991.0081

Eglinton, T., Eglinton, G., 1963. The Distribution of Alkanes. Elsevier.

Elderfield, H., Ferretti, P., Greaves, M., Crowhurst, S., McCave, I.N., Hodell, D., Piotrowski, A.M., 2012. Evolution of Ocean Temperature and Ice Volume Through the Mid-Pleistocene Climate Transition. Science 337, 704–709. https://doi.org/10.1126/science.1221294

Feakins, S.J., 2013. Pollen-corrected leaf wax D/H reconstructions of northeast African hydrological changes during the late Miocene. Palaeogeogr. Palaeoclimatol. Palaeoecol. 374, 62–71. https://doi.org/10.1016/j.palaeo.2013.01.004

Feakins, S.J., Bentley, L.P., Salinas, N., Shenkin, A., Blonder, B., Goldsmith, G.R., Ponton, C., Arvin, L.J., Wu, M.S., Peters, T., West, A.J., Martin, R.E., Enquist, B.J., Asner, G.P., Malhi, Y., 2016. Plant leaf wax biomarkers capture gradients in hydrogen isotopes of precipitation from the Andes and Amazon. Geochim. Cosmochim. Acta 182, 155–172. https://doi.org/10.1016/j.gca.2016.03.018

Feakins, S.J., Sessions, A.L., 2010. Controls on the D/H ratios of plant leaf waxes in an arid ecosystem. Geochim. Cosmochim. Acta 74, 2128–2141. https://doi.org/10.1016/j.gca.2010.01.016

Fedorov, G., Nolan, M., Brigham-Grette, J., Bolshiyanov, D., Schwamborn, G., Juschus, O., 2013. Preliminary estimation of Lake El'gygytgyn water balance and sediment income. Clim. Past 9, 1455–1465. https://doi.org/10.5194/cp-9-1455-2013

Ficken, K.J., Li, B., Swain, D.L., Eglinton, G., 2000. An n-alkane proxy for the sedimentary input of submerged/floating freshwater aquatic macrophytes. Org. Geochem. 31, 745–749. https://doi.org/10.1016/S0146-6380(00)00081-4

Fitzpatrick, J.J., Alley, R.B., Brigham-Grette, J., Miller, G.H., Polyak, L., White, J.W.C., 2010. Arctic Paleoclimate Synthesis Thematic Papers. Quat. Sci. Rev., Special Theme: Arctic Palaeoclimate Synthesis (PP. 1674-1790) 29, 1674–1678. https://doi.org/10.1016/j.quascirev.2009.09.016

Flanagan, K.M., McCauley, E., Wrona, F., Prowse, T., 2003. Climate change: the potential for latitudinal effects on algal biomass in aquatic ecosystems. Can. J. Fish. Aquat. Sci. 60, 635–639. https://doi.org/10.1139/f03-062

Foster, L.C., Pearson, E.J., Juggins, S., Hodgson, D.A., Saunders, K.M., Verleyen, E., Roberts, S.J., 2016. Development of a regional glycerol dialkyl glycerol tetraether (GDGT)–temperature calibration for Antarctic and sub-Antarctic lakes. Earth Planet. Sci. Lett. 433, 370–379. https://doi.org/10.1016/j.epsl.2015.11.018

G Ourisson, M Rohmer, Poralla, and K., 1987. Prokaryotic Hopanoids and other Polyterpenoid Sterol Surrogates. Annu. Rev. Microbiol. 41, 301–333. https://doi.org/10.1146/annurev.mi.41.100187.001505

Gasson, E.G.W., DeConto, R.M., Pollard, D., Clark, C.D., 2018. Numerical simulations of a kilometre-thick Arctic ice shelf consistent with ice grounding observations. Nat. Commun. 9, 1510. https://doi.org/10.1038/s41467-018-03707-w

Glushkova, O.Y., 2001. Geomorphological correlation of Late Pleistocene glacial complexes of Western and Eastern Beringia. Quat. Sci. Rev., Beringian Paleoenvironments - Festschrift in Honour of D.M. Hopkins 20, 405–417. https://doi.org/10.1016/S0277-3791(00)00108-6

Glushkova, O.Y., Smirnov, V.N., 2006. Pliocene to Holocene geomorphic evolution and paleogeography of the El'gygytgyn Lake region, NE Russia. J. Paleolimnol. 37, 37–47. https://doi.org/10.1007/s10933-006-9021-x

Gore, D.B., 1997. Blanketing snow and ice; constraints on radiocarbon dating deglaciation in East Antarctic oases. Antarct. Sci. 9, 336–346. https://doi.org/10.1017/S0954102097000412

Griffiths, K., Michelutti, N., Sugar, M., Douglas, M.S.V., Smol, J.P., 2017. Ice-cover is the principal driver of ecological change in High Arctic lakes and ponds. PLOS ONE 12, e0172989. https://doi.org/10.1371/journal.pone.0172989

Hall, I.R., McCave, I.N., Shackleton, N.J., Weedon, G.P., Harris, S.E., 2001. Intensified deep Pacific inflow and ventilation in Pleistocene glacial times. Nature 412, 809–812. https://doi.org/10.1038/35090552

Haltia, E.M., Nowaczyk, N.R., 2013. Magnetostratigraphy of sediments from Lake El'gygytgyn ICDP Site 5011-1: paleomagnetic age constraints for the longest paleoclimate record from the continental Arctic. Clim Past Discuss 9, 5077–5122. https://doi.org/10.5194/cpd-9-5077-2013

Hao, Q., Wang, L., Oldfield, F., Guo, Z., 2015. Extra-long interglacial in Northern Hemisphere during MISs 15-13 arising from limited extent of Arctic ice sheets in glacial MIS 14. Sci. Rep. 5, 12103. https://doi.org/10.1038/srep12103

Haug, G.H., Maslin, M.A., Sarnthein, M., Stax, R., Tiedemann, R., 1995. Evolution of northwest Pacific sedimentation patterns since 6 Ma (Site 882). In: Rea, D.K., Basov, I.A., Scholl, D.W., and Allen, J.F. (Eds.). Proc. Ocean Drill. Program Sci. Results 145, 293–314.

Healey, F.P., Hendzel, L.L., 1980. Physiological Indicators of Nutrient Deficiency in Lake Phytoplankton. Can. J. Fish. Aquat. Sci. 37, 442–453. https://doi.org/10.1139/f80-058

Hecky, R.E., 1993. The eutrophication of Lake Victoria. SIL Proc. 1922-2010 25, 39–48. https://doi.org/10.1080/03680770.1992.11900057

Herfort, L., Schouten, S., Boon, J.P., Woltering, M., Baas, M., Weijers, J.W.H., Sinninghe Damsté, J.S., 2006. Characterization of transport and deposition of terrestrial organic matter in the southern North Sea using the BIT index. Limnol. Oceanogr. 51, 2196–2205. https://doi.org/10.4319/lo.2006.51.5.2196

Hobbie, J.E., Bahr, M., Bettez, N., Rublee, P.A., 2000. Microbial food webs in oligotrophic arctic lakes, in: Microbial Biosystems: New Frontiers, Proceedings of the 8th International Symposium on Microbial Ecology, Atlantic Canada Society for Microbial Ecology, Halifax, Canada. pp. 293–298.

Holland, A.R., Petsch, S.T., Castañeda, I.S., Wilkie, K.M., Burns, S.J., Brigham-Grette, J., 2013. A biomarker record of Lake El'gygytgyn, Far East Russian Arctic: investigating sources of organic matter and carbon cycling during marine isotope stages 1–3. Clim. Past 9, 243–260. https://doi.org/10.5194/cp-9-243-2013

Hopmans, E.C., Weijers, J.W.H., Schefuß, E., Herfort, L., Sinninghe Damsté, J.S., Schouten, S., 2004. A novel proxy for terrestrial organic matter in sediments based on branched and isoprenoid tetraether lipids. Earth Planet. Sci. Lett. 224, 107–116. https://doi.org/10.1016/j.epsl.2004.05.012

Hou, J., D'Andrea, W.J., Huang, Y., 2008. Can sedimentary leaf waxes record D/H ratios of continental precipitation? Field, model, and experimental assessments. Geochim. Cosmochim. Acta 72, 3503–3517. https://doi.org/10.1016/j.gca.2008.04.030

Hou, J., D'Andrea, W.J., MacDonald, D., Huang, Y., 2007. Hydrogen isotopic variability in leaf waxes among terrestrial and aquatic plants around Blood Pond, Massachusetts (USA). Org. Geochem. 38, 977–984. https://doi.org/10.1016/j.orggeochem.2006.12.009

Hu, A., Meehl, G.A., Otto-Bliesner, B.L., Waelbroeck, C., Han, W., Loutre, M.-F., Lambeck, K., Mitrovica, J.X., Rosenbloom, N., 2010. Influence of Bering Strait flow and North Atlantic circulation on glacial sea-level changes. Nat. Geosci. 3, 118–121. https://doi.org/10.1038/ngeo729

Huang, Y., Shuman, B., Wang, Y., Webb, T., 2002. Hydrogen isotope ratios of palmitic acid in lacustrine sediments record late Quaternary climate variations. Geology 30, 1103–1106. https://doi.org/10.1130/0091-7613(2002)030<1103:HIROPA>2.0.CO;2

Huybers, P., 2011. Combined obliquity and precession pacing of late Pleistocene deglaciations. Nature 480, 229–232. https://doi.org/10.1038/nature10626

IPCC, 2013. IPCC Working Group I [WWW Document]. URL http://www.climatechange2013.org/ (accessed 4.25.16).

Jaccard, S.L., Galbraith, E.D., Sigman, D.M., Haug, G.H., 2010. A pervasive link between Antarctic ice core and subarctic Pacific sediment records over the past 800 kyrs. Quat. Sci. Rev., Climate of the Last Million Years: New Insights from EPICA and Other Records 29, 206–212. https://doi.org/10.1016/j.quascirev.2009.10.007

Jacob, J., Disnar, J.-R., Boussafir, M., Spadano Albuquerque, A.L., Sifeddine, A., Turcq, B., 2005. Pentacyclic triterpene methyl ethers in recent lacustrine sediments (Lagoa do Caçó, Brazil). Org. Geochem. 36, 449–461. https://doi.org/10.1016/j.orggeochem.2004.09.005

Jansen, J.H., Kuijpers, A., Troelstra, S.R., 1986. A mid-brunhes climatic event: long-term changes in global atmosphere and ocean circulation. Science 232, 619–622. https://doi.org/10.1126/science.232.4750.619

Jouzel, J., Masson-Delmotte, V., Cattani, O., Dreyfus, G., Falourd, S., Hoffmann, G., Minster, B., Nouet, J., Barnola, J.M., Chappellaz, J., Fischer, H., Gallet, J.C., Johnsen, S., Leuenberger, M., Loulergue, L., Luethi, D., Oerter, H., Parrenin, F., Raisbeck, G., Raynaud, D., Schilt, A., Schwander, J., Selmo, E., Souchez, R., Spahni, R., Stauffer, B., Steffensen, J.P., Stenni, B., Stocker, T.F., Tison, J.L., Werner, M., Wolff, E.W., 2007. Orbital and Millennial Antarctic Climate Variability over the Past 800,000 Years. Science 317, 793–796. https://doi.org/10.1126/science.1141038

Juschus, O., Melles, M., Gebhardt, A.C., Niessen, F., 2009. Late Quaternary mass movement events in Lake El′gygytgyn, North-eastern Siberia. Sedimentology 56, 2155–2174. https://doi.org/10.1111/j.1365-3091.2009.01074.x

Juschus, O., Preusser, F., Melles, M., Radtke, U., 2007. Applying SAR-IRSL methodology for dating fine-grained sediments from Lake El'gygytgyn, north-eastern Siberia. Quat. Geochronol. 1–4, 187–194. https://doi.org/10.1016/j.quageo.2006.05.006

Kahmen, A., Hoffmann, B., Schefuß, E., Arndt, S.K., Cernusak, L.A., West, J.B., Sachse, D., 2013a. Leaf water deuterium enrichment shapes leaf wax n-alkane δD values of angiosperm plants II: Observational evidence and global implications. Geochim. Cosmochim. Acta 111, 50–63. https://doi.org/10.1016/j.gca.2012.09.004

Kahmen, A., Schefuß, E., Sachse, D., 2013b. Leaf water deuterium enrichment shapes leaf wax n-alkane δD values of angiosperm plants I: Experimental evidence and mechanistic insights. Geochim. Cosmochim. Acta 111, 39–49. https://doi.org/10.1016/j.gca.2012.09.003

Kaufman, D.S., Axford, Y.L., Henderson, A.C.G., McKay, N.P., Oswald, W.W., Saenger, C., Anderson, R.S., Bailey, H.L., Clegg, B., Gajewski, K., Hu, F.S., Jones, M.C., Massa, C., Routson, C.C., Werner, A., Wooller, M.J., Yu, Z., 2016. Holocene climate changes in eastern Beringia (NW North America) – A systematic review of multi-proxy evidence. Quat. Sci. Rev., Special Issue: PAST Gateways (Palaeo-Arctic Spatial and Temporal Gateways) 147, 312–339. https://doi.org/10.1016/j.quascirev.2015.10.021

Keisling, B.A., Castañeda, I.S., Brigham-Grette, J., 2016. Hydrological and temperature change in Arctic Siberia during the intensification of Northern Hemisphere Glaciation. Earth Planet. Sci. Lett. https://doi.org/10.1016/j.epsl.2016.09.058

Kim, J.-H., Ludwig, W., Schouten, S., Kerhervé, P., Herfort, L., Bonnin, J., Sinninghe Damsté, J.S., 2007. Impact of flood events on the transport of terrestrial organic matter to the ocean: A study of the Têt River (SW France) using the BIT index. Org. Geochem. 38, 1593–1606. https://doi.org/10.1016/j.orggeochem.2007.06.010

Knudson, K.P., Ravelo, A.C., 2015. North Pacific Intermediate Water circulation enhanced by the closure of the Bering Strait: NPIW ENHANCED WITH BERING STRAIT CLOSURE. Paleoceanography n/a-n/a. https://doi.org/10.1002/2015PA002840

Kopec, B.G., Feng, X., Michel, F.A., Posmentier, E.S., 2016. Influence of sea ice on Arctic precipitation. Proc. Natl. Acad. Sci. 113, 46–51. https://doi.org/10.1073/pnas.1504633113

Kurita, N., Yoshida, N., Inoue, G., Chayanova, E.A., 2004. Modern isotope climatology of Russia: A first assessment: ISOTOPIC COMPOSITION OVER RUSSIA. J. Geophys. Res. Atmospheres 109, n/a-n/a. https://doi.org/10.1029/2003JD003404

Lang, N., Wolff, E.W., 2011. Interglacial and glacial variability from the last 800 ka in marine, ice and terrestrial archives. Clim. Past 7, 361–380. https://doi.org/10.5194/cp-7-361-2011

Laskar, J., Robutel, P., Joutel, F., Gastineau, M., Correia, A.C.M., Levrard, B., 2004. A long-term numerical solution for the insolation quantities of the Earth. Astron. Astrophys. 428, 261–285. https://doi.org/10.1051/0004-6361:20041335

Lattaud, J., Dorhout, D., Schulz, H., Castañeda, I.S., Schefuß, E., Sinninghe Damsté, J.S., Schouten, S., 2017. The C32 alkane-1,15-diol as a proxy of late Quaternary riverine input in coastal margins. Clim Past 13, 1049–1061. https://doi.org/10.5194/cp-13-1049-2017

Lattaud, Julie, Kim, J.-H., De Jonge, C., Zell, C., Sinninghe Damsté, J.S., Schouten, S., 2017. The C32 alkane-1,15-diol as a tracer for riverine input in coastal seas. Geochim. Cosmochim. Acta 202, 146–158. https://doi.org/10.1016/j.gca.2016.12.030

Lattaud, J., Lo, L., Huang, J.-J., Chou, Y.-M., Gorbarenko, S.A., Damsté, J.S.S., Schouten, S., 2018. A Comparison of Late Quaternary Organic Proxy-Based Paleotemperature Records of the Central Sea of Okhotsk. Paleoceanogr. Paleoclimatology 33, 732–744. https://doi.org/10.1029/2018PA003388

Lawrence, K.T., Herbert, T.D., Brown, C.M., Raymo, M.E., Haywood, A.M., 2009. High-amplitude variations in North Atlantic sea surface temperature during the early Pliocene warm period. Paleoceanography 24, PA2218. https://doi.org/10.1029/2008PA001669

Layer, P.W., 2000. Argon-40/argon-39 age of the El'gygytgyn impact event, Chukotka, Russia. Meteorit. Planet. Sci. 35, 591–599.

Li, C., Sessions, A.L., Kinnaman, F.S., Valentine, D.L., 2009. Hydrogen-isotopic variability in lipids from Santa Barbara Basin sediments. Geochim. Cosmochim. Acta 73, 4803–4823. https://doi.org/10.1016/j.gca.2009.05.056

Lisiecki, L.E., Raymo, M.E., 2005. A Pliocene-Pleistocene stack of 57 globally distributed benthic $\delta^{18}$O records: PLIOCENE-PLEISTOCENE BENTHIC STACK. Paleoceanography 20, n/a-n/a. https://doi.org/10.1029/2004PA001071

Liu, J., An, Z., 2018. A hierarchical framework for disentangling different controls on leaf wax δDn-alkane values in terrestrial higher plants. Quat. Sci. Rev. 201, 409–417. https://doi.org/10.1016/j.quascirev.2018.10.026

Liu, J., Liu, W., An, Z., Yang, H., 2016. Different hydrogen isotope fractionations during lipid formation in higher plants: Implications for paleohydrology reconstruction at a global scale. Sci. Rep. 6, 19711. https://doi.org/10.1038/srep19711

Liu, W., Huang, Y., 2005. Compound specific D/H ratios and molecular distributions of higher plant leaf waxes as novel paleoenvironmental indicators in the Chinese Loess Plateau. Org. Geochem. 36, 851–860. https://doi.org/10.1016/j.orggeochem.2005.01.006

Liu, W., Yang, H., 2008. Multiple controls for the variability of hydrogen isotopic compositions in higher plant *n* -alkanes from modern ecosystems. Glob. Change Biol. 14, 2166–2177. https://doi.org/10.1111/j.1365-2486.2008.01608.x

Lo, L., Belt, S.T., Lattaud, J., Friedrich, T., Zeeden, C., Schouten, S., Smik, L., Timmermann, A., Cabedo-Sanz, P., Huang, J.-J., Zhou, L., Ou, T.-H., Chang, Y.-P., Wang, L.-C., Chou, Y.-M., Shen, C.-C., Chen, M.-T., Wei, K.-Y., Song, S.-R., Fang, T.-H., Gorbarenko, S.A., Wang, W.-L., Lee, T.-Q., Elderfield, H., Hodell, D.A., 2018. Precession and atmospheric CO2 modulated variability of sea ice in the central Okhotsk Sea since 130,000 years ago. Earth Planet. Sci. Lett. 488, 36–45. https://doi.org/10.1016/j.epsl.2018.02.005

Loomis, S.E., Russell, J.M., Heureux, A.M., D'Andrea, W.J., Sinninghe Damsté, J.S., 2014. Seasonal variability of branched glycerol dialkyl glycerol tetraethers (brGDGTs) in a temperate lake system. Geochim. Cosmochim. Acta 144, 173–187. https://doi.org/10.1016/j.gca.2014.08.027

Loomis, S.E., Russell, J.M., Ladd, B., Street-Perrott, F.A., Sinninghe Damsté, J.S., 2012. Calibration and application of the branched GDGT temperature proxy on East African lake sediments. Earth Planet. Sci. Lett. 357–358, 277–288. https://doi.org/10.1016/j.epsl.2012.09.031

Loutre, M.F., Berger, A., 2003. Marine Isotope Stage 11 as an analogue for the present interglacial. Glob. Planet. Change 36, 209–217. https://doi.org/10.1016/S0921-8181(02)00186-8

Lozhkin, A.V., Anderson, P.M., 2013. Vegetation responses to interglacial warming in the Arctic: examples from Lake El'gygytgyn, Far East Russian Arctic. Clim. Past 9, 1211–1219. https://doi.org/10.5194/cp-9-1211-2013

Lozhkin, A.V., Anderson, P.M., Matrosova, T.V., Minyuk, P.S., 2007a. The pollen record from El'gygytgyn Lake: implications for vegetation and climate histories of northern Chukotka since the late middle Pleistocene. J. Paleolimnol. 37, 135–153. https://doi.org/10.1007/s10933-006-9018-5

Lozhkin, A.V., Anderson, P.M., Matrosova, T.V., Minyuk, P.S., Brigham-Grette, J., Melles, M., 2007b. Continuous record of environmental changes in Chukotka during the last 350 thousand years. Russ. J. Pac. Geol. 1, 550–555. https://doi.org/10.1134/S1819714007060048

Lozhkin, A.V., Minyuk, P.S., Anderson, P.M., Nedorubova, E.Y., Korzun, J.V., 2017. Variability in landscape and lake system responses to glacial and interglacial climates during the Middle Pleistocene based on palynological and geochemical data from Lake El'gygytgyn, Eastern Arctic. Rev. Palaeobot. Palynol. 246, 1–13. https://doi.org/10.1016/j.revpalbo.2017.06.004

Lüthi, D., Le Floch, M., Bereiter, B., Blunier, T., Barnola, J.-M., Siegenthaler, U., Raynaud, D., Jouzel, J., Fischer, H., Kawamura, K., Stocker, T.F., 2008. High-resolution carbon dioxide concentration record 650,000–800,000 years before present. Nature 453, 379–382. https://doi.org/10.1038/nature06949

Martínez-Garcia, A., Rosell-Melé, A., McClymont, E.L., Gersonde, R., Haug, G.H., 2010. Subpolar Link to the Emergence of the Modern Equatorial Pacific Cold Tongue. Science 328, 1550–1553. https://doi.org/10.1126/science.1184480

Marzen, R.E., DeNinno, L.H., Cronin, T.M., 2016. Calcareous microfossil-based orbital cyclostratigraphy in the Arctic Ocean. Quat. Sci. Rev. 149, 109–121. https://doi.org/10.1016/j.quascirev.2016.07.004

McFarlin, J.M., Axford, Y., Osburn, M.R., Kelly, M.A., Osterberg, E.C., Farnsworth, L.B., 2018. Pronounced summer warming in northwest Greenland during the Holocene and Last Interglacial. Proc. Natl. Acad. Sci. 115, 6357–6362. https://doi.org/10.1073/pnas.1720420115

McInerney, F.A., Helliker, B.R., Freeman, K.H., 2011. Hydrogen isotope ratios of leaf wax n-alkanes in grasses are insensitive to transpiration. Geochim. Cosmochim. Acta 75, 541–554. https://doi.org/10.1016/j.gca.2010.10.022

McKay, N.P., Kaufman, D.S., Routson, C.C., Erb, M.P., Zander, P.D., 2018. The Onset and Rate of Holocene Neoglacial Cooling in the Arctic. Geophys. Res. Lett. 45, 12,487-12,496. https://doi.org/10.1029/2018GL079773

McKay, R., Naish, T., Powell, R., Barrett, P., Scherer, R., Talarico, F., Kyle, P., Monien, D., Kuhn, G., Jackolski, C., Williams, T., 2012. Pleistocene variability of Antarctic Ice Sheet extent in the Ross Embayment. Quat. Sci. Rev. 34, 93–112. https://doi.org/10.1016/j.quascirev.2011.12.012

Melles, M., Brigham-Grette, J., Glushkova, O.Y., Minyuk, P.S., Nowaczyk, N.R., Hubberten, H.-W., 2007. Sedimentary geochemistry of core PG1351 from Lake El'gygytgyn—a sensitive record of climate variability in the East Siberian Arctic during the past three glacial–interglacial cycles. J. Paleolimnol. 37, 89–104. https://doi.org/10.1007/s10933-006-9025-6

Melles, M., Brigham-Grette, J., Minyuk, P., Koeberl, C., Andreev, A., Cook, T., Fedorov, G., Gebhardt, C., Haltia-Hovi, E., Kukkonen, M., others, 2011. The Lake El'gygytgyn Scientific Drilling Project—conquering Arctic challenges through continental drilling. Sci. Drill. 11, 29–40.

Melles, M., Brigham-Grette, J., Minyuk, P.S., Nowaczyk, N.R., Wennrich, V., DeConto, R.M., Anderson, P.M., Andreev, A.A., Coletti, A., Cook, T.L., Haltia-Hovi, E., Kukkonen, M., Lozhkin, A.V., Rosen, P., Tarasov, P., Vogel, H., Wagner, B., 2012. 2.8 Million Years of Arctic Climate Change from Lake El'gygytgyn, NE Russia. Science 337, 315–320. https://doi.org/10.1126/science.1222135

Members, N. community, Dahl-Jensen, D., Albert, M.R., Aldahan, A., Azuma, N., Balslev-Clausen, D., Baumgartner, M., Berggren, A.-M., Bigler, M., Binder, T., Blunier, T., Bourgeois, J.C., Brook, E.J., Buchardt, S.L., Buizert, C., Capron, E., Chappellaz, J., Chung, J., Clausen, H.B., Cvijanovic, I., Davies, S.M., Ditlevsen, P., Eicher, O., Fischer, H., Fisher, D.A., Fleet, L.G., Gfeller, G., Gkinis, V., Gogineni, S., Goto-Azuma, K., Grinsted, A., Gudlaugsdottir, H., Guillevic, M., Hansen, S.B., Hansson, M., Hirabayashi, M., Hong, S., Hur, S.D., Huybrechts, P., Hvidberg, C.S., Iizuka, Y., Jenk, T., Johnsen, S.J., Jones, T.R., Jouzel, J., Karlsson, N.B., Kawamura, K., Keegan, K., Kettner, E., Kipfstuhl, S., Kjær, H.A., Koutnik, M., Kuramoto, T., Köhler, P., Laepple, T., Landais, A., Langen, P.L., Larsen, L.B., Leuenberger, D., Leuenberger, M., Leuschen, C., Li, J., Lipenkov, V., Martinerie, P., Maselli, O.J., Masson-Delmotte, V., McConnell, J.R., Miller, H., Mini, O., Miyamoto, A., Montagnat-Rentier, M., Mulvaney, R., Muscheler, R., Orsi, A.J., Paden, J., Panton, C., Pattyn, F., Petit, J.-R., Pol, K., Popp, T., Possnert, G., Prié, F., Prokopiou, M., Quiquet, A., Rasmussen, S.O., Raynaud, D., Ren, J., Reutenauer, C., Ritz, C., Röckmann, T., Rosen, J.L., Rubino, M., Rybak, O., Samyn, D., Sapart, C.J., Schilt, A., Schmidt, A.M.Z., Schwander, J., Schüpbach, S., Seierstad, I., Severinghaus, J.P., Sheldon, S., Simonsen, S.B., Sjolte, J., Solgaard, A.M., Sowers, T., Sperlich, P., Steen-Larsen, H.C., Steffen, K., Steffensen, J.P., Steinhage, D., Stocker, T.F., Stowasser, C., Sturevik, A.S., Sturges, W.T., Sveinbjörnsdottir, A., Svensson, A., Tison, J.-L., Uetake, J., Vallelonga, P., Wal, R.S.W. van de, Wel, G. van der, Vaughn, B.H., Vinther, B., Waddington, E., Wegner, A., Weikusat, I., White, J.W.C., Wilhelms, F., Winstrup, M., Witrant, E., Wolff, E.W., Xiao, C., Zheng, J., 2013. Eemian interglacial reconstructed from a Greenland folded ice core. Nature 493, 489–494. https://doi.org/10.1038/nature11789

Members, N.G.I.C.P., Andersen, K.K., Azuma, N., Barnola, J.-M., Bigler, M., Biscaye, P., Caillon, N., Chappellaz, J., Clausen, H.B., Dahl-Jensen, D., Fischer, H., Flückiger, J., Fritzsche, D., Fujii, Y., Goto-Azuma, K., Grønvold, K., Gundestrup, N.S., Hansson, M., Huber, C., Hvidberg, C.S., Johnsen, S.J., Jonsell, U., Jouzel, J., Kipfstuhl, S., Landais, A., Leuenberger, M., Lorrain, R., Masson-Delmotte, V., Miller, H., Motoyama, H., Narita, H., Popp, T., Rasmussen, S.O., Raynaud, D., Rothlisberger, R., Ruth, U., Samyn, D., Schwander, J., Shoji, H., Siggard-Andersen, M.-L., Steffensen, J.P., Stocker, T., Sveinbjörnsdóttir, A.E., Svensson, A., Takata, M., Tison, J.-L., Thorsteinsson, T., Watanabe, O., Wilhelms, F., White, J.W.C., 2004. High-resolution record of Northern Hemisphere climate extending into the last interglacial period. Nature 431, 147–151. https://doi.org/10.1038/nature02805

Meyer-Jacob, C., Vogel, H., Gebhardt, A.C., Wennrich, V., Melles, M., Rosén, P., 2014. Biogeochemical variability during the past 3.6 million years recorded by FTIR spectroscopy in the sediment record of Lake El'gygytgyn, Far East Russian Arctic. Clim. Past 10, 209–220. https://doi.org/10.5194/cp-10-209-2014

Meyers, P.A., 2003. Applications of organic geochemistry to paleolimnological reconstructions: a summary of examples from the Laurentian Great Lakes. Org. Geochem. 34, 261–289. https://doi.org/10.1016/S0146-6380(02)00168-7

Meyers, P.A., Ishiwatari, R., 1993. Lacustrine organic geochemistry—an overview of indicators of organic matter sources and diagenesis in lake sediments. Org. Geochem. 20, 867–900. https://doi.org/10.1016/0146-6380(93)90100-P

Meyers, S.R., 2012. Seeing red in cyclic stratigraphy: Spectral noise estimation for astrochronology. Paleoceanography 27, PA3228. https://doi.org/10.1029/2012PA002307

Miller, D.R., Habicht, M.H., Keisling, B.A., Castañeda, I.S., Bradley, R.S., 2018. A 900-year New England temperature reconstruction from in situ seasonally produced branched glycerol dialkyl glycerol tetraethers (brGDGTs). Clim. Past 14, 1653–1667. https://doi.org/10.5194/cp-14-1653-2018

Miller, G.H., Brigham-Grette, J., Alley, R.B., Anderson, L., Bauch, H.A., Douglas, M.S.V., Edwards, M.E., Elias, S.A., Finney, B.P., Fitzpatrick, J.J., Funder, S.V., Herbert, T.D., Hinzman, L.D., Kaufman, D.S., MacDonald, G.M., Polyak, L., Robock, A., Serreze, M.C., Smol, J.P., Spielhagen, R., White, J.W.C., Wolfe, A.P., Wolff, E.W., 2010. Temperature and precipitation history of the Arctic. Quat. Sci. Rev., Special Theme: Arctic Palaeoclimate Synthesis (PP. 1674-1790) 29, 1679–1715. https://doi.org/10.1016/j.quascirev.2010.03.001

Milne, G.A., Mitrovica, J.X., 2008. Searching for eustasy in deglacial sea-level histories. Quat. Sci. Rev. 27, 2292–2302. https://doi.org/10.1016/j.quascirev.2008.08.018

Minyuk, P.S., Brigham-Grette, J., Melles, M., Borkhodoev, V.Y., Glushkova, O.Y., 2006. Inorganic geochemistry of El'gygytgyn Lake sediments (northeastern Russia) as an indicator of paleoclimatic change for the last 250 kyr. J. Paleolimnol. 37, 123–133. https://doi.org/10.1007/s10933-006-9027-4

Mock, C.J., Bartlein, P.J., Anderson, P.M., 1998. Atmospheric circulation patterns and spatial climatic variations in Beringia. Int. J. Climatol. 18, 1085–1104.

Moossen, H., Bendle, J., Seki, O., Quillmann, U., Kawamura, K., 2015. North Atlantic Holocene climate evolution recorded by high-resolution terrestrial and marine biomarker records. Quat. Sci. Rev. 129, 111–127. https://doi.org/10.1016/j.quascirev.2015.10.013

Naish, T., Powell, R., Levy, R., Wilson, G., Scherer, R., Talarico, F., Krissek, L., Niessen, F., Pompilio, M., Wilson, T., Carter, L., DeConto, R., Huybers, P., McKay, R., Pollard, D., Ross, J., Winter, D., Barrett, P., Browne, G., Cody, R., Cowan, E., Crampton, J., Dunbar, G., Dunbar, N., Florindo, F., Gebhardt, C., Graham, I., Hannah, M., Hansaraj, D., Harwood, D., Helling, D., Henrys, S., Hinnov, L., Kuhn, G., Kyle, P., Läufer, A., Maffioli, P., Magens, D., Mandernack, K., McIntosh, W., Millan, C., Morin, R., Ohneiser, C., Paulsen, T., Persico, D., Raine, I., Reed, J., Riesselman, C., Sagnotti, L., Schmitt, D., Sjunneskog, C., Strong, P., Taviani, M., Vogel, S., Wilch, T., Williams, T., 2009. Obliquity-paced Pliocene West Antarctic ice sheet oscillations. Nature 458, 322–328. https://doi.org/10.1038/nature07867

Niedermeyer, E.M., Schefuß, E., Sessions, A.L., Mulitza, S., Mollenhauer, G., Schulz, M., Wefer, G., 2010. Orbital- and millennial-scale changes in the hydrologic cycle and vegetation in the western African Sahel: insights from individual plant wax δD and δ13C. Quat. Sci. Rev. 29, 2996–3005. https://doi.org/10.1016/j.quascirev.2010.06.039

Nishimura, M., Koyama, T., 1977. The occurrence of stanols in various living organisms and the behavior of sterols in contemporary sediments. Geochim. Cosmochim. Acta 41, 379–385. https://doi.org/10.1016/0016-7037(77)90265-4
Nolan, M., 2013. Quantitative and qualitative constraints on hind-casting the formation of multiyear lake-ice covers at Lake El'gygytgyn. Clim. Past 9, 1253–1269. https://doi.org/10.5194/cp-9-1253-2013
Nolan, M., 2012. Analysis of local AWS and NCEP/NCAR reanalysis data at Lake El'gygtytgyn, and its implications for maintaining multi-year lake-ice covers. Clim. Past Discuss. 8, 1443–1483. https://doi.org/10.5194/cpd-8-1443-2012
Nolan, M., Brigham-Grette, J., 2007. Basic hydrology, limnology, and meteorology of modern Lake El'gygytgyn, Siberia. J. Paleolimnol. 37, 17–35. https://doi.org/10.1007/s10933-006-9020-y
Nolan, M., Cassano, E.N., Cassano, J.J., 2013. Synoptic climatology and recent climate trends at Lake El'gygytgyn. Clim. Past 9, 1271–1286. https://doi.org/10.5194/cp-9-1271-2013
Noone, D., 2008. The influence of midlatitude and tropical overturning circulation on the isotopic composition of atmospheric water vapor and Antarctic precipitation. J. Geophys. Res. 113. https://doi.org/10.1029/2007JD008892
Nowaczyk, N.R., Haltia, E.M., Ulbricht, D., Wennrich, V., Sauerbrey, M.A., Rosén, P., Vogel, H., Francke, A., Meyer-Jacob, C., Andreev, A.A., Lozhkin, A.V., 2013. Chronology of Lake El'gygytgyn sediments – a combined magnetostratigraphic, palaeoclimatic and orbital tuning study based on multi-parameter analyses. Clim. Past 9, 2413–2432. https://doi.org/10.5194/cp-9-2413-2013
Nürnberg, D., Dethleff, D., Tiedemann, R., Kaiser, A., Gorbarenko, S.A., 2011. Okhotsk Sea ice coverage and Kamchatka glaciation over the last 350ka — Evidence from ice-rafted debris and planktonic δ18O. Palaeogeogr. Palaeoclimatol. Palaeoecol. 310, 191–205. https://doi.org/10.1016/j.palaeo.2011.07.011
Ogbebo, F.E., Evans, M.S., Waiser, M.J., Tumber, V.P., Keating, J.J., 2009. Nutrient limitation of phytoplankton growth in Arctic lakes of the lower Mackenzie River Basin, northern Canada. Can. J. Fish. Aquat. Sci. 66, 247–260. https://doi.org/10.1139/F08-202
Opel, T., Dereviagin, A.Y., Meyer, H., Schirrmeister, L., Wetterich, S., 2011. Palaeoclimatic information from stable water isotopes of Holocene ice wedges on the Dmitrii Laptev Strait, northeast Siberia, Russia. Permafr. Periglac. Process. 22, 84–100. https://doi.org/10.1002/ppp.667
Ourisson, G., Albrecht, P., 1992. Hopanoids. 1. Geohopanoids: the most abundant natural products on Earth? Acc. Chem. Res. 25, 398–402. https://doi.org/10.1021/ar00021a003
Overland, J.E., Francis, J.A., Hanna, E., Wang, M., 2012. The recent shift in early summer Arctic atmospheric circulation. Geophys. Res. Lett. 39. https://doi.org/10.1029/2012GL053268

Pagani, M., Pedentchouk, N., Huber, M., Sluijs, A., Schouten, S., Brinkhuis, H., Sinninghe Damsté, J.S., Dickens, G.R., Expedition 302 Scientists, Backman, J., Clemens, S., Cronin, T., Eynaud, F., Gattacceca, J., Jakobsson, M., Jordan, R., Kaminski, M., King, J., Koc, N., Martinez, N.C., McInroy, D., Moore Jr, T.C., O'Regan, M., Onodera, J., Pälike, H., Rea, B., Rio, D., Sakamoto, T., Smith, D.C., St John, K.E.K., Suto, I., Suzuki, N., Takahashi, K., Watanabe, M., Yamamoto, M., 2006. Arctic hydrology during global warming at the Palaeocene/Eocene thermal maximum. Nature 442, 671–675. https://doi.org/10.1038/nature05043

Past Interglacials Working Group of PAGES, 2016. Interglacials of the last 800,000 years: Interglacials of the Last 800,000 Years. Rev. Geophys. 54, 162–219. https://doi.org/10.1002/2015RG000482

Pautler, B.G., Reichart, G.-J., Sanborn, P.T., Simpson, M.J., Weijers, J.W.H., 2014. Comparison of soil derived tetraether membrane lipid distributions and plant-wax δD compositions for reconstruction of Canadian Arctic temperatures. Palaeogeogr. Palaeoclimatol. Palaeoecol. 404, 78–88. https://doi.org/10.1016/j.palaeo.2014.03.038

Pearson, E.J., Juggins, S., Talbot, H.M., Weckström, J., Rosén, P., Ryves, D.B., Roberts, S.J., Schmidt, R., 2011. A lacustrine GDGT-temperature calibration from the Scandinavian Arctic to Antarctic: Renewed potential for the application of GDGT-paleothermometry in lakes. Geochim. Cosmochim. Acta 75, 6225–6238. https://doi.org/10.1016/j.gca.2011.07.042

Peters, K.E., Walters, C.C., Moldowan, J.M., 2005. The Biomarker Guide: Biomarkers and isotopes in the environment and human history. Cambridge University Press.

Peterse, F., Martínez-García, A., Zhou, B., Beets, C.J., Prins, M.A., Zheng, H., Eglinton, T.I., 2014. Molecular records of continental air temperature and monsoon precipitation variability in East Asia spanning the past 130,000 years. Quat. Sci. Rev. 83, 76–82. https://doi.org/10.1016/j.quascirev.2013.11.001

Pienitz, R., Douglas, M.S., Smol, J.P., Hamilton, P.B., 2004. Algal indicators of environmental change in arctic and antarctic lakes and ponds. Long-Term Environ. Change Arct. Antarct. Lakes 117–157.

Polissar, P.J., Freeman, K.H., 2010. Effects of aridity and vegetation on plant-wax δD in modern lake sediments. Geochim. Cosmochim. Acta 74, 5785–5797. https://doi.org/10.1016/j.gca.2010.06.018

Pollard, D., DeConto, R.M., 2009. Modelling West Antarctic ice sheet growth and collapse through the past five million years. Nature 458, 329–332. https://doi.org/10.1038/nature07809

Porter, T.J., Froese, D.G., Feakins, S.J., Bindeman, I.N., Mahony, M.E., Pautler, B.G., Reichart, G.-J., Sanborn, P.T., Simpson, M.J., Weijers, J.W.H., 2016. Multiple water isotope proxy reconstruction of extremely low last glacial temperatures in Eastern Beringia (Western Arctic). Quat. Sci. Rev. 137, 113–125. https://doi.org/10.1016/j.quascirev.2016.02.006

Post, E., Forchhammer, M.C., Bret-Harte, M.S., Callaghan, T.V., Christensen, T.R., Elberling, B., Fox, A.D., Gilg, O., Hik, D.S., Høye, T.T., Ims, R.A., Jeppesen, E., Klein, D.R., Madsen, J., McGuire, A.D., Rysgaard, S., Schindler, D.E., Stirling, I., Tamstorf, M.P., Tyler, N.J.C., Wal, R. van der, Welker, J., Wookey, P.A., Schmidt, N.M., Aastrup, P., 2009. Ecological Dynamics Across the Arctic Associated with Recent Climate Change. Science 325, 1355–1358. https://doi.org/10.1126/science.1173113

Poynter, J., Eglinton, G., 1990. 14. Molecular composition of three sediments from hole 717c: The Bengal fan, in: Proceedings of the Ocean Drilling Program: Scientific Results. pp. 155–161.

Prokopenko, A.A., Bezrukova, E.V., Khursevich, G.K., Solotchina, E.P., Kuzmin, M.I., Tarasov, P.E., 2010. Climate in continental interior Asia during the longest interglacial of the past 500 000 years: the new MIS 11 records from Lake Baikal, SE Siberia. Clim Past 6, 31–48. https://doi.org/10.5194/cp-6-31-2010

Prokopenko, A.A., Hinnov, L.A., Williams, D.F., Kuzmin, M.I., 2006. Orbital forcing of continental climate during the Pleistocene: a complete astronomically tuned climatic record from Lake Baikal, SE Siberia. Quat. Sci. Rev. 25, 3431–3457. https://doi.org/10.1016/j.quascirev.2006.10.002

Prokopenko, A.A., Karabanov, E.B., Williams, D.F., Kuzmin, M.I., Shackleton, N.J., Crowhurst, S.J., Peck, J.A., Gvozdkov, A.N., King, J.W., 2001. Biogenic Silica Record of the Lake Baikal Response to Climatic Forcing during the Brunhes. Quat. Res. 55, 123–132. https://doi.org/10.1006/qres.2000.2212

Rach, O., Brauer, A., Wilkes, H., Sachse, D., 2014. Delayed hydrological response to Greenland cooling at the onset of the Younger Dryas in western Europe. Nat. Geosci. 7, 109–112. https://doi.org/10.1038/ngeo2053

Rach, O., Kahmen, A., Brauer, A., Sachse, D., 2017. A dual-biomarker approach for quantification of changes in relative humidity from sedimentary lipid <i>D</i>/<i>H</i> ratios. Clim. Past 13, 741–757. https://doi.org/10.5194/cp-13-741-2017

Rampen, S.W., Abbas, B.A., Schouten, S., Sinninghe Damste, J.S., 2010. A comprehensive study of sterols in marine diatoms (Bacillariophyta): Implications for their use as tracers for diatom productivity. Limnol. Oceanogr. 55, 91–105. https://doi.org/10.4319/lo.2010.55.1.0091

Rampen, S.W., Willmott, V., Kim, J.-H., Uliana, E., Mollenhauer, G., Schefuß, E., Sinninghe Damsté, J.S., Schouten, S., 2012. Long chain 1,13- and 1,15-diols as a potential proxy for palaeotemperature reconstruction. Geochim. Cosmochim. Acta 84, 204–216. https://doi.org/10.1016/j.gca.2012.01.024

Rohling, E.J., Foster, G.L., Grant, K.M., Marino, G., Roberts, A.P., Tamisiea, M.E., Williams, F., 2014. Sea-level and deep-sea-temperature variability over the past 5.3 million years. Nature 508, 477–482. https://doi.org/10.1038/nature13230

Rouse, W.R., Douglas, M.S.V., Hecky, R.E., Hershey, A.E., Kling, G.W., Lesack, L., Marsh, P., Mcdonald, M., Nicholson, B.J., Roulet, N.T., Smol, J.P., 1997. Effects of Climate Change on the Freshwaters of Arctic and Subarctic North America. Hydrol. Process. 11, 873–902. https://doi.org/10.1002/(SICI)1099-1085(19970630)11:8<873::AID-HYP510>3.0.CO;2-6

Rozanski, K., Araguás-Araguás, L., Gonfiantini, R., 2013. Isotopic Patterns in Modern Global Precipitation, in: Swart, P.K., Lohmann, K.C., Mckenzie, J., Savin, S. (Eds.), Geophysical Monograph Series. American Geophysical Union, Washington, D. C., pp. 1–36. https://doi.org/10.1029/GM078p0001

Sachse, D., Billault, I., Bowen, G.J., Chikaraishi, Y., Dawson, T.E., Feakins, S.J., Freeman, K.H., Magill, C.R., McInerney, F.A., Meer, M.T.J. van der, Polissar, P., Robins, R.J., Sachs, J.P., Schmidt, H.-L., Sessions, A.L., White, J.W.C., West, J.B., Kahmen, A., 2012. Molecular Paleohydrology: Interpreting the Hydrogen-Isotopic Composition of Lipid Biomarkers from Photosynthesizing Organisms [WWW Document]. Httpdxdoiorg101146annurev-Earth-042711-105535. URL http://www.annualreviews.org/eprint/5GnXw65Req33cYHmIEEj/full/10.1146/annurev-earth-042711-105535 (accessed 12.16.16).

Sachse, D., Radke, J., Gleixner, G., 2006. δD values of individual n-alkanes from terrestrial plants along a climatic gradient – Implications for the sedimentary biomarker record. Org. Geochem. 37, 469–483. https://doi.org/10.1016/j.orggeochem.2005.12.003

Sachse, D., Radke, J., Gleixner, G., 2004. Hydrogen isotope ratios of recent lacustrine sedimentary n-alkanes record modern climate variability. Geochim. Cosmochim. Acta 68, 4877–4889. https://doi.org/10.1016/j.gca.2004.06.004

Sauer, P.E., Eglinton, T.I., Hayes, J.M., Schimmelmann, A., Sessions, A.L., 2001. Compound-specific D/H ratios of lipid biomarkers from sediments as a proxy for environmental and climatic conditions. Geochim. Cosmochim. Acta 65, 213–222. https://doi.org/10.1016/S0016-7037(00)00520-2

Schoon, P.L., de Kluijver, A., Middelburg, J.J., Downing, J.A., Sinninghe Damsté, J.S., Schouten, S., 2013. Influence of lake water pH and alkalinity on the distribution of core and intact polar branched glycerol dialkyl glycerol tetraethers (GDGTs) in lakes. Org. Geochem. 60, 72–82. https://doi.org/10.1016/j.orggeochem.2013.04.015

Schwamborn, G., Meyer, H., Fedorov, G., Schirrmeister, L., Hubberten, H.-W., 2006. Ground ice and slope sediments archiving Late Quaternary paleoenvironment and paleoclimate signals at the margins of Elgygytgyn Crater, NE Siberia. Quat. Res. 66, 259–272. https://doi.org/Schwamborn, G. , Meyer, H. , Fedorov, G. , Schirrmeister, L. and Hubberten, H. W. (2006) Ground ice and slope sediments archiving Late Quaternary paleoenvironment and paleoclimate signals at the margins of Elgygytgyn Crater, NE Siberia , Quaternary research, 66 (2), pp. 259-272 . doi:10.1016/j.yqres.2006.06.007 <http://doi.org/10.1016/j.yqres.2006.06.007> , hdl:10013/epic.23731

Shanahan, T.M., Hughen, K.A., Ampel, L., Sauer, P.E., Fornace, K., 2013a. Environmental controls on the 2H/1H values of terrestrial leaf waxes in the eastern Canadian Arctic. Geochim. Cosmochim. Acta 119, 286–301. https://doi.org/10.1016/j.gca.2013.05.032

Shanahan, T.M., Hughen, K.A., Van Mooy, B.A.S., 2013b. Temperature sensitivity of branched and isoprenoid GDGTs in Arctic lakes. Org. Geochem. 64, 119–128. https://doi.org/10.1016/j.orggeochem.2013.09.010

Shepherd, T., Wynne Griffiths, D., 2006. The effects of stress on plant cuticular waxes. New Phytol. 171, 469–499. https://doi.org/10.1111/j.1469-8137.2006.01826.x

Sime, L.C., Risi, C., Tindall, J.C., Sjolte, J., Wolff, E.W., Masson-Delmotte, V., Capron, E., 2013. Warm climate isotopic simulations: what do we learn about interglacial signals in Greenland ice cores? Quat. Sci. Rev. 67, 59–80. https://doi.org/10.1016/j.quascirev.2013.01.009

Smith, F.A., Freeman, K.H., 2006. Influence of physiology and climate on δD of leaf wax n-alkanes from C3 and C4 grasses. Geochim. Cosmochim. Acta 70, 1172–1187. https://doi.org/10.1016/j.gca.2005.11.006

Snyder, J., Cheraponova, M., Bryan, A., 2013. Dynamic Diatom Response to Changing Climate 0-1.2 Ma at Lake El'Gygytgyn, Far East Russian Arctic. Clim. Past 1309–1319. https://doi.org/10.5194/cp-9-1309-2013

Sodemann, H., Schwierz, C., Wernli, H., 2008. Interannual variability of Greenland winter precipitation sources: Lagrangian moisture diagnostic and North Atlantic Oscillation influence. J. Geophys. Res. Atmospheres 113. https://doi.org/10.1029/2007JD008503

Stauch, G., Lehmkuhl, F., 2010. Quaternary glaciations in the Verkhoyansk Mountains, Northeast Siberia. Quat. Res. 74, 145–155. https://doi.org/10.1016/j.yqres.2010.04.003

Stevenson, R.J., Smol, J.P., 2003. Use of algae in environmental assessments. Academic Press, San Diego, CA.

Sugimoto, A., Naito, D., Yanagisawa, N., Ichiyanagi, K., Kurita, N., Kubota, J., Kotake, T., Ohata, T., Maximov, T.C., Fedorov, A.N., 2003. Characteristics of soil moisture in permafrost observed in East Siberian taiga with stable isotopes of water. Hydrol. Process. 17, 1073–1092. https://doi.org/10.1002/hyp.1180

Summons, R.E., Jahnke, L.L., Hope, J.M., Logan, G.A., 1999. 2-Methylhopanoids as biomarkers for cyanobacterial oxygenic photosynthesis. Nature 400, 554–557. https://doi.org/10.1038/23005

Sun, Q., Chu, G., Liu, M., Xie, M., Li, S., Ling, Y., Wang, X., Shi, L., Jia, G., Lü, H., 2011. Distributions and temperature dependence of branched glycerol dialkyl glycerol tetraethers in recent lacustrine sediments from China and Nepal. J. Geophys. Res. 116. https://doi.org/10.1029/2010JG001365

Sun, Y., Clemens, S.C., Morrill, C., Lin, X., Wang, X., An, Z., 2012. Influence of Atlantic meridional overturning circulation on the East Asian winter monsoon. Nat. Geosci. 5, 46–49. https://doi.org/10.1038/ngeo1326

Sundqvist, H.S., Kaufman, D.S., McKay, N.P., Balascio, N.L., Briner, J.P., Cwynar, L.C., Sejrup, H.P., Seppä, H., Subetto, D.A., Andrews, J.T., Axford, Y., Bakke, J., Birks, H.J.B., Brooks, S.J., de Vernal, A., Jennings, A.E., Ljungqvist, F.C., Rühland, K.M., Saenger, C., Smol, J.P., Viau, A.E., 2014. Arctic Holocene proxy climate database – new approaches to assessing geochronological accuracy and encoding climate variables. Clim Past 10, 1605–1631. https://doi.org/10.5194/cp-10-1605-2014

Svendsen, J.I., Alexanderson, H., Astakhov, V.I., Demidov, I., Dowdeswell, J.A., Funder, S., Gataullin, V., Henriksen, M., Hjort, C., Houmark-Nielsen, M., Hubberten, H.W., Ingólfsson, Ó., Jakobsson, M., Kjær, K.H., Larsen, E., Lokrantz, H., Lunkka, J.P., Lyså, A., Mangerud, J., Matiouchkov, A., Murray, A., Möller, P., Niessen, F., Nikolskaya, O., Polyak, L., Saarnisto, M., Siegert, C., Siegert, M.J., Spielhagen, R.F., Stein, R., 2004. Late Quaternary ice sheet history of northern Eurasia. Quat. Sci. Rev., Quaternary Environments of the Eurasian North (QUEEN) 23, 1229–1271. https://doi.org/10.1016/j.quascirev.2003.12.008

Svendsen, J.I., Astakhov, V.I., Bolshiyanov, D.Y., Demidov, I., Dowdeswell, J.A., Gataullin, V., Hjort, C., Hubberten, H.W., Larsen, E., Mangerud, J., Melles, M., Möller, P., Saarnisto, M., Siegert, M.J., 1999. Maximum extent of the Eurasian ice sheets in the Barents and Kara Sea region during the Weichselian. Boreas 28, 234–242. https://doi.org/10.1111/j.1502-3885.1999.tb00217.x

SWIPA, 2017. Snow, Water, Ice and Permafrost in the Arctic (SWIPA) 2017.

Takahashi, K., Ravelo, A.C., Alvarez Zarikian, C., 2011. IODP Expedition 323—Pliocene and Pleistocene Paleoceanographic Changes in the Bering Sea. Sci. Drill. https://doi.org/10.2204/iodp.sd.11.01.2011

Talbot, H.M., Summons, R.E., Jahnke, L.L., Cockell, C.S., Rohmer, M., Farrimond, P., 2008. Cyanobacterial bacteriohopanepolyol signatures from cultures and natural environmental settings. Org. Geochem. 39, 232–263. https://doi.org/10.1016/j.orggeochem.2007.08.006

Tang, C., Yang, H., Pancost, R.D., Griffiths, M.L., Xiao, G., Dang, X., Xie, S., 2017. Tropical and high latitude forcing of enhanced megadroughts in Northern China during the last four terminations. Earth Planet. Sci. Lett. 479, 98–107. https://doi.org/10.1016/j.epsl.2017.09.012

Thomas, E.K., Briner, J.P., Ryan-Henry, J.J., Huang, Y., 2016a. A major increase in winter snowfall during the middle Holocene on western Greenland caused by reduced sea ice in Baffin Bay and the Labrador Sea. Geophys. Res. Lett. 43, 2016GL068513. https://doi.org/10.1002/2016GL068513

Thomas, E.K., Castañeda, I.S., McKay, N.P., Briner, J.P., Salacup, J.M., Nguyen, K.Q., Schweinsberg, A.D., 2018. A Wetter Arctic Coincident With Hemispheric Warming 8,000 Years Ago. Geophys. Res. Lett. 45, 10,637-10,647. https://doi.org/10.1029/2018GL079517

Thomas, E.K., Clemens, S.C., Prell, W.L., Herbert, T.D., Huang, Y., Liu, Z., Damsté, J.S.S., Sun, Y., Wen, X., 2014. Temperature and leaf wax δ2H records demonstrate seasonal and regional controls on Asian monsoon proxies. Geology 42, 1075–1078. https://doi.org/10.1130/G36289.1

Thomas, E.K., Clemens, S.C., Sun, Y., Prell, W.L., Huang, Y., Gao, L., Loomis, S., Chen, G., Liu, Z., 2016b. Heterodynes dominate precipitation isotopes in the East Asian monsoon region, reflecting interaction of multiple climate factors. Earth Planet. Sci. Lett. 455, 196–206. https://doi.org/10.1016/j.epsl.2016.09.044

Thomas, E.K., McGrane, S., Briner, J.P., Huang, Y., 2012. Leaf wax δ2H and varve-thickness climate proxies from proglacial lake sediments, Baffin Island, Arctic Canada. J. Paleolimnol. 48, 193–207. https://doi.org/10.1007/s10933-012-9584-7

Thompson, R.S., Fleming, R.F., 1996. Middle Pliocene vegetation: reconstructions, paleoclimatic inferences, and boundary conditions for climate modeling. Mar. Micropaleontol., Climates and Climate Variability of the Pliocene 27, 27–49. https://doi.org/10.1016/0377-8398(95)00051-8

Tierney, J.E., deMenocal, P.B., 2013. Abrupt Shifts in Horn of Africa Hydroclimate Since the Last Glacial Maximum. Science 342, 843–846. https://doi.org/10.1126/science.1240411

Tierney, J.E., Russell, J.M., 2009. Distributions of branched GDGTs in a tropical lake system: Implications for lacustrine application of the MBT/CBT paleoproxy. Org. Geochem. 40, 1032–1036. https://doi.org/10.1016/j.orggeochem.2009.04.014

Tierney, J.E., Russell, J.M., Eggermont, H., Hopmans, E.C., Verschuren, D., Sinninghe Damsté, J.S., 2010. Environmental controls on branched tetraether lipid distributions in tropical East African lake sediments. Geochim. Cosmochim. Acta 74, 4902–4918. https://doi.org/10.1016/j.gca.2010.06.002

Tierney, J.E., Russell, J.M., Huang, Y., Damste, J.S.S., Hopmans, E.C., Cohen, A.S., 2008. Northern Hemisphere Controls on Tropical Southeast African Climate During the Past 60,000 Years. Science 322, 252–255. https://doi.org/10.1126/science.1160485

Tranvik, L.J., Downing, J.A., Cotner, J.B., Loiselle, S.A., Striegl, R.G., Ballatore, T.J., Dillon, P., Finlay, K., Fortino, K., Knoll, L.B., others, 2009. Lakes and reservoirs as regulators of carbon cycling and climate. Limnol. Oceanogr. 54, 2298–2314.

Tzedakis, P.C., Channell, J.E.T., Hodell, D.A., Kleiven, H.F., Skinner, L.C., 2012a. Determining the natural length of the current interglacial. Nat. Geosci. 5, 138–141. https://doi.org/10.1038/ngeo1358

Tzedakis, P.C., Wolff, E.W., Skinner, L.C., Brovkin, V., Hodell, D.A., McManus, J.F., Raynaud, D., 2012b. Can we predict the duration of an interglacial? Clim. Past 8, 1473–1485. https://doi.org/10.5194/cp-8-1473-2012

van Bree, L.G.J., Peterse, F., van der Meer, M.T.J., Middelburg, J.J., Negash, A.M.D., De Crop, W., Cocquyt, C., Wieringa, J.J., Verschuren, D., Sinninghe Damsté, J.S., 2018. Seasonal variability in the abundance and stable carbon-isotopic composition of lipid biomarkers in suspended particulate matter from a stratified equatorial lake (Lake Chala, Kenya/Tanzania): Implications for the sedimentary record. Quat. Sci. Rev. 192, 208–224. https://doi.org/10.1016/j.quascirev.2018.05.023

van Dongen, B.E., Semiletov, I., Weijers, J.W.H., Gustafsson, Ö., 2008. Contrasting lipid biomarker composition of terrestrial organic matter exported from across the Eurasian Arctic by the five great Russian Arctic rivers. Glob. Biogeochem. Cycles 22, GB1011. https://doi.org/10.1029/2007GB002974

Vaughn, D.R., Caissie, B.E., 2017. Effects of sea-level, sea-ice extent, and nutrient availability on primary production at the Umnak Plateau, Bering Sea (IODP Site U1339) during Marine Isotope Stage (MIS) 5. Palaeogeogr. Palaeoclimatol. Palaeoecol. 485, 283–292. https://doi.org/10.1016/j.palaeo.2017.06.020

Veillette, J., Martineau, M.-J., Antoniades, D., Sarrazin, D., Vincent, W.F., 2010. Effects of loss of perennial lake ice on mixing and phytoplankton dynamics: insights from High Arctic Canada. Ann. Glaciol. 51, 56–70. https://doi.org/10.3189/172756411795931921

Vernal, A. de, Hillaire-Marcel, C., 2008. Natural Variability of Greenland Climate, Vegetation, and Ice Volume During the Past Million Years. Science 320, 1622–1625. https://doi.org/10.1126/science.1153929

Vincent, W.F., Laurion, I., Pienitz, R., Walter Anthony, K.M., 2012. Climate Impacts on Arctic Lake Ecosystems, in: Goldman, C.R., Kumagai, M., Robarts, R.D. (Eds.), Climatic Change and Global Warming of Inland Waters. John Wiley & Sons, Ltd, Chichester, UK, pp. 27–42. https://doi.org/10.1002/9781118470596.ch2

Voelker, A.H.L., Rodrigues, T., Billups, K., Oppo, D., McManus, J., Stein, R., Hefter, J., Grimalt, J.O., 2010. Variations in mid-latitude North Atlantic surface water properties during the mid-Brunhes (MIS 9–14) and their implications for the thermohaline circulation. Clim. Past 6, 531–552. https://doi.org/10.5194/cp-6-531-2010

Vogel, H., Meyer-Jacob, C., Melles, M., Brigham-Grette, J., Andreev, A.A., Wennrich, V., Tarasov, P.E., Rosén, P., 2013. Detailed insight into Arctic climatic variability during MIS 11c at Lake El'gygytgyn, NE Russia. Clim. Past 9, 1467–1479. https://doi.org/10.5194/cp-9-1467-2013

Volkman, 1986 (OLs) (geoq) [WWW Document], n.d. . Scribd. URL https://www.scribd.com/doc/57770267/Volkman-1986-OLs-geoq (accessed 3.17.15).

Volkman, J., 2003. Sterols in microorganisms. Appl. Microbiol. Biotechnol. 60, 495–506. https://doi.org/10.1007/s00253-002-1172-8

Volkman, J.K., Barrett, S.M., Blackburn, S.I., Mansour, M.P., Sikes, E.L., Gelin, F., 1998. Microalgal biomarkers: A review of recent research developments. Org. Geochem. 29, 1163–1179. https://doi.org/10.1016/S0146-6380(98)00062-X

Volkman, J.K., Barrett, S.M., Dunstan, G.A., Jeffrey, S.W., 1992. C30□C32 alkyl diols and unsaturated alcohols in microalgae of the class Eustigmatophyceae. Org. Geochem. 18, 131–138. https://doi.org/10.1016/0146-6380(92)90150-V

Volkman, J.K., Rijpstra, W.I.C., de Leeuw, J.W., Mansour, M.P., Jackson, A.E., Blackburn, S.I., 1999. Sterols of four dinoflagellates from the genus Prorocentrum. Phytochemistry 52, 659–668. https://doi.org/10.1016/S0031-9422(99)00251-4

Waelbroeck, C., Labeyrie, L., Michel, E., Duplessy, J.C., McManus, J.F., Lambeck, K., Balbon, E., Labracherie, M., 2002. Sea-level and deep water temperature changes derived from benthic foraminifera isotopic records. Quat. Sci. Rev. 21, 295–305. https://doi.org/10.1016/S0277-3791(01)00101-9

Walsh, J.E., 2014. Intensified warming of the Arctic: Causes and impacts on middle latitudes. Glob. Planet. Change 117, 52–63. https://doi.org/10.1016/j.gloplacha.2014.03.003

Weber, Y., De Jonge, C., Rijpstra, W.I.C., Hopmans, E.C., Stadnitskaia, A., Schubert, C.J., Lehmann, M.F., Sinninghe Damsté, J.S., Niemann, H., 2015. Identification and carbon isotope composition of a novel branched GDGT isomer in lake sediments: Evidence for lacustrine branched GDGT production. Geochim. Cosmochim. Acta 154, 118–129. https://doi.org/10.1016/j.gca.2015.01.032

Wei, J.H., Finkelstein, D.B., Brigham-Grette, J., Castañeda, I.S., Nowaczyk, N., 2014. Sediment colour reflectance spectroscopy as a proxy for wet/dry cycles at Lake El'gygytgyn, Far East Russia, during Marine Isotope Stages 8 to 12. ResearchGate 61. https://doi.org/10.1111/sed.12116

Weijers, J.W.H., Schouten, S., van den Donker, J.C., Hopmans, E.C., Sinninghe Damsté, J.S., 2007. Environmental controls on bacterial tetraether membrane lipid distribution in soils. Geochim. Cosmochim. Acta 71, 703–713. https://doi.org/10.1016/j.gca.2006.10.003

Werner, M., Heimann, M., Hoffmann, G., 2001. Isotopic composition and origin of polar precipitation in present and glacial climate simulations. Tellus B 53, 53–71. https://doi.org/10.1034/j.1600-0889.2001.01154.x

Wilkie, K., 2012. Compound--Specific Hydrogen Isotopes of Lipid Biomarkers in Lake El'gygytgyn, Ne Russia. Dissertations.

Wilkie, K.M.K., Chapligin, B., Meyer, H., Burns, S., Petsch, S., Brigham-Grette, J., 2013. Modern isotope hydrology and controls on δD of plant leaf waxes at Lake El'gygytgyn, NE Russia. Clim. Past 9, 335–352. https://doi.org/10.5194/cp-9-335-2013

Woelders, L., Lenaerts, J.T.M., Hagemans, K., Akkerman, K., van Hoof, T.B., Hoek, W.Z., 2018. Recent climate warming drives ecological change in a remote high-Arctic lake. Sci. Rep. 8. https://doi.org/10.1038/s41598-018-25148-7

Woodgate, R.A., Aagaard, K., 2005. Revising the Bering Strait freshwater flux into the Arctic Ocean. Geophys. Res. Lett. 32, L02602. https://doi.org/10.1029/2004GL021747

Wu, M.S., West, A.J., Feakins, S.J., 2019. Tropical soil profiles reveal the fate of plant wax biomarkers during soil storage. Org. Geochem. 128, 1–15. https://doi.org/10.1016/j.orggeochem.2018.12.011

Yang, H., Huang, Y., 2003. Preservation of lipid hydrogen isotope ratios in Miocene lacustrine sediments and plant fossils at Clarkia, northern Idaho, USA. Org. Geochem. 34, 413–423. https://doi.org/10.1016/S0146-6380(02)00212-7

Yang, H., Liu, W., Leng, Q., Hren, M.T., Pagani, M., 2011. Variation in n-alkane δD values from terrestrial plants at high latitude: Implications for paleoclimate reconstruction. Org. Geochem. 42, 283–288. https://doi.org/10.1016/j.orggeochem.2011.01.006

Yau, A.M., Bender, M.L., Robinson, A., Brook, E.J., 2016. Reconstructing the last interglacial at Summit, Greenland: Insights from GISP2. Proc. Natl. Acad. Sci. 113, 9710–9715. https://doi.org/10.1073/pnas.1524766113

Yin, Q., 2013. Insolation-induced mid-Brunhes transition in Southern Ocean ventilation and deep-ocean temperature. Nature 494, 222–225. https://doi.org/10.1038/nature11790

Yin, Q.Z., Berger, A., 2010. Insolation and CO2 contribution to the interglacial climate before and after the Mid-Brunhes Event. Nat. Geosci. 3, 243–246. https://doi.org/10.1038/ngeo771

Zell, C., Kim, J.-H., Moreira-Turcq, P., Abril, G., Hopmans, E.C., Bonnet, M.-P., Sobrinho, R.L., Damsté, J.S.S., 2013. Disentangling the origins of branched tetraether lipids and crenarchaeol in the lower Amazon River: Implications for GDGT-based proxies. Limnol. Oceanogr. 58, 343–353. https://doi.org/10.4319/lo.2013.58.1.0343

Zhou, Y., Grice, K., Stuart-Williams, H., Farquhar, G.D., Hocart, C.H., Lu, H., Liu, W., 2010. Biosynthetic origin of the saw-toothed profile in δ13C and δ2H of n-alkanes and systematic isotopic differences between n-, iso- and anteiso-alkanes in leaf waxes of land plants. Phytochemistry 71, 388–403. https://doi.org/10.1016/j.phytochem.2009.11.009

Zhu, C., Weijers, J.W.H., Wagner, T., Pan, J.-M., Chen, J.-F., Pancost, R.D., 2011. Sources and distributions of tetraether lipids in surface sediments across a large river-dominated continental margin. Org. Geochem. 42, 376–386. https://doi.org/10.1016/j.orggeochem.2011.02.002

Zink, K.-G., Vandergoes, M.J., Mangelsdorf, K., Dieffenbacher-Krall, A.C., Schwark, L., 2010. Application of bacterial glycerol dialkyl glycerol tetraethers (GDGTs) to develop modern and past temperature estimates from New Zealand lakes. Org. Geochem., Advances in Organic Geochemistry 2009 Proceedings of the 24th International Meeting on Organic Geochemistry 41, 1060–1066. https://doi.org/10.1016/j.orggeochem.2010.03.004